AAA Fuels Handbook

by

Yeon Soo Kim and G. L. Hofman

Argonne National Laboratory, Argonne, Illinois, 60439
operated by The University of Chicago
for the United States Department of Energy
under Contract W-31-109-Eng-38

Table of Contents

PART A Metal Alloy Fuels

Section		Page
Preface		A-ii
Section 1	General	A.1-1
1.1	Unit Conversion	A.1-1
1.2	Fundamental Constants	A.1-3
1.3	Metal Element Data	A.1-3
1.4	References for Section 1	A.1-4
Section 2	Enthalpy and Heat Capacity	A.2-1
2.1	Zirconium	A.2-1
2.2	Plutonium	A.2-8
2.3	Americium	A.2-14
2.4	Neptunium	A.2-19
2.5	Zr-Pu-Am-Np Alloy	A.2-24
2.6	Uranium	A.2-29
2.7	Curium	A.2-34
2.8	References for Section 2	A.2-36
Section 3	Vapor Pressure	A.3-1
3.1	Americium	A.3-1
3.2	Plutonium and Pu-Zr alloy	A.3-1
3.3	Neptunium	A.3-6
3.4	Zirconium	A.3-8
3.5	Curium	A.3-8
3.6	Uranium	A.3-8
3.7	References for Section 3	A.3-9

Section		Page
Section 4	Phase Equilibrium	A.4-1
4.1	Phase and Crystal Structures of Elements	A.4-1
4.2	Binary Systems	A.4-2
4.3	Ternary Systems	A.4-9
4.4	References for Section 4	A.4-12
Section 5	Thermal Expansion and Density	A.5-1
5.1	Theory	A.5-1
5.2	Elemental Data	A.5-4
5.3	Zr-Pu Binary Alloy	A.5-5
5.4	TRU-Zr Alloy	A.5-5
5.5	References for Section 5	A.5-12
Section 6	Thermal Conductivity	A.6-1
6.1	Elemental Thermal Conductivity	A.6-1
6.2	Theory of Alloy Thermal Conductivity	A.6-6
6.3	Zr-U Alloy	A.6-8
6.4	Zr-Pu Alloy	A.6-11
6.5	Zr-Pu-Am and TRU-Zr Alloys	A.6-16
6.6	References for Section 6	A.6-17
Section 7	Diffusion Coefficient	A.7-1
7.1	Elemental Self Diffusion	A.7-1
7.2	Pu-Ga and Pu-Al Alloy Interdiffusion	A.7-3
7.3	Pu-Zr Alloy Interdiffusion	A.7-3
7.4	Constituent Redistribution	A.7-8
7.5	References for Section 7	A.7-13
Section 8	Elastic Constants	A.8-1
8.1	Modulus of Elasticity	A.8-1

Section Page

8.2 Poisson's Ratio A.8-5

8.3 References for Section 8 ..... A.8-8

Section 9 Creep A.9-1

9.1 U-Zr Alloy A.9-1

9.2 Zr-Pu Alloy A.9-3

9.3 TRU-Zr Alloy A.9-3

9.4 References for Section 9 ..... A.9-5

Section 10 Swelling A.10-1

10.1 Basic Swelling Correlation A.10-1

10.2 Swelling under External Stress A.10-2

10.3 Swelling with Fission Gas Release A.10-3

10.4 Other Consideration: Effect of He Generation from Americium A.10-4

10.5 References for Section 10 ..... A.10-8

Section 11 Gas Release A.11-1

11.1 Fission Gas Release A.11-1

11.2 He Gas Release A.11-1

11.3 References for Section 11 ..... A.11-3

List of Figures

PART A Metal Alloy Fuels

Figure		Page
2-1	Heat capacity data of zirconium in the literature ..……..……	A.2-3
2-2	Enthalpy of zirconium in the literature ……...……..…….	A.2-5
2-3	Comparison of plutonium heat capacity from Hultgren [1], Oetting [7] and Oetting [8] ...…….……..	A.2-9
2-4	Comparison of enthalpy of plutonium from Hultgren [1], Oetting [7] and Oetting [8] ..……...…..	A.2-11
2-5	Heat Capacity of americium taken from Ref.7 ……...	A.2-15
2-6	Enthalpy of americium …….……...	A.2-17
2-7	Heat capacity of neptunium taken from Ref.7 ……	A.2-20
2-8	Enthalpy of neptunium from Ref.7 …….	A.2-22
2-9	Comparison of TRU-Zr element heat capacities and estimated heat capacity of 60 wt%(Zr)+34 wt%(Pu)+4 wt%(Am)+2 wt%(Np) ……...	A.2-25
2-10	Comparison of TRU-Zr element enthalpies and estimated enthalpy of 60 wt%(Zr)+34 wt%(Pu)+4 wt%(Am)+2 wt%(Np) ……	A.2-26
2-11	Uranium metal heat capacity taken from Ref.7 ……..	A.2-30

Figure		Page
2-12	Uranium metal enthalpy taken from Ref.7 …….	A.2-32
3-1	Recommended vapor pressure of solid plutonium compared to the Alcock data ……...…….	A.3-3
3-2	Model predictions for vapor pressure of liquid plutonium compared to data from the literature ……...……	A.3-4
3-3	Predicted vapor pressure of liquid phase neptunium compared with data from the literature ……...……...…….	A.3-7
4-1	Phase diagram of Pu-Zr binary alloy [2] ……...…..	A.4-3
4-2	Phase diagram of plutonium-americium alloy [4] ……...……...	A.4-5
4-3	Phase diagram of plutonium-americium alloy [6] ……..	A.4-6
4-4	Phase diagram of neptunium-americium alloy [6] ……..	A.4-7
4-5	Phase diagram of Pu-Zr alloy [4] ……...…..…..	A.4-8
4-6	Section of the Pu-Am-Np phase diagram at 1000 K [6] …….....	A.4-10
4-7	Section of the Pu-Am-Np phase diagram at 1000 K [6] ….……	A.4-11
5-1	Comparison of Pu densities between the solid phase and the liquid phase	A.5-9
5-2	Fractional linear thermal expansion of 60 wt%Zr-40 wt%Pu alloy …….....	A.5-11

Figure Page

6-1 Thermal conductivity of TRU elements. The thermal conductivities of U and Zr are included for comparison ……..…….... A.6-5

6-2 Comparison between correlation predictions (lines) and data (symbols) from Touloukian [1] and from Fink [3]. (a) U-rich Zr-U alloys, (b) Zr-rich Zr-U alloys. The coefficient in front of Zr designates the weight percent if Zr in the alloy ……..……...……. A.6-10

6-3 Thermal conductivity of Zr-Pu alloys versus Zr content at the temperature range of 540 – 870 K. The dashed lines indicate the phase transitions ……..…….…….……..... A.6-14

6-4 Thermal conductivity of Zr-Pu alloys versus Zr content at the temperature range of 873 – 1532 K. The dashed line shows the phase transition (solidus line) …….……...…….... A.6-15

7-1 Intrinsic diffusion coefficients of Pu and Zr in (ε-Pu,β-Zr) solid solution at 1000K …….……..... A.7-7

7-2 Constituent redistribution profiles of U-Pu-Zr fuel at 1.9 at% burnup [20] A.7-9

7-3 Postirradiation results of X501 test: (a) Postirradiation optical image, (b) Wavelength dispersive spectroscopy (WDS) signals. The fuel was composed of U-20.2Pu-9.1Zr-1.2Am-1.3Np (wt%) and irradiated to ~6at% burnup [25] …….. A.7-12

8-1 Dynamic modulus of elasticity of pure Zr ……...……... A.8-3

8-2 Dynamic modulus of elasticity of pure Pu ……..…… A.8-4

Figure Page

8-3 Poisson's ratio of Pu-Zr alloys for Pu concentrations up to 0.5 in weight fraction ……..……... A.8-7

10-1 Swelling of fuel versus burnup for irradiated Zr-U alloys ……...……... A.10-6

10-2 Zr-Pu fuel swelling versus burnup under 20 MPa external pressure with fission gas release …….……...……... A.10-7

11-1 Comparison of fission gas release data and predictions by Eq.(1) …….. A.11-2

List of Tables

PART A Metal Alloy Fuels

Table		Page
1-1	Fundamental Constants ……...……	A.1-3
1-2	Metal Element Data [1-3] ……...……	A.1-3
2-1	Zirconium Phase Transition Temperatures (K) ...……..…….……	A.2-1
2-2	Recommended Values of Heat Capacity and Enthalpy of Zirconium ….....	A.2-6
2-3	Enthalpies of Transitions of Zirconium (kJ/mole) ……...…….……..	A.2-7
2-4	Plutonium Phase Transition Temperatures (K) ……..……...…..	A.2-8
2-5	Recommended Values of Heat Capacity and Enthalpy of Plutonium ….....	A.2-12
2-6	Enthalpies of Transitions of Plutonium (kJ/mole) …….…..……...	A.2-13
2-7	Phase Transition Temperatures and Enthalpies of Transitions of Americium ……..……	A.2-14
2-8	Recommended Heat Capacity and Enthalpy of Americium ……..…….	A.2-18
2-9	Phase transition temperatures and Enthalpies of Transitions of Neptunium	A.2-19
2-10	Recommended Heat Capacity and Enthalpy of Neptunium ……	A.2-23
2-11	Recommended Heat Capacity Values for TRU Elements and Alloy ……..	A.2-27

Table		Page
2-12	Recommended Enthalpy Values for TRU Elements and Alloy …..…….	A.2-28
2-13	Phase Transition temperatures and Enthalpy of Transitions of Uranium ...	A.2-29
2-14	Recommended Heat Capacity and Enthalpy of Uranium ……...…	A.2-33
2-15	Phase transition Temperatures and Enthalpy of Transitions of Curium ….	A.2-34
2-16	Recommended Heat Capacity and Enthalpy of Curium …….....	A.2-35
3-1	Vapor Pressure of Plutonium over Pu-Zr Alloys ……...…….	A.3-5
4-1	Crystal Structure and Phase Transitions of TRU and Zr Elements …….	A.4-1
5-1	Thermal Expansion Coefficient and Density of Zirconium [2] ……..……	A.5-6
5-2	Thermal Expansion Coefficient and Density of Plutonium [2] ……...	A.5-7
5-3	Thermal Expansion Coefficient and Density of Neptunium [3] …….....	A.5-8
5-4	Thermal Expansion Coefficient and Density of Zr-40Pu Alloy ……...….	A.5-10
7-1	Plutonium Self-diffusion Coefficient ……..	A.7-1
7-2	Diffusion of Actinides in Uranium Dioxide ……	A.7-2
7-3	Interdiffusion Coefficient of Pu Alloys ……...	A.7-3
7-4	Diffusion Coefficient in (ε-Pu,β-Zr) ……..……..……...……	A.7-5

Table		Page
7-5	Diffusion Coefficients of Pu and Zr in Pu-Zr alloys for the Pu Concentration Range of 20 –50 at% ……...…….…....	A.7-6
7-6	Interdiffusion Coefficient of Pu-Zr Alloys ……...…...……...	A.7-6
9-1	Creep Data for Zr-rich Zr-U Alloys ……...…….	A.9-4

Table of Contents

PART B Nitride Fuels

Section		Page
Preface		B-ii
Section 1	General	B.1-1
1.5	Unit Conversion	B.1-1
1.6	Fundamental Constants	B.1-3
1.7	Metal Element and Nitride Data	B.1-3
1.8	References for Section 1	B.1-5
Section 2	Heat Capacity	B.2-1
2.9	ZrN	B.2-1
2.10	PuN	B.2-1
2.11	(Pu,Zr)N	B.2-2
2.12	(TRU,Zr)N	B.2-2
2.13	References for Section 2	B.2-8
Section 3	Vapor Pressure	B.3-1
3.8	Vapor Pressures over PuN	B.3-1
3.9	Vapor Pressures over (Pu,Am)N	B.3-2
3.10	Vapor Pressures over NpN	B.3-6
3.11	Vapor Pressures over ZrN	B.3-6
3.12	References for Section 3	B.3-9
Section 4	Thermal Expansion and Density	B.4-1
4.1	Theory	B.4-1
4.2	ZrN	B.4-3
4.3	PuN	B.4-5

Section Page
4.4 (Pu,Zr)N B.4-9
4.5 (TRU,Zr)N B.4-10
4.6 References for Section 4 ..... B.4-13

Section 5 Thermal Conductivity B.5-1
5.1 ZrN B.5-1
5.2 PuN B.5-1
5.3 NpN B.5-4
5.4 (Pu,Zr)N B.5-4
5.5 (TRU,Zr)N B.5-6
5.6 Porosity Effect B.5-8
5.7 References for Section 5 ..... B.5-9

Section 6 Diffusion Coefficient B.6-1
6.1 Diffusion in ZrN B.6-1
6.2 Diffusion in (U,Pu)N B.6-1
6.3 Diffusion in (Pu,Zr)N B.6-3
6.4 Radiation Enhanced Diffusion in (pu,Zr)N B.6-3
6.5 References for Section 6 ..... B.6-4

Section 7 Elastic Constants B.7-1
7.1 Young's Modulus B.7-1
7.2 Poisson's Ratio B.7-5
7.3 References for Section 7 ..... B.7-7

Section 8 Creep B.8-1
8.1 Fully Dense (Pu,Zr)N B.8-1
8.2 Porosity correction B.8-1
8.3 Irradiation Effect B.8-2
8.4 References for Section 8 ..... B.8-3

Section Page

Section 9 Swelling ..…… B.9-1

9.1 Basic Swelling Correlation ..……..…..……... B.9-1

9.2 Swelling under External Stress ……..…..……..…. B.9-3

9.3 References for Section 9 ..……..……..……..……. B.9-6

Section 10 Gas Release ..……... B.10-1

10.1 Fission Gas Release Correlation ……...…….. B.10-1

10.2 References for Section 10 ..……. B.10-3

List of Figures

PART B Nitride Fuels

Figure		Page
2-1	Heat capacity of ZrN ……...……..…….……	B.2-4
2-2	Comparison of the heat capacity data of PuN in the literature ..……..…….	B.2-5
2-3	Comparison of the heat capacity of PuN, ZrN and (Pu,Zr)N …...…..……..	B.2-6
3-4	Vapor pressures over PuN …..……...….	B.3-4
3-5	Vapor pressures over PuN containing 0.0027 mol.% AmN [8]. N2 pressure over pure PuN by Eq.(1) is added for comparison ..……	B.3-5
3-6	Vapor pressures over ZrN. Data (symbols) and extrapolation to lower temperatures (lines) ….……..……...……..	B.3-8
4-1	Comparison of the linear thermal expansion coefficient of PuN in the literature ……...…....	B.4-7
4-2	Comparison of the linear thermal expansion coefficient of ZrN, PuN and $(Pu_{0.2}Zr_{0.8})N$ …..……...……...	B.4-12
5-1	Thermal conductivity of correlation of ZrN fitted to the data in the literature …….……..……...	B.5-2
5-2	Thermal conductivity correlation of PuN fitted to the data in the literature ……..	B.5-3

Figure Page

5-3 Comparison of thermal conductivities of UN, ZrN and PuN …….. B.5-5

5-4 Thermal conductivity of ZrN, PuN and (Pu,Zr)N solid solutions …….. B.5-7

6-1 Nitrogen diffusion coefficient in ZrN in the literature and recommended fit ……. B.6-2

7-1 Estimated Young's modulus of 100%TD ($Pu_{0.2}Zr_{0.8}$)N ……...……... B.7-3

9-1 Swelling of (Pu,Zr)N with and without external stress of 30 MPa ……..… B.9-5

10-1 Percent fission gas release from (Pu,Zr)N with 15% porosity ……..…….. B.10-2

List of Tables

PART B Nitride Fuels

Table		Page
1-1	Elemental Data ……...…….	B.1-3
1-2	Fundamental Constants ……...……	B.1-3
1-3	Metal Element Data and Nitride Data …….	B.1-4
2-1	Recommended Heat Capacity Values for PuN, ZrN and $(Pu_{0.2}Zr_{0.8})N$ …..	B.2-7
4-1	Thermal Expansion Coefficient and Density of ZrN ……..……	B.4-4
4-2	Thermal Expansion Coefficient and Density of PuN ……...……...	B.4-8
4-3	Thermal Expansion, Linea Thermal Expansion Coefficient and Density of $(Pu_{0.2}Zr_{0.8})N$ ……...…….....	B.4-11

PART A

Metal Alloy Fuels

PART A

Metal Alloy Fuels

Preface

PART A of this handbook is for metal alloy fuels.

The metal alloy of transuranic elements (i.e., Pu, Np, Am, Cm, etc) in Zr, designated as TRU-Zr, is one of the primary candidate fuel types for the AAA system.

The data found in the literature were critically reviewed and assessed to provide the recommended ones. For the convenience of the user, most of the materials properties are given in model correlations; performance models are also provided in mathematical formulas. Tabulations were made in case where these were judged to allow more flexibility for the user.

The information for the materials properties of the TRU-Zr alloy, however, is extremely scarce in general. Therefore, where no data exists, the values and models based on theoretical estimations and extrapolations from the U-Zr and U-Pu-Zr data are inevitably recommended. The justifications for this will be possible when sufficient measured data are available in the future. In this respect, this part is subject to modification whenever new data or better methods of deduction become available.

Section 1 General

1.1 Unit Conversion

Throughout this report the units in the SI (i.e., metric) system are preferentially used. Where more convenient, cgs units are also adopted. The following unit conversions are used. Any data given in English units are converted to the corresponding SI units.

1.1.1 Mass

1 lb = 0.45359 kg

1.1.2 Length

1 cm = 0.01 m
1 in. = 0.0254 m
1 ft = 0.3048 m

1.1.3 Temperature

The basic unit for temperature is the absolute temperature in Kelvin (K), which is related to the Celsius scale by

T (K) = T (^{o}C) +273.15

When a temperature is given in the other frequently appearing temperature scale, Fahrenheit (^{o}F), it is converted in Kelvin as follows:

$$T(K) = \frac{5}{9}\left[T(^{o}F) - 32\right] + 273.15$$

In the case where ^{o}F is involved in a unit conversion, however, it is transformed to K as follows:

$$K = \frac{5}{9}(^{o}F)$$

1.1.4 Pressure

Pascal is adopted as the basic unit for pressure. Pressure given in atm, bar, torr (mmHg) and psi (lb/in^2) is converted to Pa (i.e., N/m^2) as follows:

1 atm = 101325 Pa
1 atm = 760 torr
1 bar = 100,000 Pa
1 torr (mmHg) = 133.322 Pa
1 psi = 6895 Pa

1.1.5 Energy and Heat

Joule is the basic unit for energy and heat. Energy given in calorie is converted to joule by using the following unit conversion.

1 cal = 4.184 J
1 Btu = 1055 J
1 MeV = 1.602×10^{-13} J

1.1.6 Thermal Conductivity

1 Btu/hr-ft-^{o}F = 1.731 W/m-K
1 Cal/sec-cm-^{o}C = 418.7 W/m-K

1.2 Fundamental Constants

Table 1-1 Fundamental Constants

Symbol	Quantity	Value
R	Gas constant	8.314 J/mole-K
N_A	Avogadro's Number	6.02217×10^{23} mole^{-1}

1.3 Metal Element Data

Table 1-2 Metal Element Data [1–3]

Element	Atomic Number	Atomic mass [a]	Nominal density [b] (g/cm^3)
Zr	40	91.224	6.506
Pu	94	(242) [c]	19.840
Am	95	243.0614	13.670
Np	93	237.0482	20.250

a : based on ^{12}C=12.0000

b: at 293 K

c: mass number of the longest-lived isotope, Pu-242 [3]

1.4 References for Section 1

1. J.R. Lamarsh, Introduction to Nuclear Engineering, Addison-Wesley Pub. Co., Menlo Park, California (1983).
2. J. Emsley, The Elements, Clarendon Press, Oxford (1998).
3. N.N. Greenwood and A. Earnshaw , Chemistry of the Elements, 2nd edition, Butterworth, UK (1997).

Section 2 Enthalpy and Heat Capacity

2.1 Zirconium

2.1.1 Heat Capacity

Heat capacity data of Zr have been reviewed and compiled by Hultgren et al. [1], Pankratz [2], Hofman et al. [3], Barin [4], and Chase [5]. Hofman adopted Hultgren's data compilation. Barin and Chase data are the same because Barin adopted the Chase data. Kubaschewski et al. [6] recommended the heat capacity correlation formulated from the data of the earlier edition of JANAF data tables.

The $\alpha \leftrightarrow \beta$ phase transition temperature of Hultgren, Pankratz and Kubaschewski data sets is 1136 K while that of Barin and Chase data sets is 1135 K. The melting point is 2125 K for all data sets but 2128 K for Kubaschewski. For this work, the transition temperatures are taken after the Chase data. Therefore, the phase transition temperatures are 1135 K for the $\alpha \leftrightarrow \beta$ transition and 2125 K for the $\beta \leftrightarrow Liquid$ transition. The zirconium phase transition temperatures are tabulated in Table 2-1.

Table 2-1 Zirconium Phase Transition Temperatures (K)

Ref.	1,2	4,5	6	Suggested values
$\alpha - \beta$	1136	1135	1135	1135
$\beta - L$	2125	2125	2128	2125

Heat capacity data sets from Refs. 1 – 5 are compared in Fig.2-1. For α-Zr, Hultgren data and data by Pankratz are close to each other at the higher extreme and Chase data lie at the lower extreme. The Chase data are based on the data most recently reported. The recommended values for the phase are the average values of data reported by Pankratz, Kubaschewski, and Chase. The

values are tabulated in Table 2-2 and the heat capacity equation for the phase is obtained by fitting the recommended values for temperature range, $298.15 \le T \le 1135\ K$, as:

$$C_p(\alpha - Zr) = 22.839 + 9.091 \times 10^{-3}\ T - 2.132 \times 10^{4}\ T^{-2}$$

where C_p is in $J.K^{-1}.mole^{-1}$ and T in K.

For β-Zr, Pankratz data and Chase data are consistent with each other while Kubaschewski data are higher. The Hultgren data are constant with respect to temperature for the β-Zr phase, which is not supported by any further data. Therefore, the Hultgren data are rejected. The recommended values are the average values between Chase data and Pankratz data. The representing heat capacity equation is obtained by fitting the recommended values for the temperature range, $1135 \le T \le 2125\ K$, as:

$$C_p(\beta - Zr) = 12.885 + 9.976 \times 10^{-3}\ T + 5.158 \times 10^{6}\ T^{-2}$$

No data for liquid phase heat capacity of zirconium is available in the literature. Therefore, all of the values available in the data compilations are estimated ones. Liquid phase heat capacity is constant with respect to temperature for all three data sets. The values from all of the data sets are very close to each other except the Chase data, which are approximately 25% higher than the others. Therefore, the recommended values are obtained by averaging the values from all data sets except Chase data. Therefore, heat capacity for the temperature range, $2125\ K \le T$, is represented by

$$C_p(Liquid - Zr) = 33.471\ \text{J.K}^{-1}.\text{mole}^{-1}$$

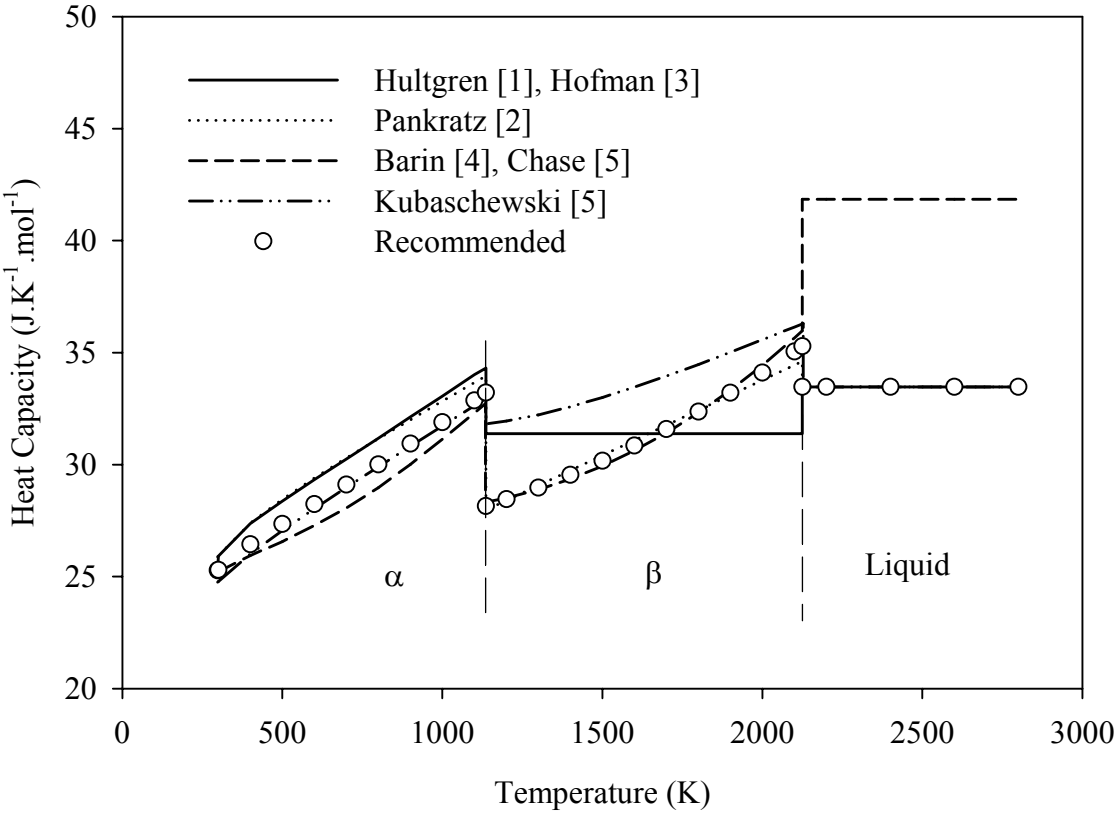

Fig.2-1 Heat capacity data of zirconium in the literature

2.1.2 Enthalpy

Enthalpy data for zirconium are available from Refs. 1, 2 and 5 and they are compared in Fig.2-2. Generally, the data are consistent for all Zr phases. Enthalpy values for the α-Zr phase are obtained by averaging Pankratz data and Chase data. The enthalpy for $298.15 \le T \le 1135\ K$ is formulated based on the recommended values as:

$$H - H_{298}(\alpha - Zr) = -7.341 + 2.340 \times 10^{-2}\ T + 4.160 \times 10^{-6}\ T^2,$$

where H is in kJ.mole^{-1} and T in K.

Enthalpy values for the β-Zr phase are also obtained by averaging Pankratz data and Chase data. The enthalpy equation for $1135 \le T \le 2125\ K$ is fitted to the recommended values as:

$$H - H_{298}(\beta - Zr) = 1.877 + 1.950 \times 10^{-2}\ T + 3.604 \times 10^{-6}\ T^2,$$

Similarly, the average values of Hultgran data and Pankratz data are selected for the enthalpy of liquid Zr. The ehthalpy equation for liquid Zr ($2125\ K \le T$) is

$$H - H_{298}(Liquid - Zr) = 8.146 + 3.350 \times 10^{-2}\ T.$$

The recommended values of enthalpy are tabulated in Table 2-2.

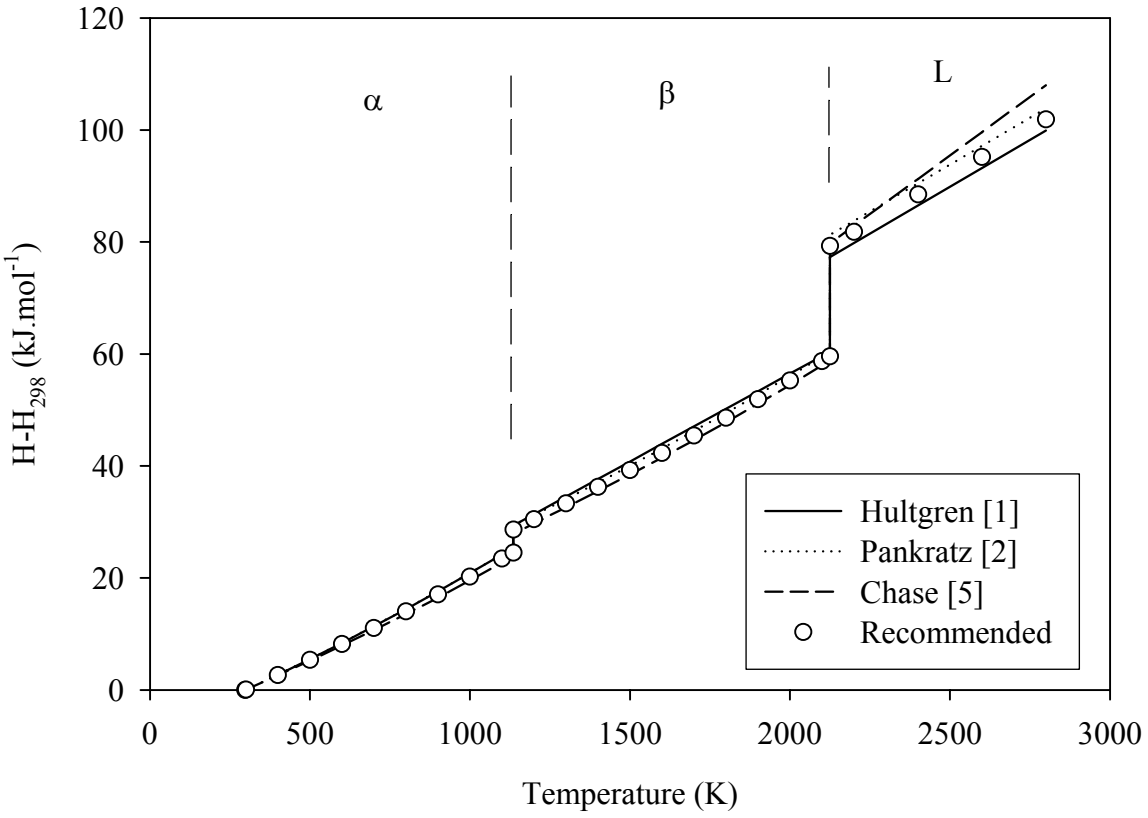

Fig.2-2 Enthalpy of zirconium in the literature

Table 2-2 Recommended Values of Heat Capacity and Enthalpy of Zirconium

T (K)	C_p ($J.K^{-1}.mole^{-1}$)	$H-H_{298}$ ($kJ.mole^{-1}$)
298.15	25.280	0.000
300	25.305	0.047
400	26.442	2.665
500	27.354	5.373
600	28.235	8.166
700	29.104	11.041
800	30.005	14.003
900	30.937	17.055
1000	31.893	20.204
1100	32.864	23.450
1135 (α)	33.209	24.493
1135 (β)	28.145	28.626
1200	28.452	30.451
1300	28.971	33.323
1400	29.544	36.247
1500	30.172	39.233
1600	30.850	42.284
1700	31.583	45.405
1800	32.368	48.602
1900	33.208	51.881
2000	34.101	55.246
2100	35.045	58.703
2125 (β)	35.289	59.581
2125 (L)	33.471	79.274
2200	33.471	81.785
2400	33.471	88.479
2600	33.471	95.173
2800	33.471	101.868

2.1.3 Phase transition enthalpy of zirconium

The enthalpies of phase transition are available from the literature. For the $\alpha \leftrightarrow \beta$ phase transition, $\Delta H_t(\alpha \leftrightarrow \beta) = 3.937$ kJ.mole^{-1} from Hultgren [1], 3.979 kJ.mole^{-1} from Pankratz [2], 4.017 kJ.mole^{-1} from Barin [4] and Chase [5], and 3.9 kJ.mole^{-1} from Kubaschewski [6]. The suggested value is by Chase.

For the $\beta \leftrightarrow L$ phase transition, the transition enthalpy is reported as $\Delta H_t(\beta \leftrightarrow L) = 16.90$ kJ.mole^{-1} from Hultgren [1], 18.8 kJ.mole^{-1} from Kubaschewski [6] and 20.92 kJ.mole^{-1} from Pankratz [2], Barin [4] and Chase [5]. The recommended value is taken from Chase.

The recommended values of transition enthalpies are given in Table 2-3.

Table 2-3 Enthalpies of Transitions of Zirconium (kJ.mole^{-1})

Ref.	$\Delta H_t(\alpha \leftrightarrow \beta)$	ΔH_m
1	3.937	16.90
2	3.979	20.92
4	4.017	20.92
5	4.017	20.92
6	3.9	18.8
Suggested values	4.017	20.92

2.2 Plutonium

2.2.1 Heat capacity

Plutonium has six allotropic forms between room temperature and its melting point, 913 K. The phase transition temperatures were changes as well as the heat capacity and enthalpy data. The phase transition temperatures are compared in Table 2-4.

Table 2-4 Plutonium Phase Transition Temperatures (K)

Ref.	1	7	8	9	Suggested values
$\alpha - \beta$	395	395 ± 4	397.6 ± 1.0	399.6 ± 0.6	397.6
$\beta - \gamma$	480	480 ± 5	487.9 ± 1.0	489.7 ± 0.9	487.9
$\gamma - \delta$	588	588 ± 3	593.1 ± 1.0	592.6 ± 0.2	593.1
$\delta - \delta'$	730	730 ± 2	736	NA	736
$\delta' - \varepsilon$	753	752 ± 4	755.7	NA	755.7
$\varepsilon - L$	913	913 ± 2	913	NA	913

NA: Not available

Heat capacity and enthalpy of pure plutonium can be found several places [1-4,7,8]. Barin [4] adopted Hultgren data [1]. Hultgren data were compiled from the original data available before 1965. Oetting [7] data were available in 1976. Pankratz [2] and Hofman [3] adopted Oetting data. Oetting and Adams [8] reported the more updated results in 1983.

As shown in Fig.2-3, the Hultgren and Oetting [7] are close except the α-phase. Oetting [8] is generally lower except the α-phase and liquid phases. In the liquid phase Oetting [7] and Oetting [8] are almost identical. For the present report, Oetting [8] data are selected. The data are tabulated in Table 2-5.

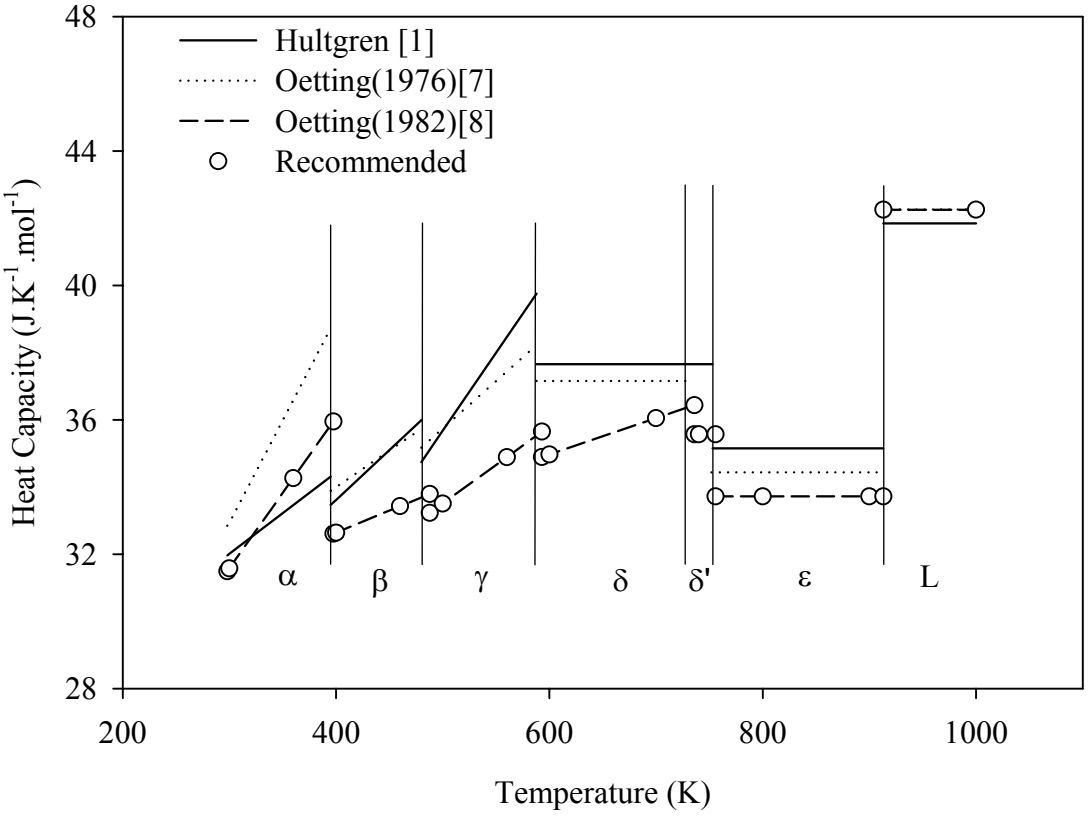

Fig.2-3 Comparison of Plutonium Heat Capacity from Hultgren [1], Oetting [7] and Oetting [8]

The heat capacity equations of plutonium are obtained by fitting the selected data as follows:

$$C_p(\alpha - Pu) = 18.126 + 4.482\times10^{-2}\,T \qquad (298.15 \le T \le 397.6\ K),$$

$$C_p(\beta - Pu) = 27.416 + 1.306\times10^{-2}\,T \qquad (397.6 \le T \le 487.9\ K),$$

$$C_p(\gamma - Pu) = 22.023 + 2.296\times10^{-2}\,T \qquad (487.9 \le T \le 593.1\ K),$$

$$C_p(\delta - Pu) = 28.478 + 1.081\times10^{-2}\,T \qquad (593.1 \le T \le 736\ K),$$

$$C_p(\delta' - Pu) = 35.560 \qquad (736 \le T \le 755.7\ K),$$

$$C_p(\varepsilon - Pu) = 33.720 \qquad (755.7 \le T \le 913\ K),$$

$$C_p(L - Pu) = 42.248 \qquad (913\ K \le T),$$

where heat capacity is given in $J.K^{-1}.mole^{-1}$ and T in K.

2.2.2 Enthalpy

A comparison of enthalpy data of plutonium is illustrated in Fig.2-4. The compared data sets are in good consistency. Oetting and Adams [8] is the most up-to-date data set and selected for the present report.

$$H - H_{298}(\alpha - Pu) = -7.396 + 1.812\times10^{-2}\,T + 2.241\times10^{-5}\,T^2 \quad (298.15 \le T \le 397.6\ K),$$

$$H - H_{298}(\beta - Pu) = -4.875 + 2.742\times10^{-2}\,T + 6.525\times10^{-6}\,T^2 \quad (397.6 \le T \le 487.9\ K),$$

$$H - H_{298}(\gamma - Pu) = -2.944 + 2.203\times10^{-2}\,T + 1.148\times10^{-5}\,T^2 \quad (487.9 \le T \le 593.1\ K),$$

$$H - H_{298}(\delta - Pu) = -3.921 + 2.848\times10^{-2}\,T + 5.403\times10^{-6}\,T^2 \quad (593.1 \le T \le 736\ K),$$

$$H - H_{298}(\delta' - Pu) = -2.937 + 2.702\times10^{-2}\,T + 5.726\times10^{-6}\,T^2 \quad (736 \le T \le 755.7\ K),$$

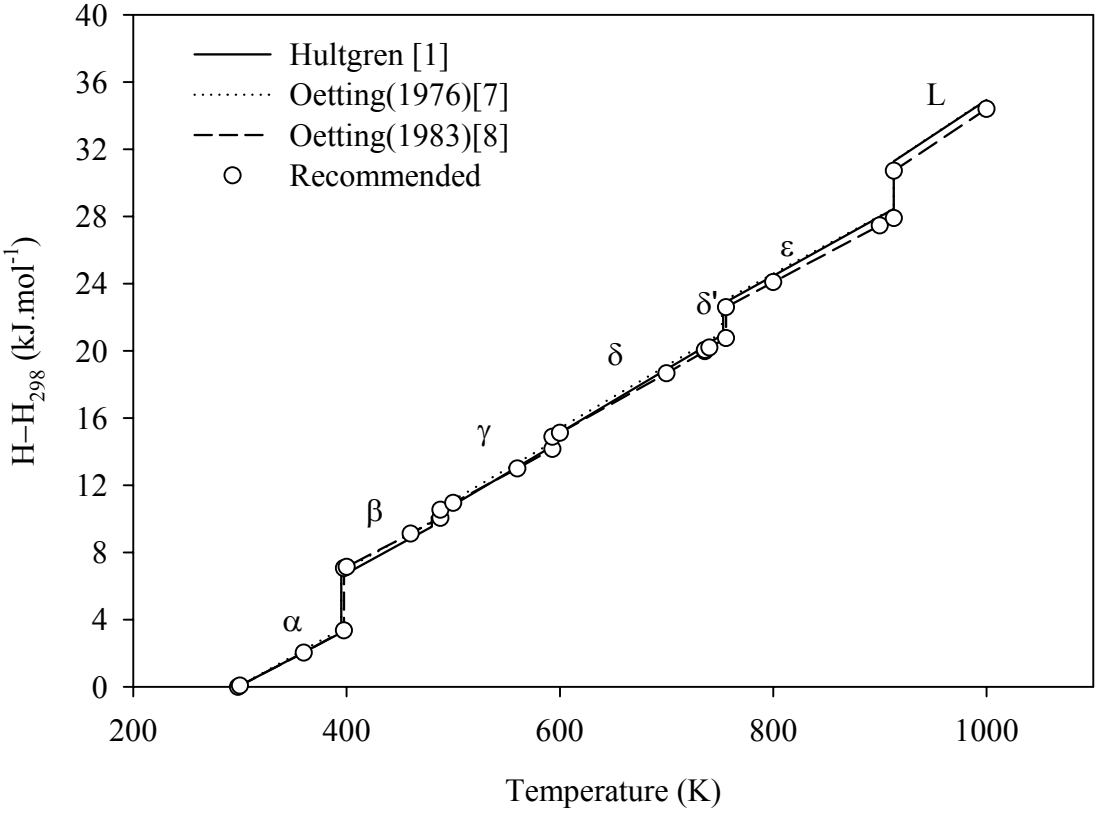

Fig.2-4 Comparison of Enthalpy of Plutonium from Hultgren [1], Oetting [7] and Oetting [8]

Table 2-5 Recommended Values of Heat Capacity and Enthalpy of Plutonium

T (K)	C_p ($J.K^{-1}.mole^{-1}$)	$H–H_{298}$ ($kJ.mole^{-1}$)
298.15	31.489	0.000
300	31.572	0.058
360	34.261	2.033
397.6 (α)	35.946	3.353
397.6 (β)	32.609	7.059
400	32.640	7.138
460	33.424	9.119
487.9 (β)	33.788	10.057
487.9 (γ)	33.225	10.535
500	33.503	10.939
560	34.880	12.990
593.1 (γ)	35.640	14.157
593.1 (δ)	34.888	14.870
600	34.962	15.111
700	36.043	18.662
736 (δ)	36.432	19.966
736 (δ′)	35.560	20.050
740	35.560	20.192
755.7 (δ′)	35.560	20.751
755.7 (ε)	33.720	22.592
800	33.720	24.085
900	33.720	27.458
913 (ε)	33.720	27.896
913 (L)	42.248	30.720
1000	42.248	34.395
1200	(42.248)*	(42.843)
1400	(42.248)	(51.293)
1600	(42.248)	(59.743)
1800	(42.248)	(68.193)
2000	(42.248)	(76.643)
2200	(42.248)	(85.093)
2400	(42.248)	(93.543)
2600	(42.248)	(101.993)

* Values in parentheses are extrapolated ones.

$$H - H_{298}(\varepsilon - Pu) = -2.891 + 3.372 \times 10^{-2}\, T \quad (755.7 \le T \le 913\ K),$$

$$H - H_{298}(L - Pu) = -7.857 + 4.225 \times 10^{-2}\, T \quad (913\ K \le T),$$

where enthalpies are given in kJ.mole^{-1} and T in K. The recommended values of enthalpy of plutonium are tabulated in Table 2-5.

2.2.3 Phase transition enthalpy and enthalpy of fusion

The data of the phase transition temperatures and enthalpies of transitions prior to 1976 are summarized in Ref.7. Two more new data has been added on these subjects [8,9]. The data from the literature and suggested values are found in Table.2-6.

Table 2-6 Enthalpies of Transitions of Plutonium (kJ.mole^{-1})

Ref.	$\alpha - \beta$	$\beta - \gamma$	$\gamma - \delta$	$\delta - \delta'$	$\delta' - \varepsilon$	$\varepsilon - L$
7	3.43 ± 0.08	0.57 ± 0.06	0.59 ± 0.06	0.08 ± 0.04	1.84 ± 0.08	2.82 ± 0.11
8	3.71 ± 0.00	0.48 ± 0.01	0.71 ± 0.01			
9	3.50 ± 0.14	0.49 ± 0.04	0.66 ± 0.03			
*	3.71 ± 0.00	0.48 ± 0.01	0.71 ± 0.01	0.08 ± 0.04	1.84 ± 0.08	2.82 ± 0.11

* Suggested values

2.3 Americium

2.3.1 Phase transition temperatures enthalpy of transitions

Americium has three allotropic forms. The transition temperatures and enthalpies of transitions are taken from Ref.7 and tabulated in Table 2-7.

Table 2-7 Phase Transition Temperatures and Enthalpies of Transitions of Americium

Transition	T (K)	ΔH_t (kJ.mole^{-1})
$\alpha - \beta$	923	0.774
$\beta - \gamma$	1350	5.858
$\gamma - L$	1449	14.393

2.3.2 Heat capacity

There is only one set of heat capacity data of americium in the literature [7]. The heat capacity equations are found in Ref.7 as follows:

$$C_p(\alpha - Am) = 22.150 + 1.206\times10^{-2}\,T + 1.138\times10^{-6}\,T^2 \quad (298 \le T \le 923\ K),$$

$$C_p(\beta - Am) = 21.746 + 8.206\times10^{-3}\,T + 3.093\times10^{-6}\,T^2 \quad (923 \le T \le 1350\ K),$$

$$C_p(\gamma - Am) = 39.748 \quad (1350 \le T \le 1449\ K),$$

$$C_p(L - Am) = 41.840 \quad (1449\ K \le T),$$

where heat capacity is given in J.K^{-1}.mole^{-1} and T in K. The values computed by the equations are given in Table 2-8 and plotted in Fig.2-5.

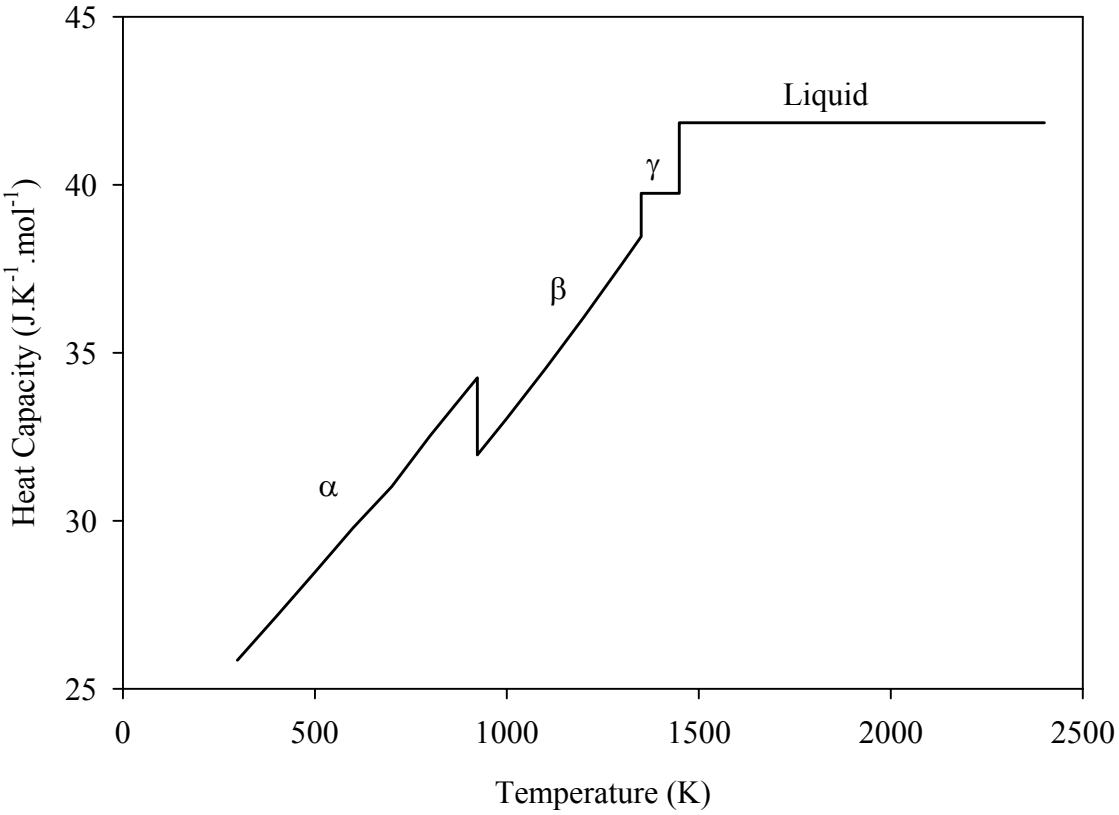

Fig.2-5 Heat capacity of americium taken from Ref.7

2.3.3 Enthalpy

Enthalpy equations are obtained by fitting the data of Ref.7 as follows:

$$H - H_{298}(\alpha - Am) = -7.079 + 2.175\times10^{-2}\,T + 6.733\times10^{-6}\,T^2 \quad (298 \le T \le 923\ K),$$

$$H - H_{298}(\beta - Am) = -3.416 + 1.781\times10^{-2}\,T + 7.608\times10^{-6}\,T^2 \quad (923 \le T \le 1350\ K),$$

$$H - H_{298}(\gamma - Am) = -13.004 + 3.932\times10^{-2}\,T + 1.525\times10^{-7}\,T^2 \quad (1350 \le T \le 1449\ K),$$

$$H - H_{298}(L - Am) = -1.941 + 4.184\times10^{-2}\,T \quad (1449\ K \le T),$$

where enthalpy is in kJ.mole^{-1} and T in K. Enthalpies as a function of temperatures are shown in Fig.2-6.

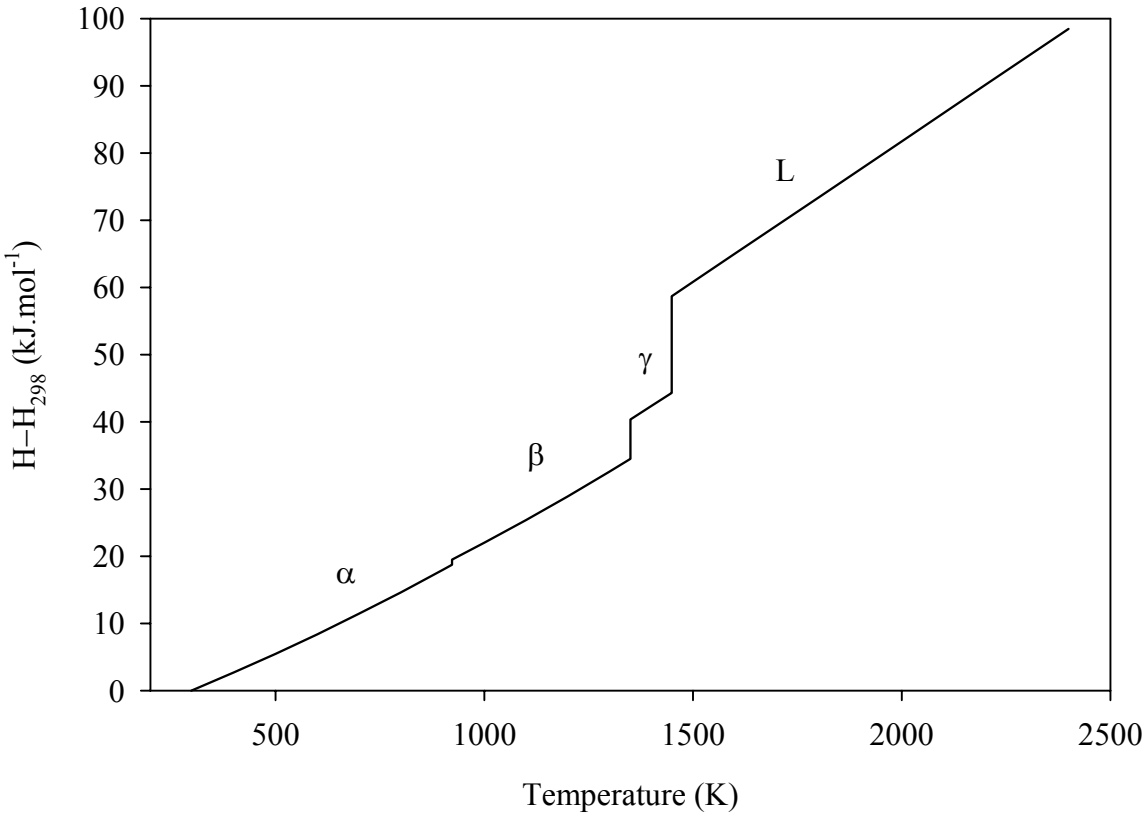

Fig.2-6 Enthalpy of americium from Ref.7

Table 2-8 Recommended Heat Capacity and Enthalpy of Americium

T (K)	C_p ($J.K^{-1}.mole^{-1}$)	$H–H_{298}$ ($kJ.mole^{-1}$)
298	25.848	0.000
300	25.872	0.048
400	27.158	2.699
500	28.467	5.480
600	29.798	8.393
700	31.015	11.441
800	32.530	14.624
900	33.930	17.947
923 (α)	34.255	18.731
923 (β)	31.955	19.505
1000	33.045	22.008
1100	34.515	25.385
1200	36.047	28.913
1300	37.641	32.597
1350 (β)	38.461	34.499
1350 (γ)	39.748	40.357
1400	39.748	42.344
1449 (γ)	39.748	44.292
1449 (L)	41.840	58.685
1500	41.840	60.819
1600	41.840	65.003
1800	41.840	73.371
2000	41.840	81.739
2200	41.840	90.107
2400	41.840	98.475

2.4 Neptunium

2.4.1 Phase transition enthalpy and heat of fusion

Like americium neptunium has three allotropic forms. The transition temperatures and enthalpies of transitions are taken from Ref.7 and tabulated in Table 2-9.

Table 2-9 Phase Transition Temperatures and Enthalpies of Transitions of Neptunium

Transition	T (K)	ΔH_t (kJ.mole^{-1})
$\alpha - \beta$	553	5.607
$\beta - \gamma$	849	5.272
$\gamma - L$	912	5.188

2.4.2 Heat capacity

The heat capacity equations are found in Ref.7 as follows:

$$C_p(\alpha - Np) = -4.054 + 8.255\times10^{-2}\,T + 8.058\times10^{5}\,T^{-2} \quad (298 \le T \le 553\ K),$$

$$C_p(\beta - Np) = 39.330 \quad (553 \le T \le 849\ K),$$

$$C_p(\gamma - Np) = 36.401 \quad (849 \le T \le 912\ K),$$

$$C_p(L - Np) = 45.396 \quad (912\ K \le T),$$

where heat capacity is given in J.K^{-1}.mole^{-1} and T in K. The values computed by the equations are given in Table 2-10 and plotted in Fig.2-7.

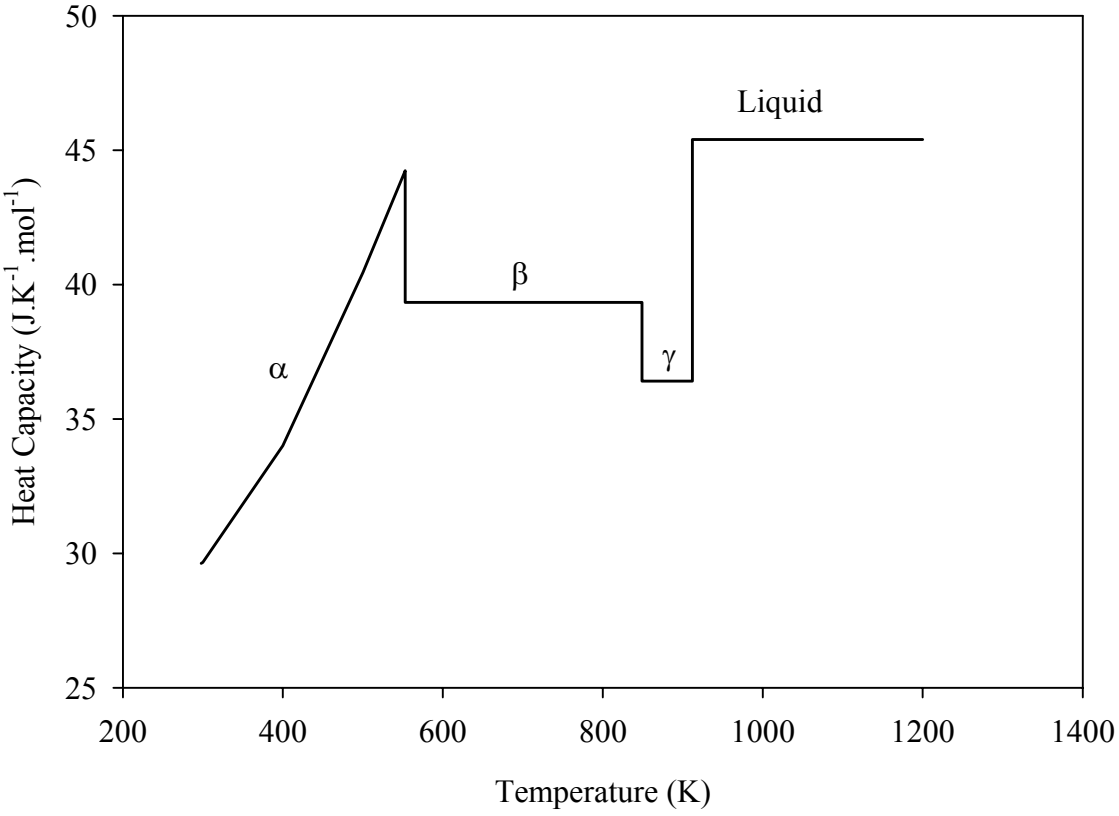

Fig.2-7 Heat capacity of neptunium taken from Ref.7

2.4.3 Enthalpy

Enthalpy equations are obtained by fitting the data of Ref.7 as follows:

$$H - H_{298}(\alpha - Np) = -5.806 + 1.063\times10^{-2}\,T + 2.971\times10^{-5}\,T^2 \quad (298 \le T \le 553\ K),$$

$$H - H_{298}(\beta - Np) = -6.986 + 3.936\times10^{-2}\,T - 1.743\times10^{-8}\,T^2 \quad (553 \le T \le 849\ K),$$

$$H - H_{298}(\gamma - Np) = 1.086 + 3.571\times10^{-2}\,T + 3.890\times10^{-7}\,T^2 \quad (849 \le T \le 912\ K),$$

$$H - H_{298}(L - Np) = -2.234 + 4.540\times10^{-2}\,T \quad (912\ K \le T),$$

where enthalpy is in kJ.mole^{-1} and T in K. Enthalpies as a function of temperatures are shown in Fig.2-8.

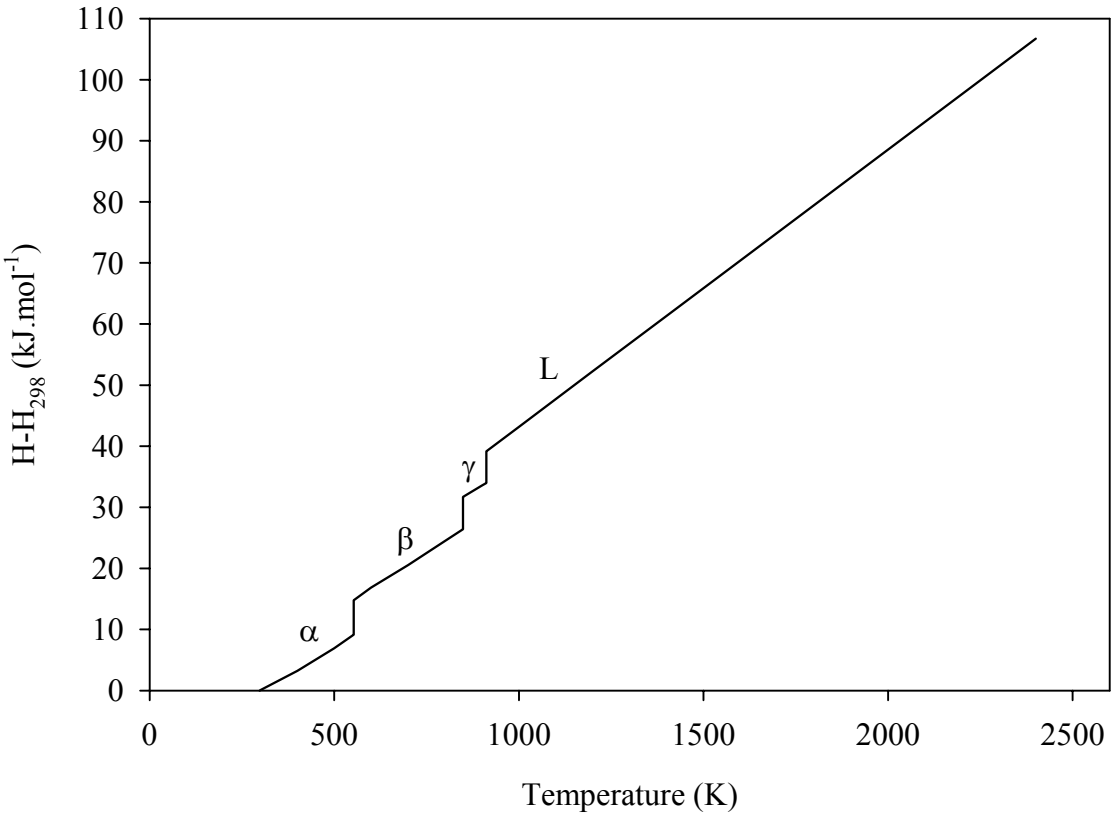

Fig.2-8 Enthalpy of neptunium from Ref.7

Table 2-10 Recommended Heat Capacity and Enthalpy of Neptunium

T (K)	C_p ($J.K^{-1}.mole^{-1}$)	$H–H_{298}$ ($kJ.mole^{-1}$)
298	29.623	0.000
300	29.664	0.055
400	34.003	3.210
500	40.446	6.923
553 (α)	44.233	9.166
553 (β)	39.330	14.772
600	39.330	16.853
700	39.330	20.554
800	39.330	24.487
849 (β)	39.330	26.414
849 (γ)	36.401	31.686
900	36.401	33.542
912 (γ)	36.401	33.979
912 (L)	45.396	39.167
1000	45.396	43.162
1200	45.396	52.241
1400	45.396	61.321
1600	45.396	70.400
1800	45.396	79.479
2000	45.396	88.558
2200	45.396	97.638
2400	45.396	106.717

2.5 Zr-Pu-Am-Np Alloy

No experimental data for heat capacity and enthalpy of Zr-Pu-Am-Np alloys is available at the present time. A theoretical estimation is necessary. The most accepted model is known as the Kopp-Neumann law [10]. According to this law, the specific heat of an alloy is equal to the sum of the products of the atomic fraction of the constituent elements and their atomic specific heat, i.e.,

$$C_p = \sum_{i=1}^{n} a_i \, C_{p,i}$$

where a_i is the atomic fraction and $C_{p,i}$ is the specific heat of the i-th element. The Zr concentration in weight percent is converted to atomic fraction by

$$C_{Zr} = \frac{M_{TRU} w_{Zr}}{M_{Zr} + (M_{TRU} - M_{Zr}) w_{Zr}},$$

where C is the atom fraction, M is the atomic mass, and w is the weight fraction. The TRU mass is approximately the average of the involving TRU elements. Consequently, the concentrations in atom fraction of each TRU element are obtained approximately as

$$C_i = \frac{w_i}{\sum w_i}\left(1 - C_{Zr}\right).$$

As an example, heat capacity and enthalpy of Zr (60 wt%) + Pu (34 wt%) + Am (4 wt%) + Np (2 wt%) alloy are estimated as follows:

$$C_{p,TRU-Zr} = 0.8\,C_{p,Zr} + 0.17\,C_{p,Pu} + 0.02\,C_{p,Am} + 0.01\,C_{p,Np},$$

$$[H - H_{298}]_{TRU-Zr} = 0.8[H - H_{298}]_{Zr} + 0.17[H - H_{298}]_{Pu} + 0.02[H - H_{298}]_{Am} + 0.01[H - H_{298}]_{Np}$$

where the coefficient in front of each term is the atomic fraction of the element.

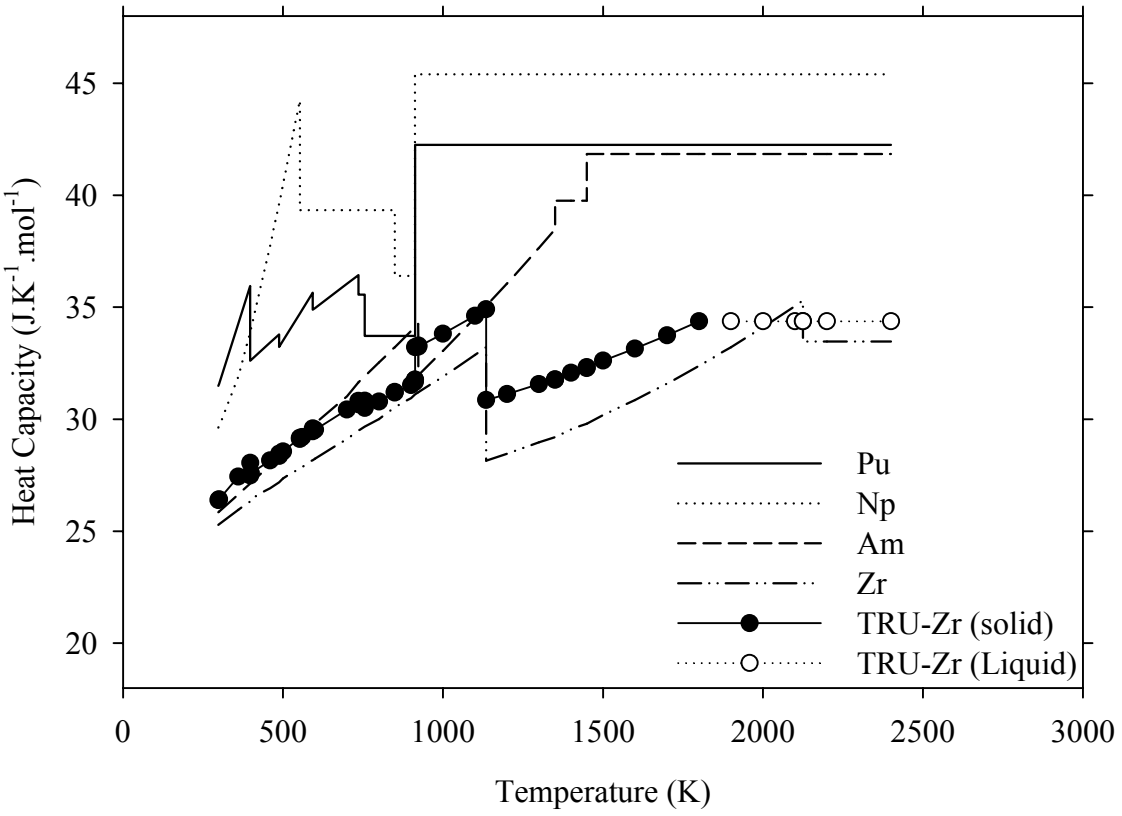

Fig.2-9 Comparison of TRU element heat capacities and estimated heat capacity of 60 wt%(Zr)+34 wt%(Pu)+4 wt%(Am)+2 wt%(Np)

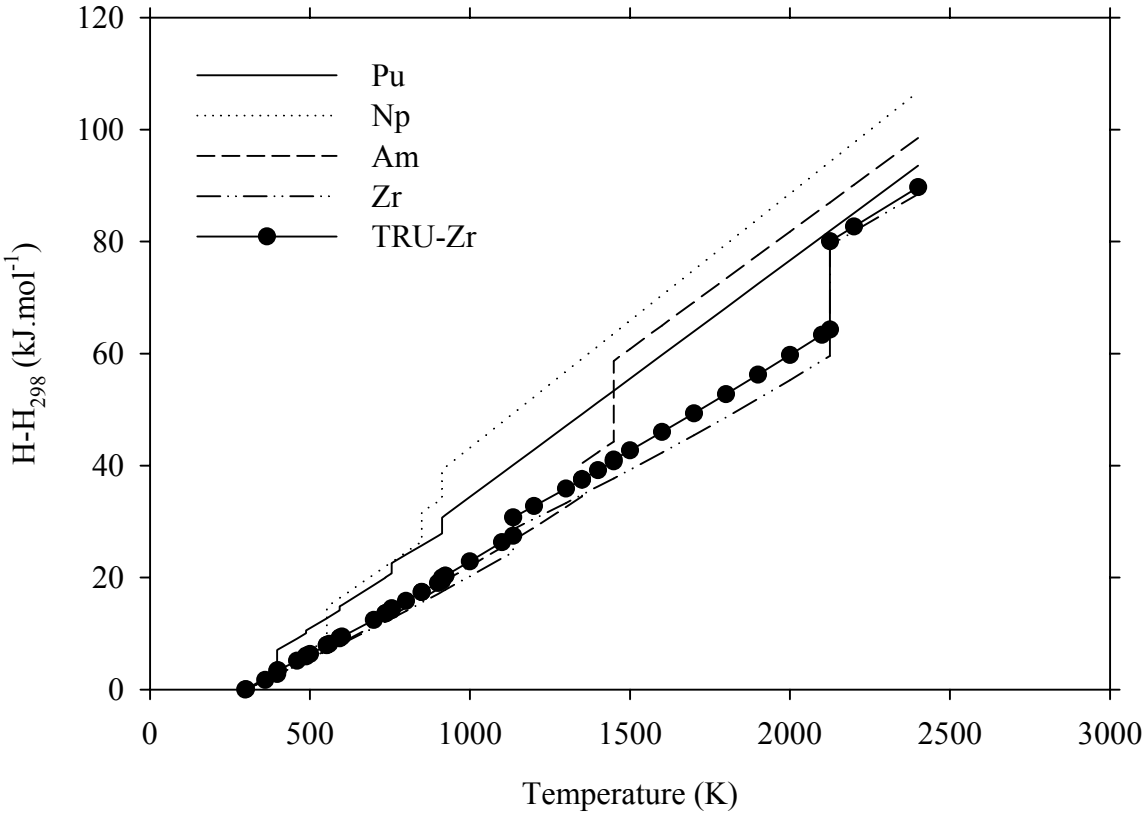

Fig.2-10 Comparison of TRU-Zr element enthalpies and estimated enthalpy of 60 wt%(Zr) + 34 wt%(Pu) + 4 wt%(Am) + 2 wt%(Np)

Table 2-11 Recommended Heat Capacity Values for TRU Elements and Alloy

Temperature (K)	Zr ($J.K^{-1}.mole^{-1}$)	Pu ($J.K^{-1}.mole^{-1}$)	Am ($J.K^{-1}.mole^{-1}$)	Np ($J.K^{-1}.mole^{-1}$)	TRU Alloy ($J.K^{-1}.mole^{-1}$)
298.15	25.280	31.489	25.848	29.623	26.390
300	25.305	31.572	25.872	29.664	26.425
397.6	26.320	35.946	27.125	33.865	28.048
397.6	26.320	32.609	27.125	33.865	27.480
400	26.442	32.640	27.158	34.003	27.585
460	26.921	33.424	27.938	37.727	28.155
487.9	27.186	33.788	28.305	39.607	28.455
487.9	27.186	33.225	28.305	39.607	28.359
500	27.354	33.503	28.467	40.446	28.553
553	27.798	34.720	29.167	44.233	29.166
553	27.798	34.720	29.167	39.330	29.117
560	27.863	34.880	29.260	39.330	29.199
593.1	28.171	35.640	29.703	39.330	29.583
593.1	28.171	34.888	29.703	39.330	29.455
600	28.235	34.962	29.798	39.330	29.521
700	29.104	36.043	31.015	39.330	30.424
736	29.492	36.432	31.643	39.330	30.813
736	29.492	35.560	31.643	39.330	30.665
740	29.528	35.560	31.698	39.330	30.695
755.7	29.673	35.560	31.914	39.330	30.815
755.7	29.673	33.720	31.914	39.330	30.502
800	30.005	33.720	32.530	39.330	30.780
849	30.529	33.720	33.209	39.330	31.213
849	30.529	33.720	33.209	36.401	31.184
900	30.937	33.720	33.930	36.401	31.524
912	31.105	33.720	34.095	36.401	31.663
912	31.105	33.720	34.095	45.396	31.753
913	31.114	33.720	34.095	45.396	31.759
913	31.114	42.248	34.095	45.396	33.209
923	31.206	42.248	34.255	45.396	33.286
923	31.206	42.248	31.955	45.396	33.240
1000	31.893	42.248	33.045	45.396	33.811
1100	32.864	42.248	34.515	45.396	34.618
1135	33.209	42.248	35.044	45.396	34.905
1135	28.145	42.248	35.044	45.396	30.853
1200	28.452	42.248	36.047	45.396	31.119
1300	28.971	42.248	37.641	45.396	31.565
1350	29.188	42.248	38.461	45.396	31.756
1350	29.188	42.248	39.748	45.396	31.781
1400	29.544	42.248	39.748	45.396	32.067
1449	29.802	42.248	39.748	45.396	32.273
1449	29.802	42.248	41.840	45.396	32.314
1500	30.172	42.248	41.840	45.396	32.610
1600	30.850	42.248	41.840	45.396	33.153
1700	31.583	42.248	41.840	45.396	33.739
1800	32.368	42.248	41.840	45.396	(34.367)*
1900	33.208	42.248	41.840	45.396	(34.367)
2000	34.101	42.248	41.840	45.396	(34.367)
2100	35.045	42.248	41.840	45.396	(34.367)
2125	35.289	42.248	41.840	45.396	(34.367)
2125	33.471	42.248	41.840	45.396	(34.367)
2200	33.471	42.248	41.840	45.396	(34.367)

* Values in parentheses are estimated ones.

Table 2-12 Recommended Enthalpy Values for TRU Elements and Alloy

Temperature (K)	Zr ($J.K^{-1}.mole^{-1}$)	Pu ($J.K^{-1}.mole^{-1}$)	Am ($J.K^{-1}.mole^{-1}$)	Np ($J.K^{-1}.mole^{-1}$)	TRU Alloy ($J.K^{-1}.mole^{-1}$)
298.15	0.000	0.000	0.000	0.000	0.000
300	0.047	0.058	0.048	0.055	0.049
397.6	2.620	3.353	2.633	3.117	2.750
397.6	2.620	7.059	2.633	3.117	3.380
400	2.665	7.138	2.699	3.210	3.431
460	4.303	9.119	4.351	5.370	5.134
487.9	5.066	10.057	5.136	6.453	5.930
487.9	5.066	10.535	5.136	6.453	6.011
500	5.373	10.939	5.480	6.923	6.337
553	6.871	12.749	7.008	9.166	7.896
553	6.871	12.749	7.008	14.772	7.952
560	7.068	12.990	7.212	15.050	8.157
593.1	8.001	14.157	8.189	16.352	9.135
593.1	8.001	14.870	8.189	16.352	9.256
600	8.166	15.111	8.393	16.621	9.436
700	11.041	18.662	11.441	20.554	12.440
736	12.135	19.966	12.576	21.974	13.573
736	12.135	20.050	12.576	21.974	13.588
740	12.253	20.192	12.703	22.131	13.710
755.7	12.718	20.751	13.203	22.748	14.194
755.7	12.718	22.592	13.203	22.748	14.507
800	14.003	24.085	14.624	24.487	15.834
849	15.524	25.737	16.240	26.414	17.384
849	15.524	25.737	16.240	31.686	17.436
900	17.055	27.458	17.947	33.542	19.006
912	17.460	27.862	18.357	33.979	19.411
912	17.460	27.862	18.357	39.167	19.463
913	17.491	27.896	18.391	39.216	19.495
913	17.491	30.720	18.391	39.216	19.975
923	17.801	31.140	18.731	39.670	20.306
923	17.801	31.140	19.505	39.670	20.322
1000	20.204	34.395	22.008	43.162	22.882
1100	23.450	38.618	25.385	47.706	26.310
1135	24.493	40.097	26.599	49.295	27.436
1135	28.626	40.097	26.599	49.295	30.742
1200	30.451	42.843	28.913	52.241	32.745
1300	33.323	47.068	32.597	56.786	35.880
1350	34.770	49.181	34.499	59.056	37.457
1350	34.770	49.181	40.357	59.056	37.575
1400	36.247	51.293	42.344	61.321	39.177
1449	37.699	53.363	44.292	63.551	40.753
1449	37.699	53.363	58.685	63.551	41.041
1500	39.233	55.518	60.819	65.866	42.699
1600	42.284	59.743	65.003	70.400	45.987
1700	45.405	63.968	69.187	74.946	49.332
1800	48.602	68.193	73.371	79.479	52.737
1900	51.881	72.418	77.555	84.026	56.207
2000	55.246	76.643	81.739	88.558	59.747
2100	58.703	80.868	85.923	93.106	63.359
2125	59.581	81.924	86.969	94.241	64.274
2125	79.274	81.924	86.969	94.241	80.028
2200	81.785	85.093	90.107	97.638	82.672
2400	88.479	93.543	98.475	106.717	89.722

The values obtained by this method are compared with those of the constituent elements in Figs.2-9 and 2-10.

As presented in Tables 2-11 and 2-12, all of the elemental phase transition temperatures from room to melting temperatures are included for other TRU-Zr alloy compositions as well as for the present estimation. For example, the first transition temperature takes place at 397.6 K because of Pu. Only Pu has a transition at this temperature, but the values for Zr, Am and Np are also included.

The melting temperature of the TRU-Zr alloy is not known. Therefore, the estimated values of the heat capacity of the TRU-Zr alloy above the solidus temperature of 60 wt%(Zr) + 40 wt% (Pu) is given in Table 2-11 and plotted in Fig.2-9.

2.6 Uranium

2.6.1 Phase transition enthalpy and heat of fusion

The transition temperatures and enthalpies of transitions are taken from Ref.7 and tabulated in Table 2 -13.

Table 2-13 Phase Transition Temperatures and Enthalpies of Transitions of Uranium

Transition	T (K)	ΔH_t (kJ.mole^{-1})
$\alpha - \beta$	942	2.791
$\beta - \gamma$	1049	4.757
$\gamma - L$	1408	9.142

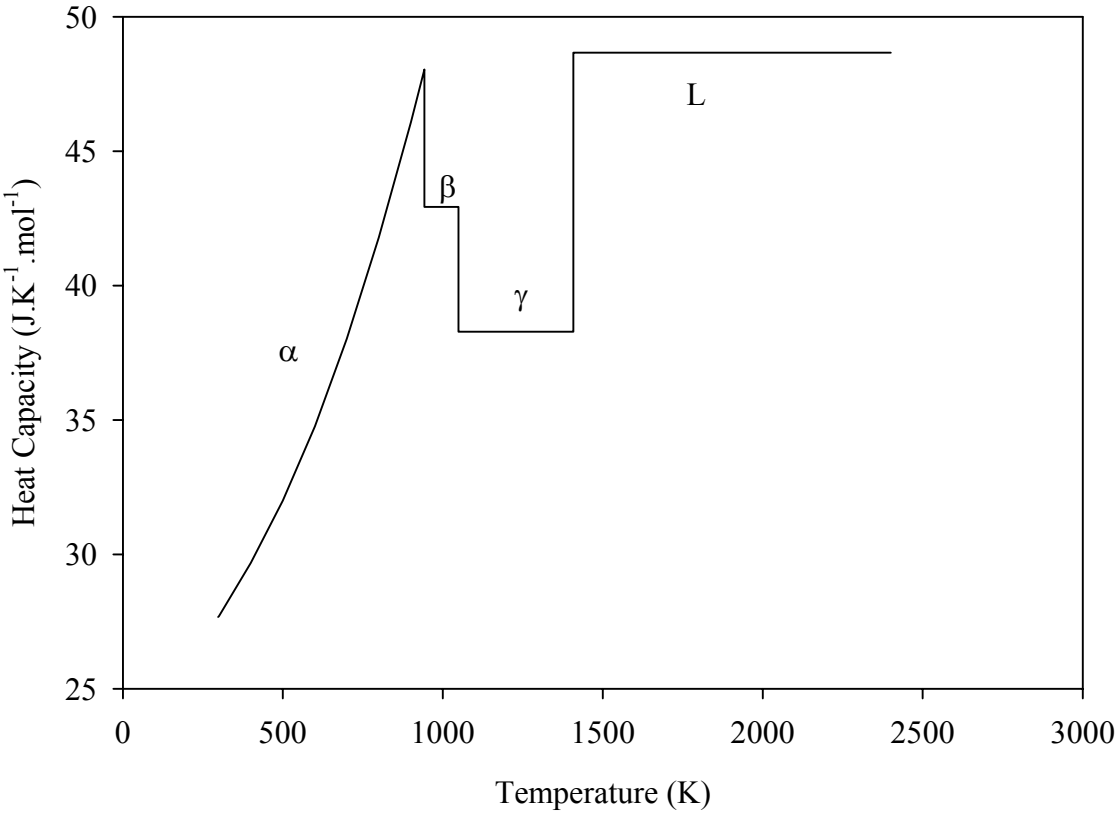

Fig.2-11 Uranium metal heat capacity taken from Ref.7

2.6.2 Heat capacity

The heat capacity data are found in Ref.7. The data are fitted to equations as follows:

$$C_p(\alpha - U) = 24.959 + 2.132\times10^{-3}\,T + 2.370\times10^{-5}\,T^2 \quad (298 \le T \le 942\ K),$$

$$C_p(\beta - U) = 42.928 \quad (942 \le T \le 1049\ K),$$

$$C_p(\gamma - U) = 38.284 \quad (1049 \le T \le 1408\ K),$$

$$C_p(L - U) = 48.660 \quad (1408\ K \le T),$$

where heat capacity is given in $J.K^{-1}.mole^{-1}$ and T in K. The values computed by the equations are given in Table 2-14 and plotted in Fig.2-11.

2.6.3 Enthalpy

Enthalpy equations are obtained by fitting the data of Ref.7 as follows:

$$H - H_{298}(\alpha - U) = -6.354 + 1.681\times10^{-2}\,T + 1.553\times10^{-5}\,T^2 \quad (298 \le T \le 942\ K),$$

$$H - H_{298}(\beta - U) = -14.324 + 4.292\times10^{-2}\,T \quad (942 \le T \le 1049\ K),$$

$$H - H_{298}(\gamma - U) = -4.698 + 3.828\times10^{-2}\,T \quad (1049 \le T \le 1408\ K),$$

$$H - H_{298}(L - U) = -10.166 + 4.866\times10^{-2}\,T \quad (1408K \le T),$$

where enthalpy is in $kJ.mole^{-1}$ and T in K. Uranium metal enthalpy is plotted in Fig.2-12.

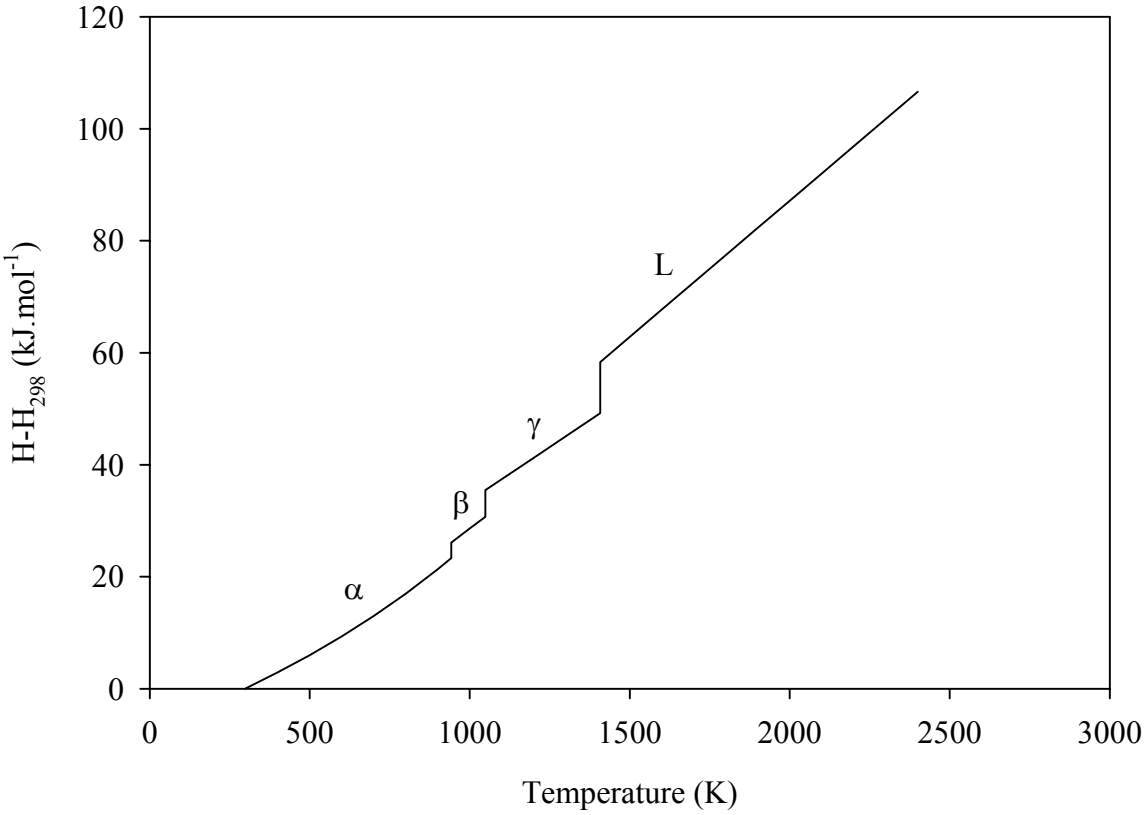

Fig.2-12 Uranium metal enthaly taken from Ref.7

Table 2-14 Recommended Heat Capacity and Enthalpy of Uranium

T (K)	C_p ($J.K^{-1}.mole^{-1}$)	$H–H_{298}$ ($kJ.mole^{-1}$)
298	27.665	0.000
300	27.700	0.051
400	29.684	2.919
500	31.997	5.999
600	34.762	9.333
700	38.021	12.968
800	41.791	16.955
900	46.081	21.344
942 (α)	48.038	23.320
942 (β)	42.928	26.111
1000	42.928	28.600
1049 (β)	42.928	30.704
1049 (γ)	38.284	35.461
1100	38.284	37.414
1200	38.284	41.242
1300	38.284	45.070
1400	38.284	48.899
1408 (γ)	38.284	49.205
1408 (L)	48.660	58.347
1500	48.660	62.824
1600	48.660	67.690
1700	48.660	72.556
1800	48.660	77.422
1900	48.660	82.288
2000	48.660	87.154
2100	48.660	92.020
2200	48.660	96.886
2400	48.660	106.618

2.7 Curium

2.7.1 Phase transition enthalpy and heat of fusion

The transition temperatures and enthalpies of transitions are taken from Ref.7 and tabulated in Table 2-15.

Table 2-15 Phase Transition Temperatures and Enthalpies of Transitions of Curium

Transition	T (K)	ΔH_t (kJ.mole^{-1})
$\alpha - \beta$	1550	3.243
$\beta - L$	1618	14.644

2.7.2 Heat capacity

The heat capacity data are found in Ref.7. The data are fitted to equations as follows:

$$C_p(\alpha - Cm) = 25.104 + 8.661 \times 10^{-3}\, T \quad (298 \le T \le 1550\ K),$$

$$C_p(\beta - Cm) = 33.472 \quad (1550 \le T \le 1618\ K),$$

$$C_p(L - Cm) = 40.166 \quad (1618\ K \le T),$$

where heat capacity is given in J.K^{-1}.mole^{-1} and T in K. The values computed by the equations are given in Table 2-16.

2.7.3 Enthalpy

Enthalpy equations are obtained by fitting the data of Ref.7 as follows:

$$H - H_{298}(\alpha - Cm) = -7.867 + 2.510\times10^{-2}\,T + 4.332\times10^{-6}\,T^2 \quad (298 \le T \le 1550\ K),$$

$$H - H_{298}(\beta - Cm) = -7.194 + 3.347\times10^{-2}\,T \quad (1550 \le T \le 1618\ K),$$

$$H - H_{298}(L - Cm) = -3.381 + 4.017\times10^{-2}\,T \quad (1618\ K \le T).$$

Table 2-16 Recommended Heat Capacity and Enthalpy of Curium

T (K)	C_p ($J.K^{-1}.mole^{-1}$)	$H-H_{298}$ ($kJ.mole^{-1}$)
298	27.686	0.000
300	27.702	0.051
400	28.568	2.865
500	29.434	5.765
600	30.301	8.752
700	31.167	11.825
800	32.033	14.985
900	32.899	18.232
1000	33.765	21.565
1100	34.631	24.985
1200	35.497	28.491
1300	36.363	32.084
1400	37.229	35.764
1500	38.095	39.530
1550 (α)	38.528	41.445
1550 (β)	33.472	44.688
1600	33.472	46.362
1618 (β)	33.472	46.964
1618 (L)	40.166	61.608
1700	40.166	64.902
1800	40.166	68.918
1900	40.166	72.935
2000	40.166	76.952
2100	40.166	80.968
2200	40.166	84.985
2400	40.166	93.018

2.8 References for Section 2

1. R. Hultgren, P.D. Desai, D.T. Hawkins, et al., Selected Values of the Thermodynamic Properties of the Elements, American Society of metals, Metals Park, Ohio (1973).
2. L.B. Pankratz, Thermodynamic Properties of Elements and Oxides, US Bureau of Mines, Bulletin 672, Washington D.C. (1982).
3. G.L. Hofman, unpublished information, Argonne National Laboratory (1985).
4. I. Barin, Thermochemical Data of Pure Substance, 3rd edition, VCH Publishers, New York (1995).
5. M.W. Chase, Journal of Physics and Chemistry Reference Data, NIST-JANAF Thermochemical Tables, 4th edition, National Institute of Standard and Technology, Gaithersburg, Maryland (1998).
6. O. Kubaschewski, C.B. Alcock and P.J. Spencer, Materials Thermochemistry, 6th edition, Pergamon Press (1993).
7. F.L. Oetting, M.H. Rand and R.J. Ackermann, The Chemical Thermodynamics of Actinide Elements and Compounds, Part 1 The Actinide Elements, International Atomic Energy Agency, Vienna (1976).
8. F.L. Oetting and R.O. Adams, Journal of Chemical Thermodynamics, 15, 537 (1983).
9. E.E. Rolon and G.F. Gallegos, Journal of Thermal Analysis, 21, 159 (1981).
10. O. Kubaschewski and C.B. Alcock, Metallurgical Thermochemistry, Fifth Ed., p184, Pergamon Press, New York (1979).

Section 3 Vapor Pressure

3.1 Americium

Vapor pressure measurement data were critically reviewed by Oetting et al. [1]. As a result, Oetting suggested the equation reported by Ward et al. [2] as the most accurate one. Ward's equation was based on data measured for $990 \le T \le 1358\ K$, given by

$$\log p = 11.584 - \frac{14315}{T}$$

where p is in Pa and T in K.

After Oetting's review was available, Alcock et al. [3] provided with a more updated equation applicable to the temperature range of $298 \le T \le 1449\ K$

$$\log p = 11.983 - \frac{14854}{T} + 0.1914\ \log T - 4.699 \times 10^{-4}\ T\ .$$

The two data sets are in very good agreement, almost undistinguishable when plotted. Alcock's equation is adopted for the present report because it is a more recent data compilation and has a wider temperature range.

3.2 Plutonium and Pu-Zr Alloy

The vapor pressure measurement of solid plutonium at temperatures below melting point is rare. Only data set found was by Alcock et al. [3]. The vapor pressure for solid plutonium is expressed by

$$\log p = 31.166 - \frac{19162}{T} - 6.6675\ \log T \quad (298 \le T \le 500\ K)\ ,$$

$$\log p = 23.864 - \frac{18460}{T} - 4.472 \log T \quad (500 \le T \le 913\ K)$$

where p is in Pa.

The recommended equation of vapor pressure for solid plutonium is developed based on the Alcock data as follows:

$$\log p = 32.525 - \frac{19234}{T} - 7.118 \log T \quad (298 \le T \le 913\ K)$$

Fig.3-1 compares the predictions of the recommended equation and those of the Alcock equation.

The liquid phase vapor pressure equation is also given by Alcock [3] as

$$\log p = 8.672 - \frac{16658}{T} \quad (913 \le T \le 2450\ K)\ .$$

This equation is generally lower than the earlier data available in the literatures [4–7]. The recommended equation is fitted for the data from Refs. 3 – 7. Fig.3-2 compares the recommended equation and data found in the literature. The recommended equation is

$$\log p = 9.504 - \frac{17254}{T} \quad (913 \le T \le 2450\ K)\ .$$

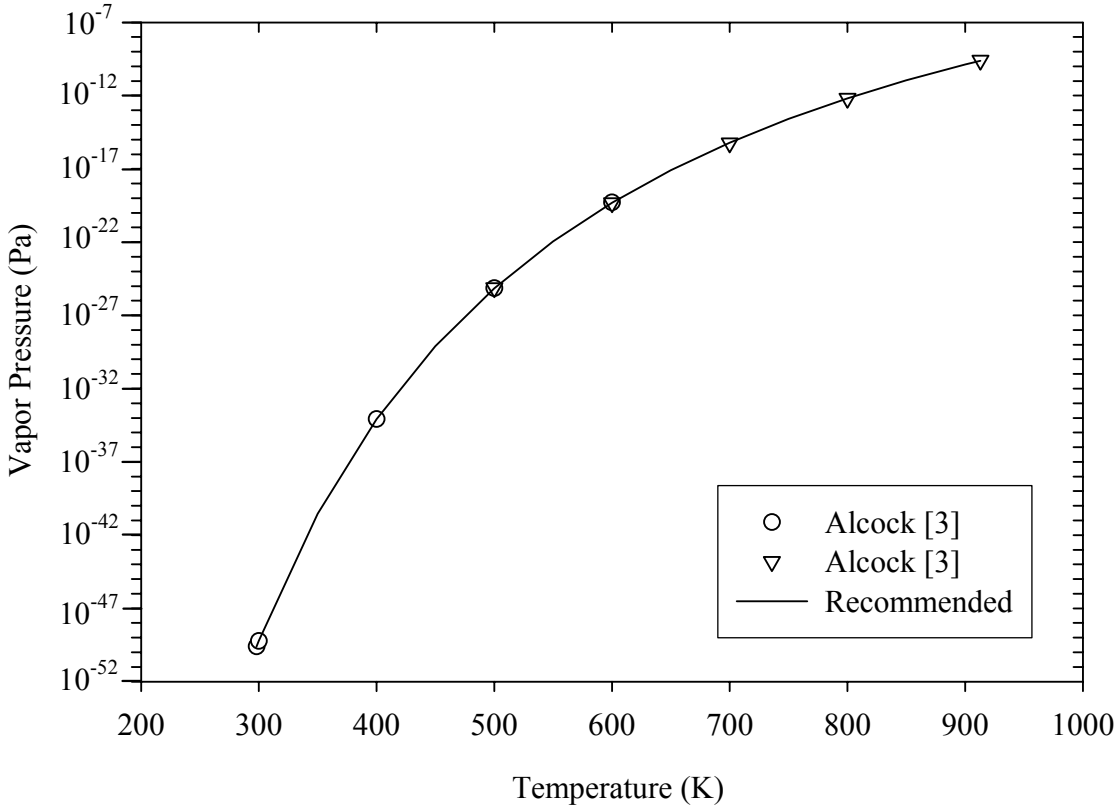

Fig.3-1 Recommended vapor pressure of solid plutonium compared to the Alcock data

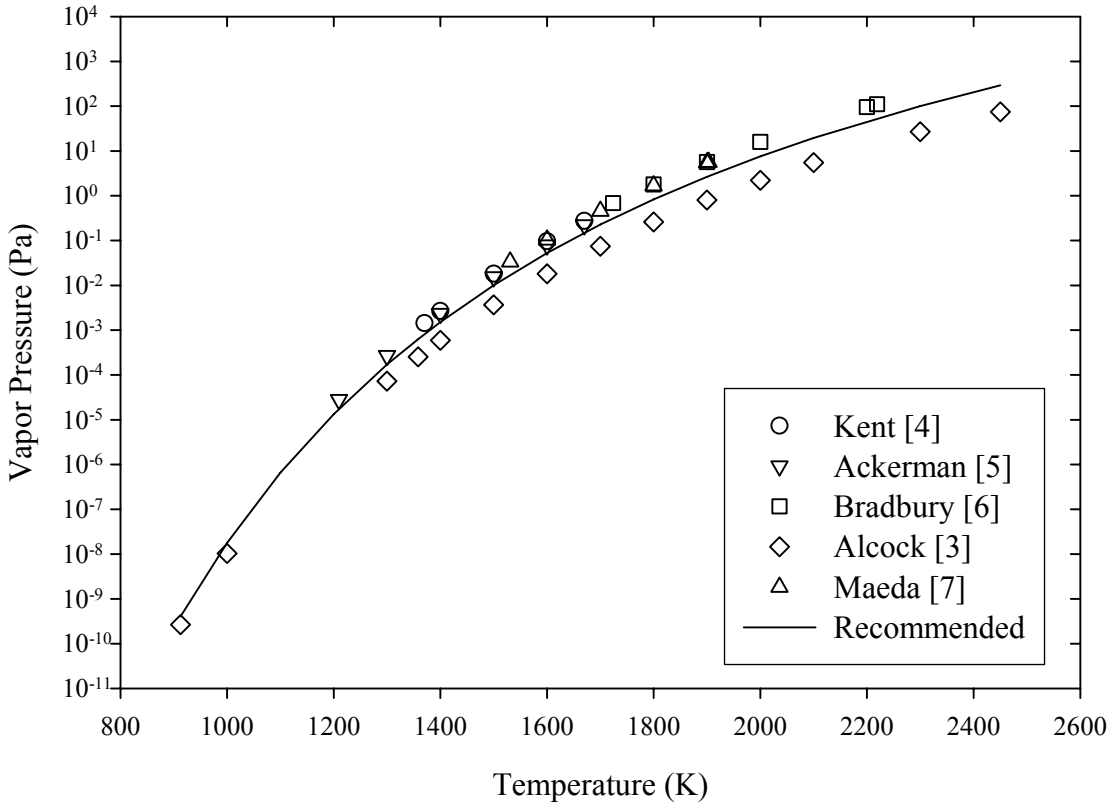

Fig.3-2 Model predictions for vapor pressure of liquid plutonium compared to data from the literature

The vapor pressure of plutonium over Pu-Zr alloys are reported by Meada et al.[7]. Table 3-1 shows vapor pressures of plutonium for several compositions.

Table 3-1 Vapor Pressure of Plutonium over Pu-Zr Alloys

Alloys	Phase	$\log p(Pa) = A + \frac{B}{T}$		Temperature Range (K)
		A	B	
Pu-20 %Zr *	Liquid	9.411	16740	1475 – 1866
Pu-50 %Zr	Solid	9.671	17207	1373 – 1439
	Liquid	9.123	16535	1623 – 1903
Pu-60 %Zr	Solid	9.261	16783	1412 – 1557
	Liquid	8.785	16082	1757 – 1903
Pu-75 %Zr	Solid	8.720	16346	1412 – 1761
Pu-82 %Zr	Solid	8.572	16244	1411 – 1814
Pu-94 %Zr	Solid	8.029	16280	1522 – 1870

* Composition in atomic %. For example, Pu-20%Zr means that the alloy is composed of 80 atom% Pu and 20 atom% Zr.

3.3 Neptunium

The vapor pressure of neptunium is found in Ref. 3 for solid phase as

$$\log p = 24.649 - \frac{24886}{T} - 3.9991 \log T \quad (298 \le T \le 912\ K).$$

where p is in Pa. Because this is the only data found, this equation is selected for this data compilation.

Alcock et al.[3] also presented the vapor pressure of neptunium for the liquid phase as

$$\log p = 15.082 - \frac{23378}{T} - 1.325 \log T \quad (912 \le T \le 2500\ K).$$

Ackermann and Rauh [5] also reported the vapor pressure of neptunium in liquid phase as

$$\log p = 10.202 - \frac{22370}{T} \quad (1540 \le T \le 2140\ K).$$

The following equation is available for the temperature range of $1617 \le T \le 2074\ K$ [8].

$$\log p = 90.442 - \frac{31522}{T} - 25.083 \log T + 4.1165 \times 10^{-3} T - 2.8679 \times 10^{-7}\ T^2$$

The recommended model is developed from the literature data as

$$\log p = 14.984 - \frac{23342}{T} - 1.303 \log T \quad (912 \le T \le 2500\ K).$$

Fig.3-3 compares the recommended equation with the data from the literature.

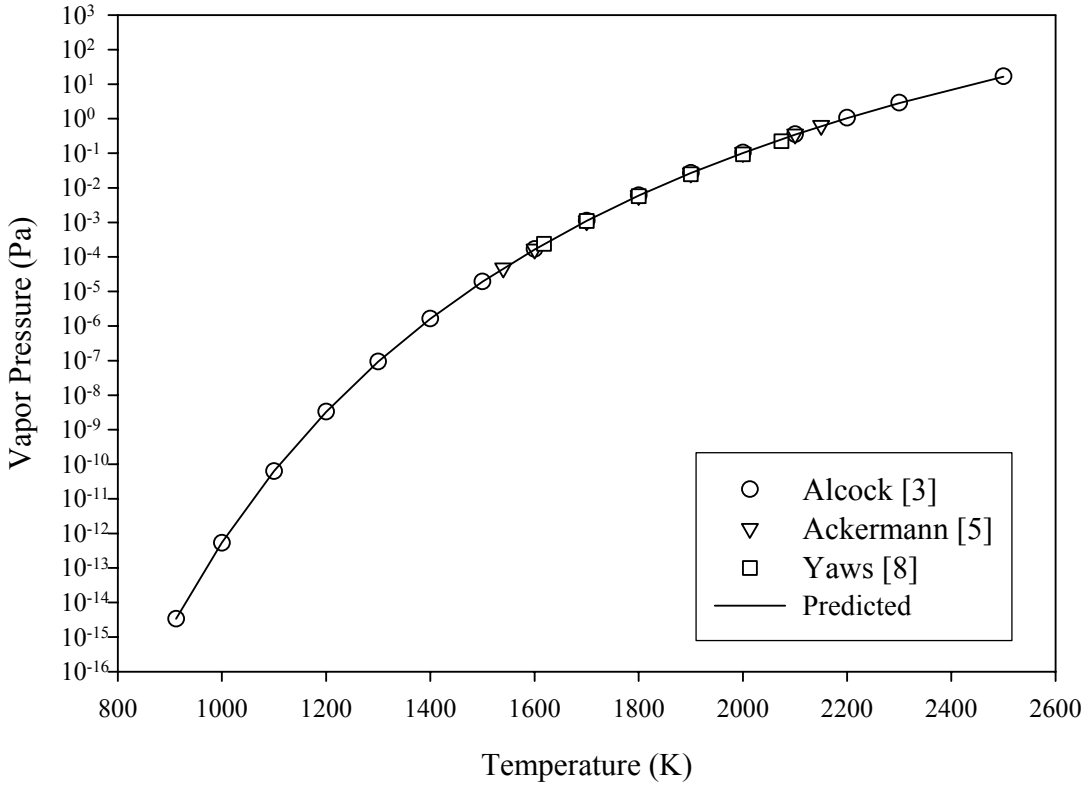

Fig.3-3 Predicted vapor pressure of liquid phase neptunium compared with data from the literature

3.4 Zirconium

The recommended vapor pressure of zirconium is found from Alcock et al. [3] for the solid phase as

$$\log p = 15.014 - \frac{31512}{T} - 0.789 \log T \quad (298 \le T \le 2125\ K),$$

and for the liquid phase as

$$\log p = 11.812 - \frac{30295}{T} \quad (2125 \le T \le 2500\ K).$$

3.5 Curium

The melting point of curium is obtained from Ref.1 as 1618 K. The recommended vapor pressure of curium is found from Alcock et al. [3] for the solid phase as

$$\log p = 13.375 - \frac{20364}{T} - 0.577 \log T \quad (298 \le T \le 1618\ K),$$

and for the liquid phase as

$$\log p = 10.229 - \frac{18292}{T} \quad (1618 \le T \le 2200\ K).$$

3.6 Uranium

The recommended vapor pressure of uranium is found from Alcock et al. [3] for the solid phase as

$$\log p = 5.776 - \frac{27729}{T} + 2.6982 \log T - 1.5471 \times 10^{-3} T \quad (298 \le T \le 1408\ K),$$

and for the liquid phase as

$$\log p = 25.741 - \frac{28776}{T} - 4.0962 \log T \quad (1408 \le T \le 2500\ K).$$

3.7 References for Section 3

1. F.L. Oetting, M.H. Rand and R.J. Ackermann, The Chemical Thermodynamics of Actinide Elements and Compounds, Part 1 The Actinide Elements, International Atomic Energy Agency, Vienna (1976).
2. J.W. Ward, W. Muller and G.F. Kramer, Transplutonium Elements, Proc. 5th Int. Conf. Baden-Baden, Sept. 1975, eds. W. Muller and R. Lindner, North-Holland Pub. Co., Amsterdam (1976).
3. C.B. Alcock, V.P. Itkin and M.K. Horrigan, Canadian Metallurg. Quart., 23 (3), 313 (1984).
4. R.A. Kent, High Temp. Sci., 1, 169 (1969).
5. R.J. Ackermann and E.G. Rauh, J. Chem. Thermodynamics, 7, 211 (1975).
6. M.H. Bradbury and R.W. Ohse, J. Chem. Phys., 70(05), 2310 (1979).
7. A. Maeda, Y. Suzuki, Y. Okamoto and T. Ohmichi, J. Alloys Compounds, 205, 35 (1994).
8. C.L. Yaws, Handbook of Vapor Pressure, Vol.4 Inorganic Compounds and Elements, Gulf Pub. Co., Houston (1995).

Section 4 Phase Equilibrium

4.1 Phases and Crystal Structures of Elements

The phases and crystal structures of TRU and Zr elements are taken from Oetting et al. [1] and summarized in Table 4-1.

Table 4-1 Crystal Structures and Phases Transitions of TRU and Zr Elements

Element	Phase	Crystal structure	Transition	Temperature (K)
Pu	α	Monoclinic	α – β	397.6
	β	b.c.m.	β – γ	487.9
	γ	f.c.o'rhombic	γ – δ	593.1
	δ	f.c.c.	δ – δ′	736
	δ′	b.c.t.	δ′ – ε	755.7
	ε	b.c.c.	ε – L	913
Am	α	d.h.c.p.	α – β	923
	β	f.c.c.	β – γ	1350
	γ	b.c.c.	γ – L	1449
Np	α	o'rhombic	α – β	553
	β	tetragonal	β – γ	849
	γ	b.c.c.	γ – L	912
Zr	α	h.c.p.	α – β	1135
	β	b.c.c.	β – L	2125

It is noticeable that the high temperature phases of all four elements have the same crystal structure, namely, body centered cubic. This enables continuous solid solution between the high temperature solids of the binary and ternary alloys of these elements.

4.2 Binary Systems

4.2.1 Pu-Zr

The phase diagram of plutonium-zirconium phase diagram is taken from Ref.2 and redrawn in Fig.4-1. Note that the phase diagram is given weight percent Zr vs. temperature in K. An additional abscissa in atom percent Zr is provided on top for reference.

The allotropic phase transitions and melting temperatures for pure plutonium from Ref.2 are consistent with the values in Sect.2. The values for pure zirconium, however, are slightly higher than those in Sect.2. These inconsistencies are corrected to conform the more reliable data from Sect.2.

The remarkable features found in the phase diagram are: continuous solid solubility between ε-Pu and β-Zr with increasing solidus from Pu to Zr; two intermediate phases; and extended δ-Pu solid solubility (to about 45 weight % Zr) which give rise to two eutectoids; and a large a-Zr solid solubility (to about 20 weight % Pu). The two intermediate phases are Pu_6Zr and $PuZr_2$. These are orthorhombic and hexagonal, respectively and have a rather broad solubility range [3].

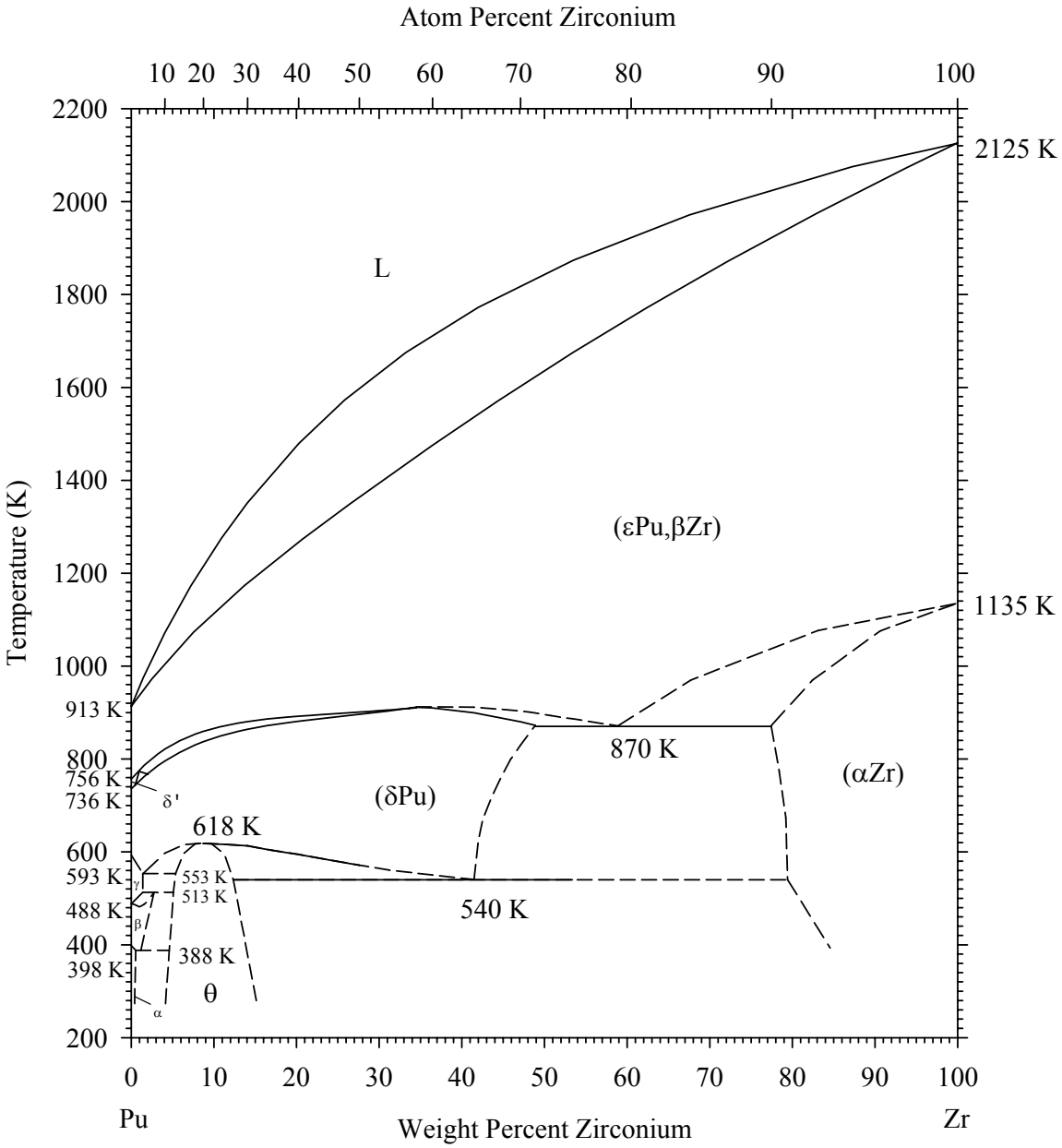

Fig.4-1 Phase diagram of Pu-Zr binary alloy [2].

4.2.2 Pu-Am

The phase diagram shown in Fig.4-2 is redrawn based on the one made available by Massalski [4]. The temperature for the $\alpha \rightarrow \beta$ allotropic transition of pure americium is modified to be consistent with the data recommended in Sect.2.

The phase diagram is incomplete toward the pure americium side, particularly for the area related to the americium $\beta \rightarrow \gamma$ allotropic transition. The Massalski phase diagram was originally redrawn from Ellinger et al. [5]. When Ellinger reported the Pu-Am phase diagram, γAm was not known. Massalski indicated the new phase in the diagram but left it without further modification. A calculation result by Ogawa [6] can be used to predict the alloying behavior of γAm with Pu. The phase diagram at high temperatures provided by Ogawa is redrawn in Fig.4-3. This phase diagram shows complete solid solubility not only between εPu and γAm, but also between δPu and βAm.

4.2.3 Am-Np

The phase diagram of neptunium-americium alloy can be found from Ogawa [6] and redrawn in Fig.4-4. This phase diagram was obtained based on model prediction by Ogawa. No measurement data, however, is available to confirm this phase diagram.

4.2.4 Pu-Np

The phase diagram of plutonium-neptunium alloy is taken from Massalski and shown in Fig.4-5.

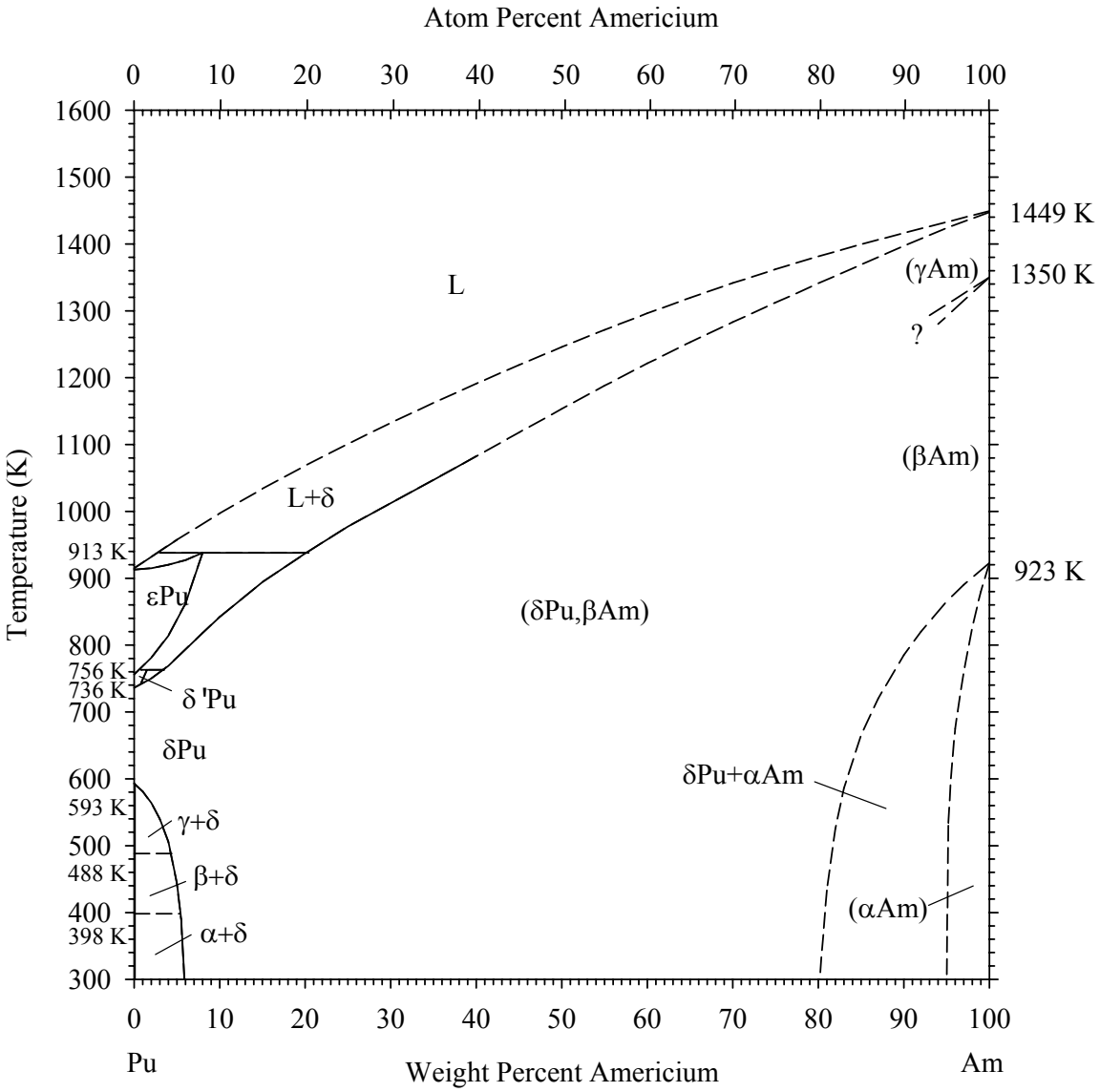

Fig.4-2 Phase diagram of plutonium-americium alloy [4].

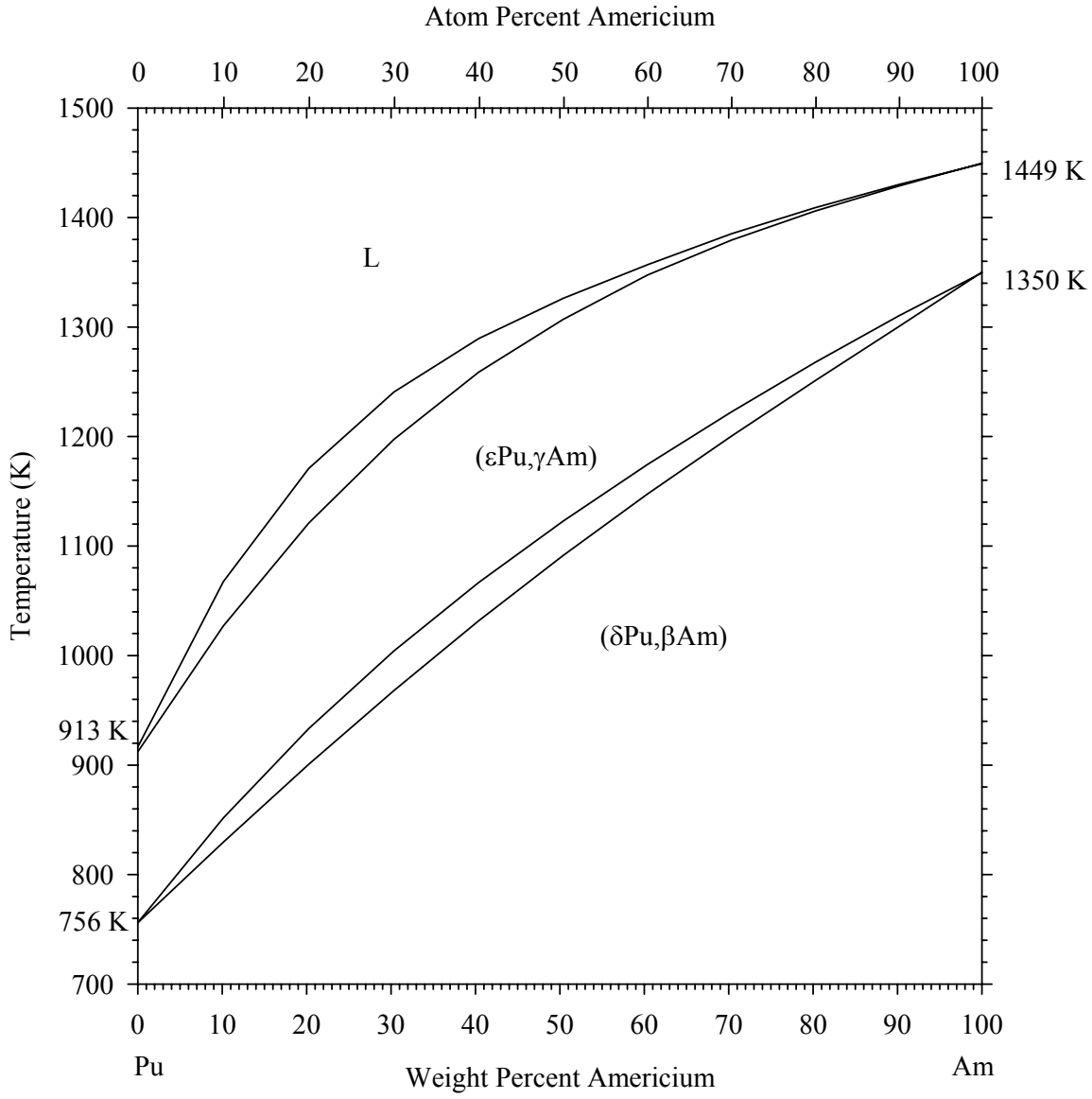

Fig.4-3 Phase diagram of plutonium-americium alloy [6].

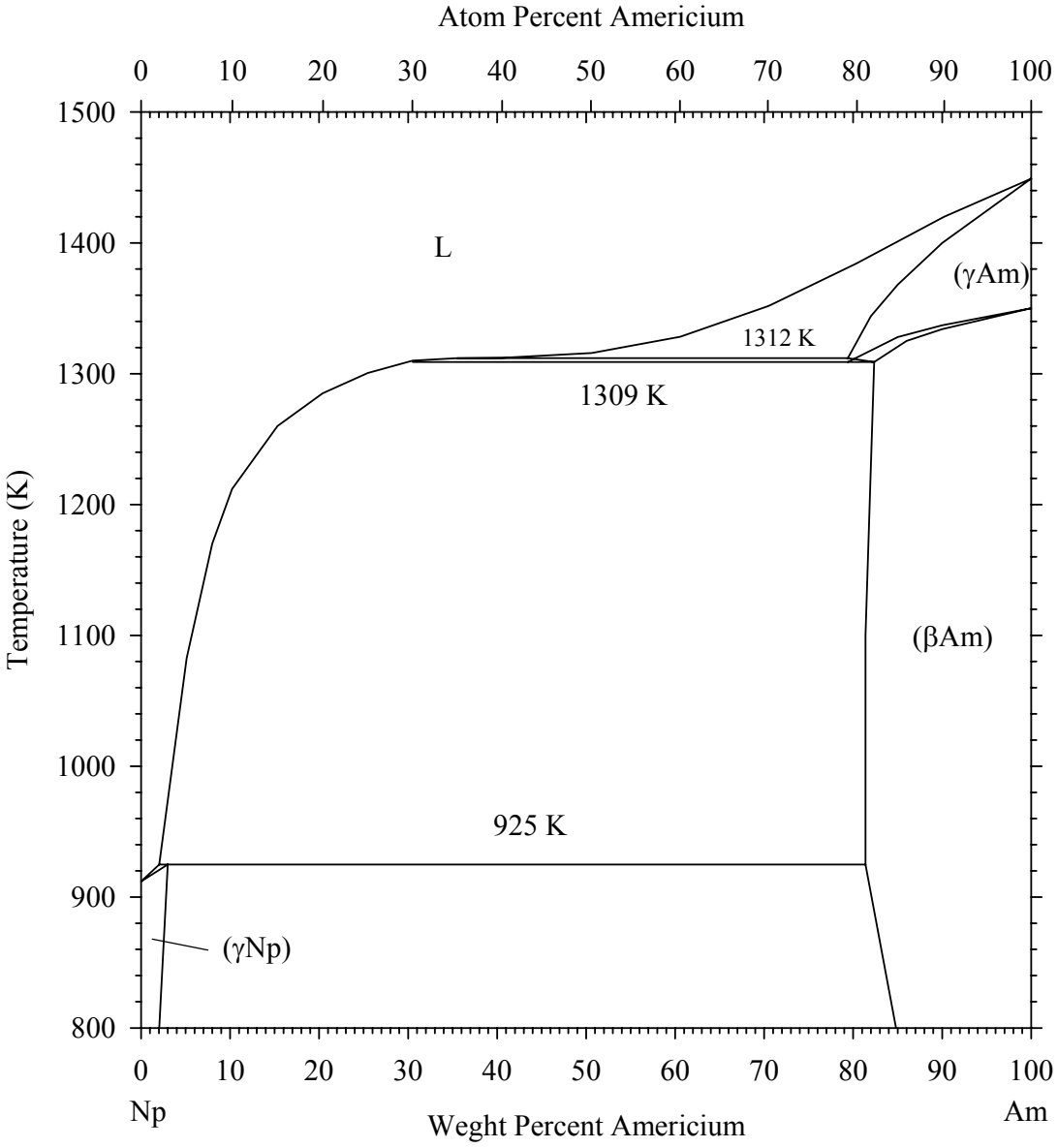

Fig.4-4 Phase diagram of neptunium-americium alloy.
Redrawn from Ogawa [6].

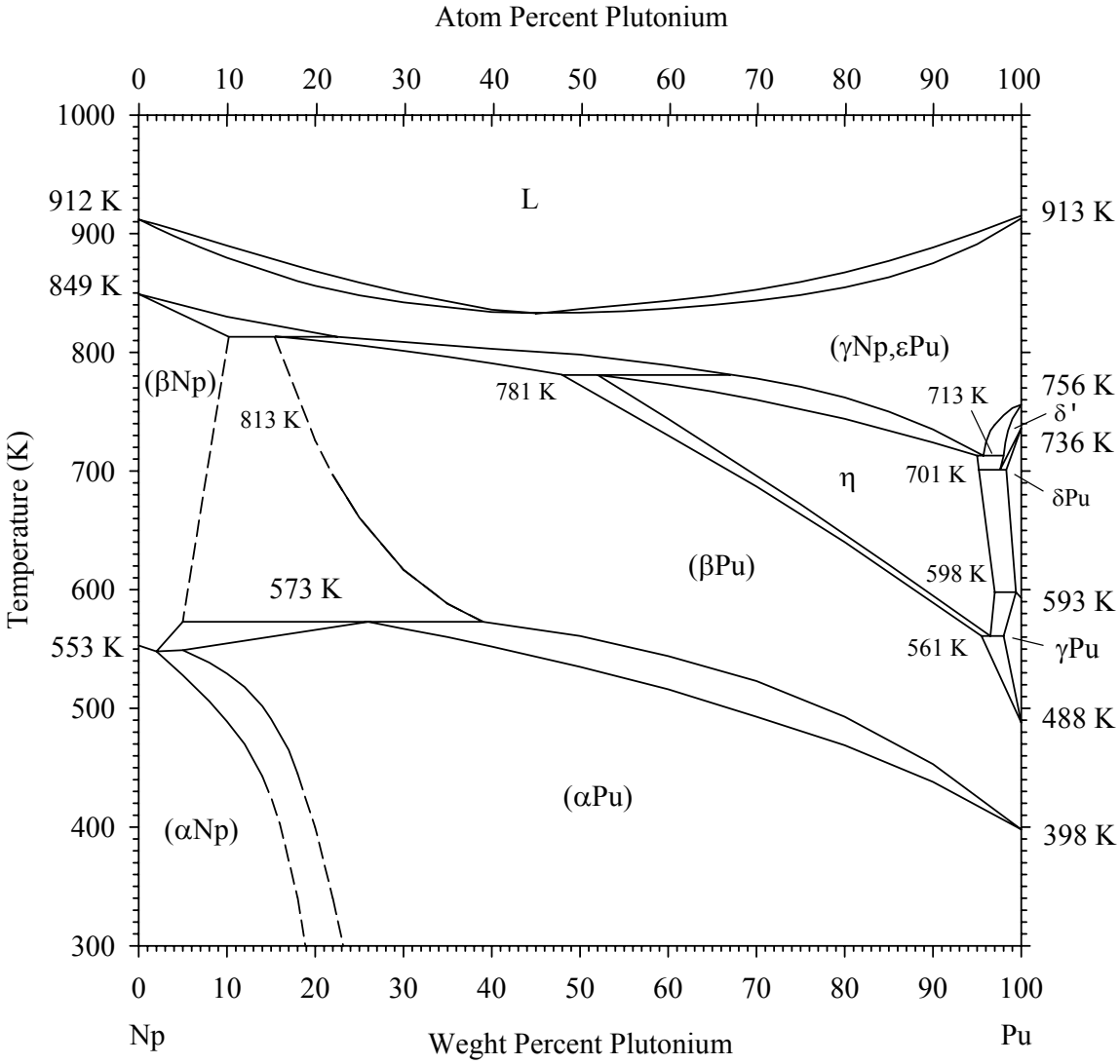

Fig.4-5 Phase diagram of neptunium-plutonium alloy [4].

4.3 Ternary Systems

There is no ternary phase diagram available for Zr-Pu-Am and Zr-Pu-Np systems. However, Ogawa calculated isotherms of the Np-Pu-Am system. He claimed that the Np-Am interaction is stronger than those of Np-Pu and Am-Pu. Figs. 4-6 and 4-7 are taken from Ogawa showing isotherms of Pu-Am-Np at 1000 K and 1300 K, respectively.

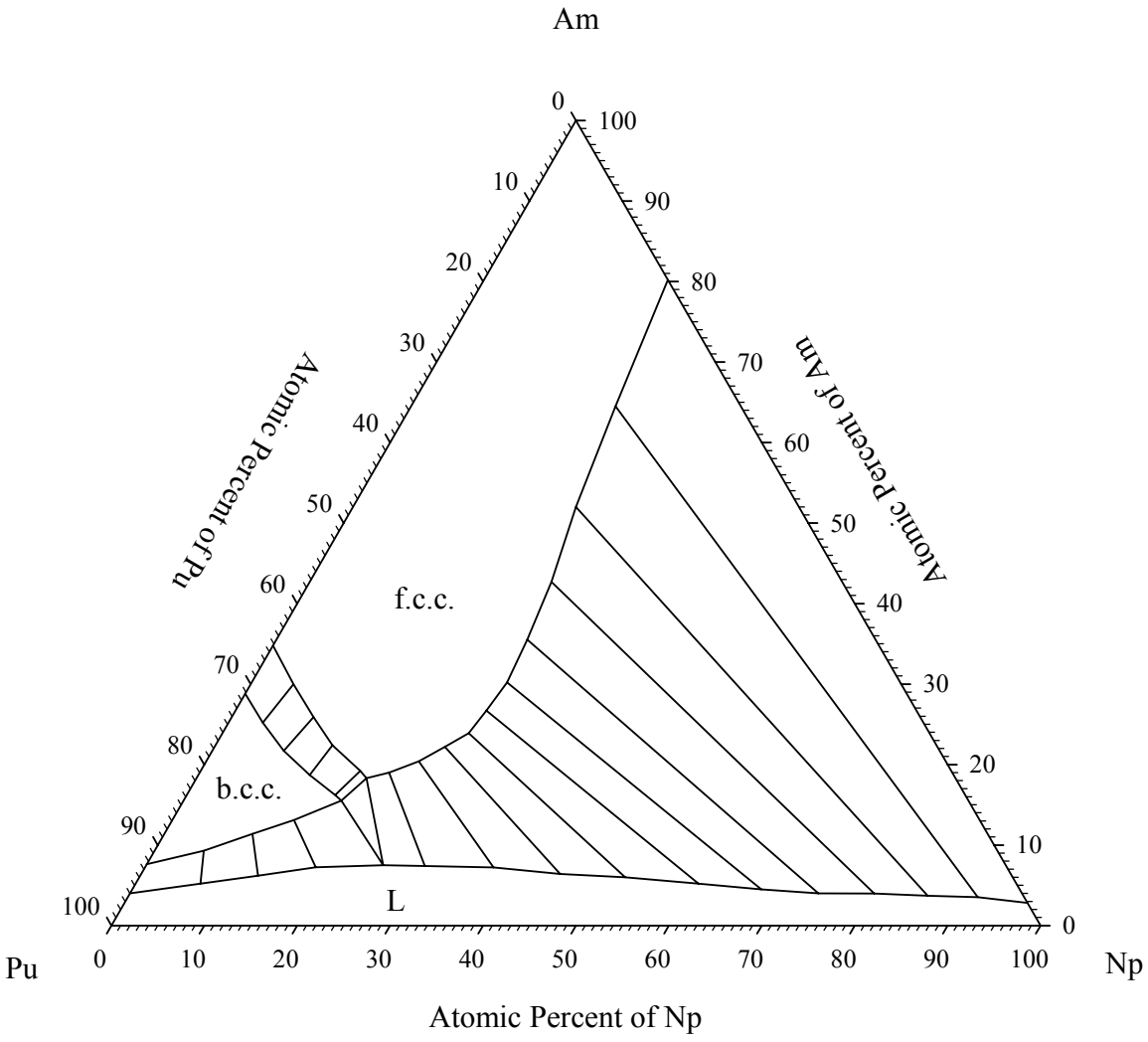

Fig.4-6 Section of the Pu-Am-Np phase diagram at 1000 K [6].

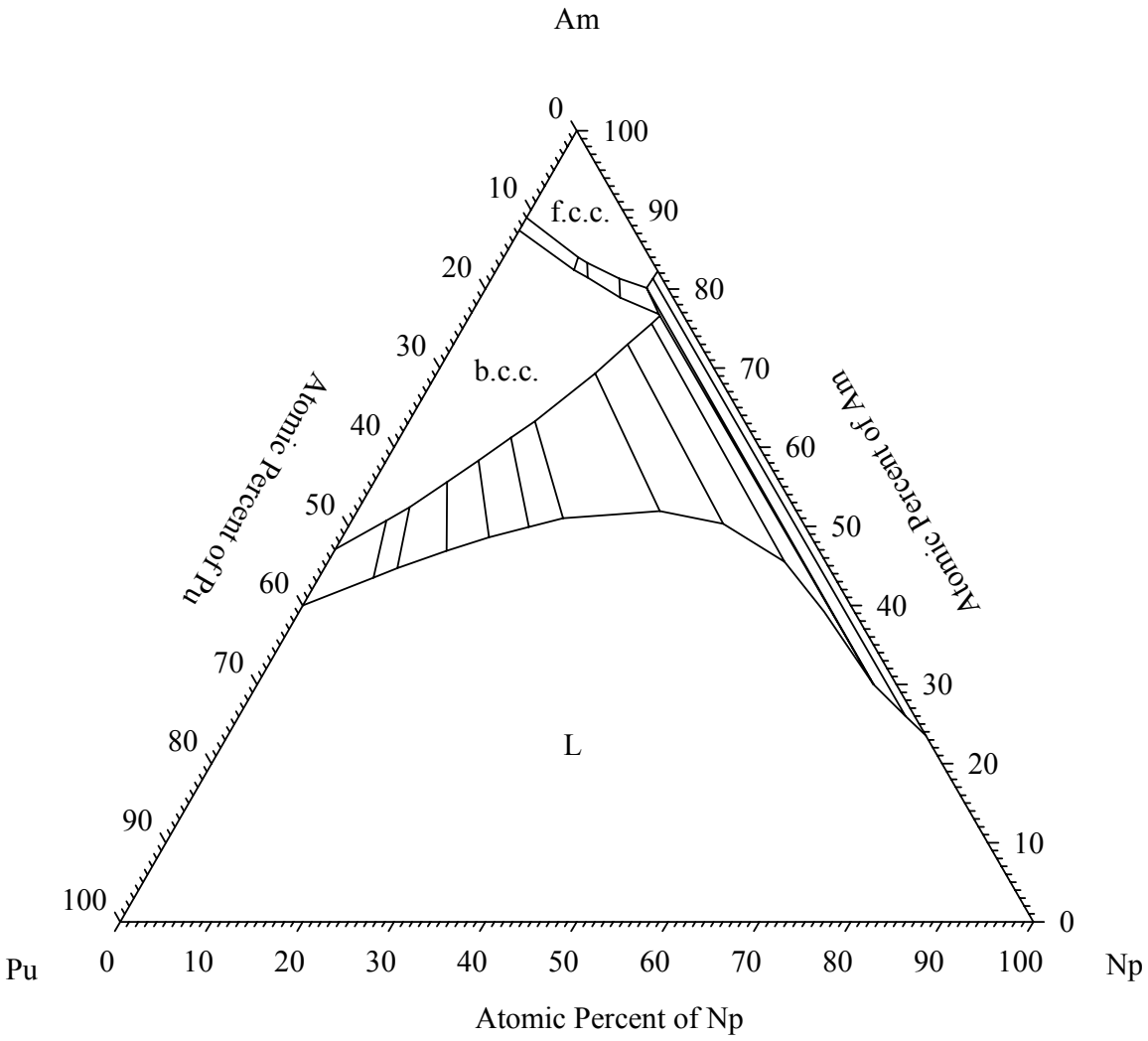

Fig.4-7 Section of the Np-Pu-Am phase diagram at 1300 K [6].

4.4 References for Section 4

1. F.L. Oetting, M.H. Rand and R.J. Ackermann, The Chemical Thermodynamics of Actinide Elements and Compounds, Part 1 The Actinide Elements, International Atomic Energy Agency, Vienna (1976).
2. H. Okamoto, in Binary Alloy Phase Diagrams, T. Massalski, ed., ASM International, June 1993 Supplement, JPE 14(3) (1993).
3. G.L. Hofman, unpublished information, Argonne National Laboratory (1985).
4. T. Massalski, Binary Alloy Phase Diagrams, pp.254-255 (1990).
5. F.H. Ellinger, K.A. Johnson and V.O. Struebing, J. Nucl. Mater., 20, 83 (1966).
6. T. Ogawa, J. Alloys Compounds, 194, 1 (1993).

Section 5 Thermal Expansion and Density

5.1 Theory

The coefficient of volumetric thermal expansion is a thermodynamic property defined as

$$\alpha = \frac{1}{V}\left(\frac{\partial V}{\partial T}\right)_p \tag{1}$$

where V is the volume and T the temperature. This is called instantaneous coefficient of thermal expansion; it is different from the mean coefficient to be described later. The subscript p implies that Eq.(1) is defined for a constant pressure process. For simplicity, however, the subscript p is dropped in the following equations. For a process where the substance volume changes $V_o \rightarrow V$ according to temperature changes $T_o \rightarrow T$, the mean coefficient is used to describe the process as

$$\overline{\alpha} = \frac{1}{V_o}\frac{V - V_o}{T - T_o} \tag{2}$$

Most measurement values are obtained for length changes and data are given in fractional (or percent) changes of length. The relevant coefficient is the instantaneous coefficient of linear thermal expansion, which is defined as

$$\alpha_l = \frac{1}{L}\left(\frac{\partial L}{\partial T}\right)_p \tag{3}$$

where L is the length of the substance. The corresponding mean coefficient is

$$\overline{\alpha}_l = \frac{1}{L_o}\frac{L - L_o}{T - T_o} \tag{4a}$$

or

$$\overline{\alpha}_l = \frac{1}{\Delta T}\frac{\Delta L}{L_o} \tag{4b}$$

where $\Delta T = T - T_o$ and $\Delta L = L - L_o$. Eq.(4b) is more useful because most data compilations are given in $\Delta L/L_o$.

If the substance is isotropic, the (instantaneous) coefficient of volume expansion is equal to three times the coefficient of linear expansion, i.e.,

$$\alpha = 3\alpha_l \tag{5}$$

The same is not true, however, for the mean coefficients. From Eq.(4) and the fact that $V=L^3$, the following can be shown

$$\frac{V}{V_o} = \left(1 + \Delta T\, \overline{\alpha}_l\right)^3 \tag{6}$$

Applying Eq.(6) into Eq.(2) yields

$$\overline{\alpha} = 3\overline{\alpha}_l + 3\Delta T\, \overline{\alpha}_l^{\,2} + \left(\Delta T\right)^2 \overline{\alpha}_l^{\,3} \tag{7}$$

Comparing between Eq.(5) and Eq.(7), the last two terms in Eq.(7) make the difference. However, the error caused by neglecting those terms in Eq.(7) is generally small.

The corresponding fractional density change can be expressed in terms of linear thermal expansion coefficient by using Eq.(6) as

$$\frac{\Delta\rho}{\rho_o} = \frac{1 - \left(1 + \Delta T\, \overline{\alpha}_l\right)^3}{\left(1 + \Delta T\, \overline{\alpha}_l\right)^3} \tag{8a}$$

where $\Delta\rho = \rho - \rho_o$. Density as a function of temperature can be found by arranging Eq.(8a) as

$$\rho = \left[1 + \frac{1 - \left(1 + \Delta L / L_o\right)^3}{\left(1 + \Delta L / L_o\right)^3} \right] \rho_o \tag{8b}$$

Conversely, the fractional length change ($\Delta V/V_o$) can be determined where the density change is known by

$$\frac{\Delta L}{L_o} = \left(\frac{\rho_o}{\rho} \right)^{\frac{1}{3}} - 1 \tag{8c}$$

5.2 Elemental Data

5.2.1 Zirconium

The thermal expansion coefficient data for polycrystalline zirconium are taken from Ref.2 and tabulated in Table 5-1. The density as a function of temperature is calculated using the relationship given in Eq.(8b). Temperature for the phase transition $\alpha \rightarrow \beta$ was adjusted to conform the information given in Sect.2.

5.2.2 Plutonium

The thermal expansion coefficient data for polycrystalline plutonium are also taken from Ref.2. The phase transition temperatures from Ref.2 are adjusted to be consistent to the more reliable ones given in Sect.2. The density values given in Table 5-2 are calculated using the relationship given in Eq.(8b).

Liquid phase Pu density is obtained from Ref.3 and compared with the solid phase values given in Table 5-2 and in Fig.5-1.

5.2.3 Neptunium

The linear expansion data and the instantaneous coefficient of thermal expansion were obtained from Ref.4. The temperature dependent density was calculated using Eq.(8b) based on room temperature value found in Ref.5. The phase transition temperatures from Ref.3 are inconsistent with those in Sect.2. Because those given in Sect.2 are considered more reliable, these discrepancies were modified.

5.2.4 Americium

Data for thermal expansion and temperature dependent density are unavailable in the literature.

5.3 Zr-Pu Binary Alloy

There is no thermal expansion data for Zr-Pu binary alloys available in the literature. The simple law of mixtures is recommend:

$$\alpha_{Zr-Pu} = \alpha_{Zr}\, v_{Zr} + \alpha_{Pu}\, v_{Pu}$$

where v is the volume fraction of the element. The density measurements of Zr-U alloys showed consistent results with calculations by the law of mixtures [6]. For a preliminary recommendation, the density of Zr-Pu alloys is also approximated by the law of mixtures.

As an example, the thermal expansion and temperature dependent density for Zr-40Pu alloy (i.e., 60 wt% Zr + 40 wt% Pu corresponding to 80 at% Zr + 20 at% Pu) were calculated and given in Table 5-4. Fig.5-2 compares $\Delta L/L_o$ of the Zr-40Pu alloy and elemental Pu, Np, and Zr.

5.4 TRU-Zr Alloy

There is no data available for Pu-Am-Np-Zr alloy thermal expansion and density as a function of temperature at the present time.

Table 5-1 Thermal Expansion Coefficient and Density of Zirconium [2]

T (K)	$\Delta L/L_o$ ($\times 10^2$) [a]	α_l ($\times 10^6$ K^{-1}) [b]	ρ ($g.cm^{-3}$) [c]
293	0.00	5.7	6.57
400	0.060 [a]	5.9	6.558
500	0.123	6.6	6.546
600	0.192	7.1	6.532
700	0.265	7.6	6.518
800	0.343	7.9	6.503
900	0.422	8.0	6.488
1000	0.505	8.2	6.471
1100	0.586	8.2	6.456
1135 (α)	0.617	8.2	6.450
1135 (β)	0.482	9.0	6.476
1200	0.539	9.1	6.465
1400	0.725	9.5	6.429
1600	0.923	10.3	6.391
1800	1.139	11.3	6.351

a: For example, this value should read as $\Delta L/L_o = 0.06 \times 10^{-2}$ at T = 400 K.

b: Instantaneous coefficient of linear expansion.

c: Calculated based on $\rho_o = 6.57$ g/cm^3 (at $T_o = 293$ K) using Eq.(8b).

Table 5-2 Thermal Expansion Coefficient and Density of Plutonium [2]

T (K)	$\Delta L/L_o$ ($\times 10^2$) [a]	α_l ($\times 10^6$ K^{-1}) [b]	ρ ($g.cm^{-3}$) [c]
293	0.00	46.7	19.750
350	0.279 [a]	49.4	19.586
397.6 (α)	0.515	51.1	19.448
397.6 (β)	3.673	37.3	17.724
400	3.682	37.3	17.720
450	3.868	37.3	17.625
487.9 (β)	4.009	37.3	17.553
487.9 (γ)	4.928	34.6	17.096
500	4.970	34.6	17.075
550	5.144	34.6	16.991
593.1 (γ)	5.294	34.6	16.918
593.1 (δ)	7.624	-8.6	15.843
600	7.618	-8.6	15.846
700	7.532	-8.6	15.884
736 (δ)	7.501	-8.6	15.898
736 (δ')	7.448	-16.1	15.921
755.7 (δ')	7.417	-16.1	15.935
755.7 (ε)	6.297	36.6	16.444
800	6.459	36.6	16.369
900	(6.825) [d]	(36.6) [d]	16.201
913 (ε)	(6.873)	(36.6)	16.179

a: For example, this value should read as $\Delta L/L_o = 0.279 \times 10^{-2}$ at T = 350 K.

b: Instantaneous coefficient of linear expansion.

c: Calculated based on ρ_o = 19.75 g/cm^3 (at T_o=293 K) using Eq.(8b).

d: Values in parentheses are estimated.

Table 5-3 Thermal Expansion Coefficient and Density of Neptunium [3]

T (K)	$\Delta L/L_o$ ($\times 10^2$) [a]	α_l ($\times 10^6$ K^{-1}) [b]	ρ ($g.cm^{-3}$) [c]
293	0.000	21.297	20.250
400	0.216 [a]	26.540	20.119
500	0.524	31.440	19.935
553	0.728	34.037	19.814
553	1.793	42.688	19.199
600	2.009	43.654	19.077
700	2.492	51.479	18.809
800	3.009	67.154	18.527
849	3.275	77.700	18.384
849	3.700	(77.700) [d]	18.159
900	(3.750)	(77.700)	18.133
912	(3.762)	(77.700)	18.129

a: For example, this value should read as $\Delta L/L_o = 0.216 \times 10^{-2}$ at T = 400 K.

b: Instantaneous coefficient of linear expansion.

c: Calculated based on $\rho_o = 20.25$ g/cm^3 (at T_o=293 K) using Eq.(8b).

d: Values in parentheses are estimated.

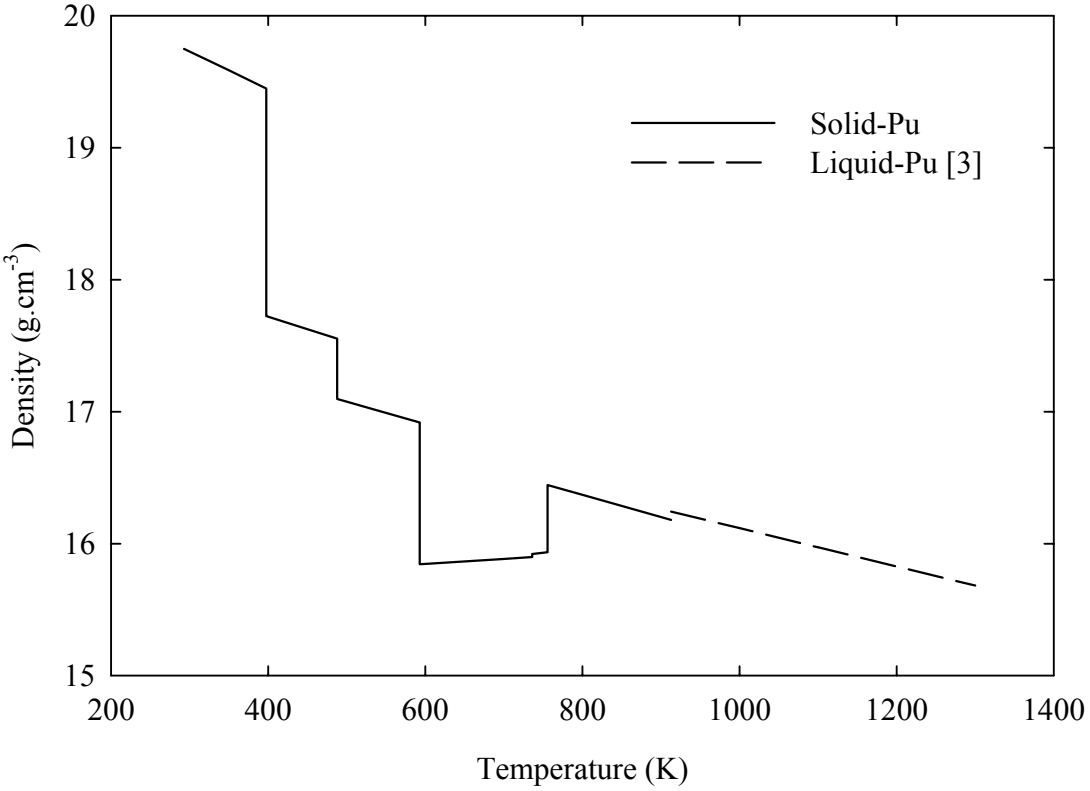

Fig.5-1 Comparison of Pu densities between the solid phase and the liquid phase

Table 5-4 Thermal Expansion Coefficient and Density of Zr-40Pu Alloy [a]

T (K)	$\Delta L/L_o$ ($\times 10^2$) [b]	α_l ($\times 10^6$ K^{-1}) [c]	ρ ($g.cm^{-3}$)
293	0.000	13.900	9.206
350	0.081 [b]	14.520	9.184
400	0.784	12.740	8.993
500	1.092	12.600	8.911
600	1.677	4.360	8.758
700	1.718	4.600	8.747
800	1.566	13.720	8.787
900	1.703	13.880	8.751

a: Alloy composition is 60 wt% Zr + 40 wt% Pu.

b: For example, this value should read as $\Delta L/L_o = 0.081 \times 10^{-2}$ at T = 350 K.

c: Instantaneous coefficient of linear expansion.

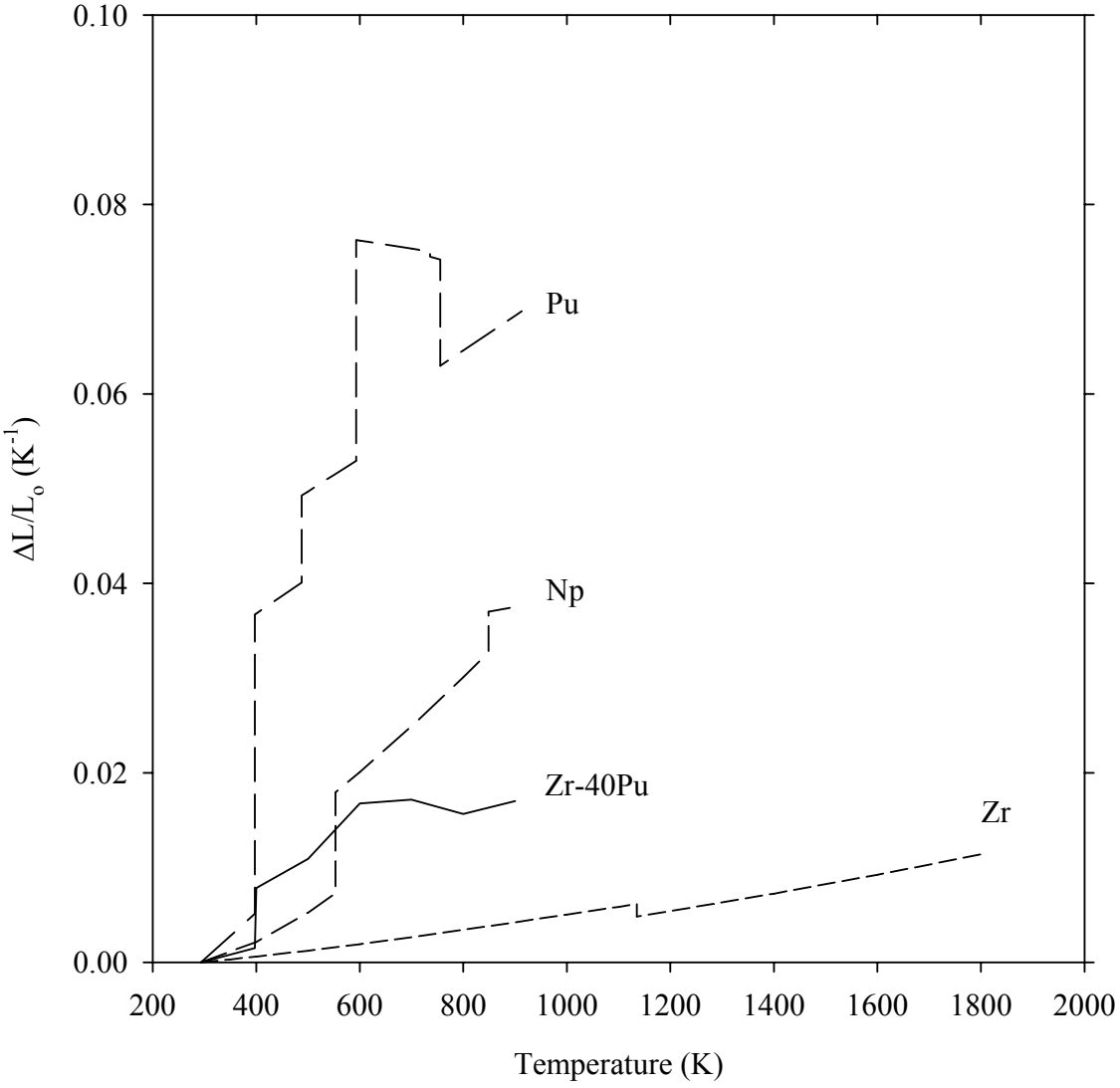

Fig.5-2 Fractional linear thermal expansion of
60 wt% Zr-40 wt% Pu alloy

5.5 References for Section 5

1. G.L. Hofman, unpublished information, Argonne National Laboratory (1985).
2. Y.S. Touloukian, R.K. Kirby, R.E. Taylor and P.D. Desai, Thermal Expansion, Thermophysical Properties of Matter, Vol.12, IFI/Plenum, New York-Washington (1975).
3. C.E. Olsen, T.A. Sandenaw and C.C. Herrick, LA-2358 Chemistry-General, TID-4500, 15th ed., Los Alamos Scientific Laboratory (1959).
4. B. Cort, J. Less-Common Metals, 135, L13 (1987).
5. J. Emsley, The Elements, 3rd ed., Clarendon Press, Oxford (1998).
6. F.A Rough, An Evaluation of Data on Zirconium-uranium Alloys, Battelle Memorial Institute, Report BMI-1030 (1955).

Section 6 Thermal Conductivity

6.1 Elemental Thermal Conductivity

The thermal conductivities of elements of Zr-TRU fuel at various temperatures are needed. Data for these elements, however, are scarce. For example, the thermal conductivity of neptunium has only two data points, both at room temperature. Americium has no data at all. To estimate the data for these elements, indirect derivations and comparisons with other actinides are made.

6.1.1 Uranium

Touloukian et al. [1] summarized the thermal conductivity data for uranium metal available before 1970. The only data added after this is by Takahashi, et al. [2]. A simple correlation for the thermal conductivity of uranium metal is generated as a polynomial using the least squares fitting of the data.

$$k_U(T) = 21.73 + 1.591\times10^{-2}\,\mathrm{T} + 5.907\times10^{-6}\,\mathrm{T}^2 . \qquad (1)$$

where k is the thermal conductivity in W/m-K and T is the temperature in K. Eq.(1) is valid in the temperature range of $255.4 \le T \le 1173.2\,\mathrm{K}$.

6.1.2 Zirconium

The thermal conductivity data of zirconium up to 1970 were reviewed and the recommended values were tabulated based on the data assessment by Touloukian [1]. Fink [3] produced a correlation including the available data available after 1970 as

$$k_{Zr}(T) = 8.853 + 7.082\times10^{-3}\,\mathrm{T} + 2.533\times10^{-6}\,\mathrm{T}^2 + 2.992\times10^{3}\,\mathrm{T}^{-1} . \qquad (2)$$

Eq.(2) is valid in the ranges of $298 \le T \le 2000\,\mathrm{K}$.

6.1.3 Plutonium

The available data for the thermal conductivity of plutonium are found only for α-Pu. The thermal conductivity for the higher temperature phases such as δ- and ε-Pu can be estimated using the Wiedemann-Franz-Lorentz law, $k = LT/\rho$, where ρ is the electrical resistivity and L is the Lorentz number. The electrical resistivity of Pu is obtained from Ref.4. The estimated thermal conductivity of Pu is as follows:

$$k_{\delta-Pu}(T) = 3.225 + 0.0296T \qquad (593 \le T \le 736\ K), \tag{3a}$$

$$k_{\varepsilon-Pu}(T) = 9.507 + 0.0184T \qquad (756 \le T \le 913\ K). \tag{3b}$$

The typical Am content in ATW TRU fuel is known to be enough to stabilize Pu to remain in δ-phase. Therefore, the data of delta stabilized Pu are rough estimates where no data for pure Pu is available. The thermal conductivity data of δ-stabilized Pu with 1 wt% Al were found from Ref.1. A polynomial correlation of the data is obtained as

$$k_{Pu-1Al} = 1.213 + 2.018\times10^{-2}\,T + 2.857\times10^{-6}\,T^2. \tag{4}$$

for the temperatures between 373 K and 873 K. As shown in Fig.6-1, Pu-1Al has generally lower thermal conductivity than pure Pu. This is attributed to the aluminum alloying effect although Al has an extremely high thermal conductivity compared to Pu.

Because of its low density, however, 1 wt% Al in the Pu-Al alloy occupies about 7 % in volume. Although small in weight percent, the large volume fraction limits the applicability of Pu-1Al data for pure Pu element. The temperature dependence, however, is useful to approximate data for other actinides whose measured data are scarce in the literature.

6.1.4 Neptunium

The thermal conductivity data for the remaining TRU elements are scarce. Therefore, estimations need to be made.

The thermal conductivity data of neptunium at room temperature were found in several places [1,5,6]. They are consistent among themselves and the value 6.3 W/m-K at 300 K is taken.

The electrical resistivity given by Lee [7] was compared at 300 K to the consistent data in the literature [1,5,6]. As a result, Lorenz number of 1.63×10^{-8} Volts^2/K^2 is found, which is also a recommended value by Touloukian [1]. Based on the electrical resistivity data by Lee [7], the thermal conductivity of neptunium is obtained using the Wiedemann-Franz-Lorentz law, and the correlation is fitted based on the data as

$$k_{Np} = 4.562 + 3.674\times10^{-3}\,T + 6.845\times10^{-6}\,T^2 \qquad (5)$$

Neptunium has a melting temperature at 912 K, which limits the validity of Eq.(5) at temperatures beyond this.

6.1.5 Americium

Touloukian's recommended thermal conductivity of americium is 10 W/m-K at room temperature [1]. Tamura [8] predicted the thermal conductivity of americium to be 22.8 W/m-K at room temperature by using an empirical correlation between the electrical conductivity and thermal conductivity. Another estimate can be made through direct application of the Wiedemann-Franz-Lorentz law. The typical Lorentz number for metals is given at room temperature as 2.44×10^{-8} Volts^2/K^2. Adopting this value and the electrical conductivity of σ=0.0015 GS/m [8] puts k at about 11 W/m-K, which is very close to the value suggested by Touloukian [1] and Muller [6]. In this work, therefore, the conservative value of 10 W/m-K is selected.

The change in the conductivity as a function of temperature is assumed to be similar to that of Pu-1Al, i.e., the expression takes the form, $k_{Am} = k_{Pu-1Al} - \left(k^0_{Pu-1Al} - k^0_{Am}\right)$ where k^0_{Pu-1Al} and k^0_{Aml} are the thermal conductivity values of Pu-1Al and Am at room temperature. Therefore, the thermal conductivity of Am is

$$k_{Am} = 4.118 + 0.018T + 5.35 \times 10^{-6} T^2 \quad (6)$$

6.1.6 Curium

The thermal conductivity of curium is 10 W/m-K at room temperature [1]. Applying the method used for americium, the thermal conductivity of Cm is estimated as

$$k_{Cm} = 4.118 + 0.018T + 5.35 \times 10^{-6} T^2 \quad (7)$$

Fig.6-1 shows the thermal conductivities of TRU elements as a function of temperature provided in Eqs. (1) – (7). The data for U and Zr are also included for a comparison purpose. Notice the similarity among the thermal conductivity increases as temperature rises between U and the TRU element, particularly Pu-1Al.

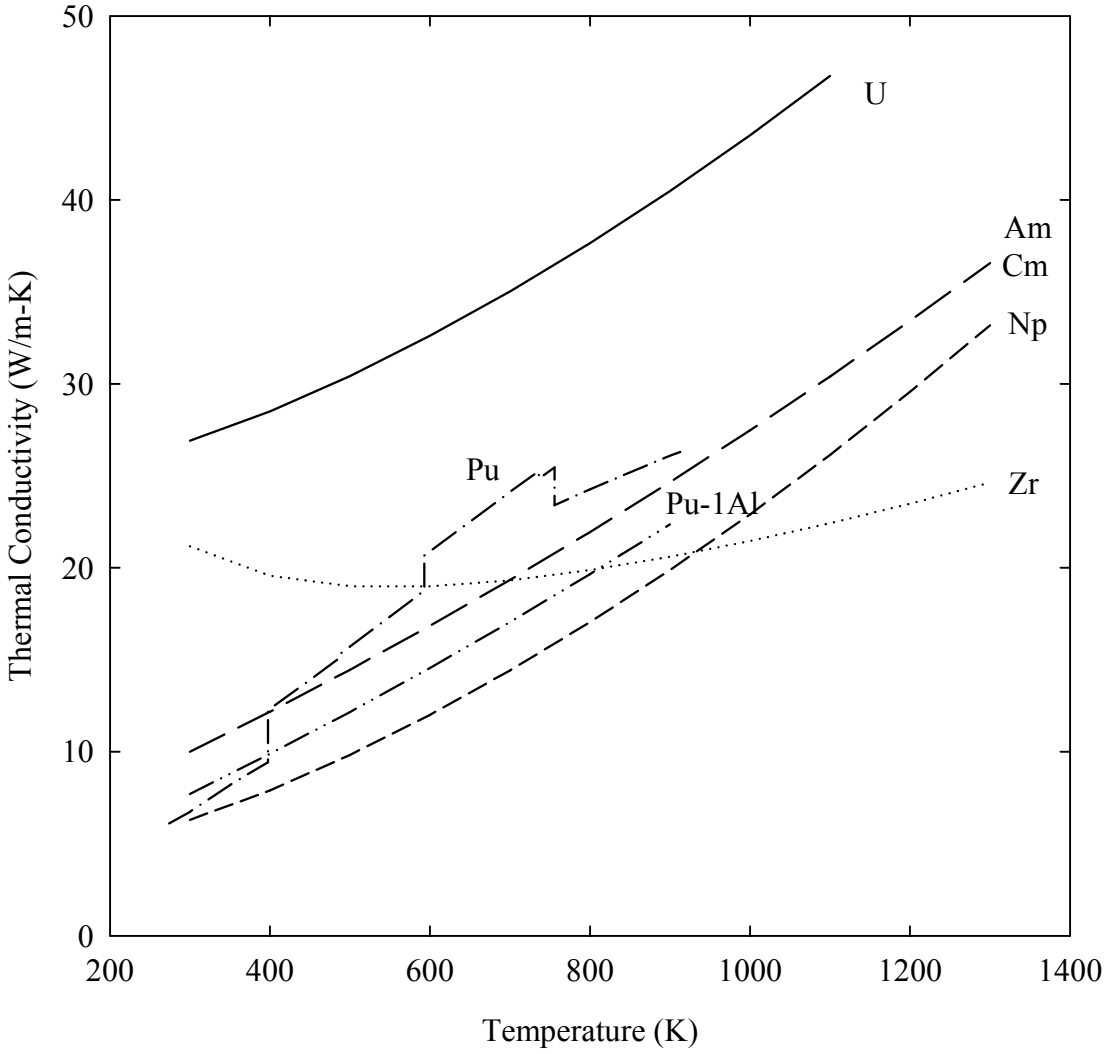

Fig.6-1 Thermal conductivity of TRU elements.
The thermal conductivities of U and Zr are included for comparison.

6.2 Theory of Alloy Thermal Conductivity

The principal heat carriers in metals are electrons and lattice wave (or phonon). The phonon contribution, however, is small except at very low temperatures. This situation can be written as $k = k_e + k_p$, where k_e is the electron contribution and k_p is the phonon one. From the Wiedemann-Franz law, the electron contribution term can be expressed as $k_e = LT/\rho$.

In the case where an alloying element dissolves into the matrix to form a solid solution, it reduces thermal conductivity by increasing the electrical resistivity of the matrix; electrons scatter additionally with impurity atoms. Assuming the Matthiessen rule [9,10] is applicable to a simple binary alloy, then $\rho = \rho_p(T) + \rho_i(c)$, where $\rho_p(T)$ is the electrical resistivity due to electron and phonon scattering which is taken to be equal to the resistivity of the pure solvent metal and $\rho_i(c)$ is the concentration dependent impurity resistivity. It is noticeable that $\rho_i(c)$ is temperature insensitive and depends on the impurity concentration. This suggests that the impurity effect will become more important at lower temperatures. Referring the Born approximation [10], $\rho_i(c) \propto c(\Delta Z)^2$, where c is the impurity concentration and ΔZ the difference between the ionic charges of the solvent and solute atoms, it is noticeable that the impurity effect becomes smaller when the solvent and solute metal atoms have similar ionic charges. For alloys with a common matrix and different alloying elements such as A-B and A-C, if B and C have similar charges, then the difference in the thermal conductivity of the two alloys will be small.

6.2.1 Bruggeman Model

Bruggeman [11] developed a method of averaging to obtain the thermal conductivity of a heterogeneous phase mixture. Landauer [12] obtained the same result for a binary metallic mixture that had a random distribution of different phases. The Bruggeman model has been proved to be the reliable method to the purpose by many authors [13 – 16]. The formula for the mixture thermal conductivity of a two-phase mixture was given as follows:

$$k = \frac{1}{4}\left[A + \left(A^2 + 8k_1k_2 \right)^{\frac{1}{2}} \right] \tag{8}$$

where $A=(3v_1 - 1)k_1 + (3v_2 - 1)k_2$. Here k is the thermal conductivity, and v the volume fraction. For a two-phase mixture, k_1 and k_2 must be the conductivities of each phase at the phase boundaries contacting the two phase, which means they also have some impurity effects in them.

The Bruggeman scheme has been proved to be the most accurate when applied to "composites" of heterogeneous phases [13 – 16]. For the solid solution cases, however, it significantly overpredicts because it does not fully appreciate the impurity effects. Therefore, the Bruggeman equation applying to a solid solution phase is considered to provide the upper limit of the thermal conductivity.

6.2.2 Ternary Solid Solution Model

Consider the ternary solid solution that is composed of A, B and C with $x_C < x_B << x_A$, where x is the atom fraction. For instance, consider an ATW fuel, which is composed of 85at%Zr–10at%Pu–5at%Am. Since A is the major component playing the dominant role, addition of C in A-B alloy, in this case Am in the Zr-Pu alloy, conserving the total impurity content the same, is replacing impurity B atoms with C atoms in the crystalline lattice of A. If the perturbation in the A crystalline lattice caused by C atoms is slightly greater than that of B atoms, the thermal conductivity of A-B-C will decrease from that of A-B. If C atoms completely replace B atoms, then the thermal conductivity becomes that of A-C. From this, it is expected that the thermal conductivity of the ternary alloy will decrease monotonically, $k_{A-C} \le k_{A-B-C} \le k_{A-B}$; there is no minimum between two bounding values, which does not hold for the binary solid solution cases. In this context, if the third element has similar size and valence to the major component, it does not penalize the alloy thermal conductivity additionally.

The thermal conductivity of ternary A-B-C alloy modeled in this manner [17–19] has the following relationship,

$$k_{A-B-C} = k_{A-B}\, v_{A-B}{}^2 + k_{A-C}\, v_{A-C}{}^2 + 4 v_{A-B} v_{A-C} \frac{k_{A-B} k_{A-C}}{k_{A-B} + k_{A-C}} \qquad (9)$$

where v is the volume fraction. The subscript denotes the corresponding alloy.

It is noticeable that, if $k_{A-B} \approx k_{A-C}$, Eq.(9) simply reduces to k_{A-B}.

6.3 Zr-U Alloy

After Touloukian reviewed and summarized the thermal conductivity data of U-Zr alloys [1], Takahashi et al. [2] were the only authors to report the measured data. Both data sets revealed that the alloy thermal conductivity is lower than the simple interpolation values between U and Zr. This is attributed to the impurity effects discussed in the previous section. This suggests that the alloying effects need to be included in the correlation instead of the simple interpolation of elemental data.

A correlation to predict the thermal conductivity of U-Zr alloys for U-rich (U > 50 wt%) cases has been developed at ANL [20]. This correlation, however, is not directly applicable to the ATW fuel cases where the Zr content is beyond the limit of the correlation. Including all the U-Zr data from Touloukian and Takahashi [1,2], and the Zr data from Fink [3], a new correlation, applicable to any Zr content, is produced as follows:

$$k_{Zr-U} = \left(1 - \sqrt{1 - x_{Zr}}\right) k_{Zr} + \sqrt{1 - x_{Zr}} \left\{ x_{Zr}\, k_{c,U} + \left(1 - x_{Zr}\right) k_U \right\} \qquad (10)$$

where x_{Zr} is the Zr weight fraction, k_U is the thermal conductivity of uranium given by Eq.(1), k_{Zr} the thermal conductivity of Zr given by Eq.(2), and $k_{c,U}$ is a thermal conductivity correction due to the alloying effect. $k_{c,U}$ was obtained by fitting the data to Eq.(10) to yield

$$k_{c,U} = -102.0 + 200.1\, x_{Zr} - 109.2\, x_{Zr}^{\,2} + 9.435\times10^{-3}\, T + 3.459\times10^{-5}\, T^2 - 0.02093\, x_{Zr}\, T$$

The standard error of estimate for data fitting was 1.29 W/m-K. Eq.(10) is applicable to any Zr content with good predictions. Fig.6-2 compares the results predicted by Eq.(10) and the recommended data compiled by Touloukian [1]. For the thermal conductivity of Zr, Fink [3] data were adopted. Generally, the prediction results are very consistent with the data. The thermal conductivity curves as a function of temperature for U-rich alloys are mostly that of U (shown in (a)) and Zr-rich alloys take that of Zr.

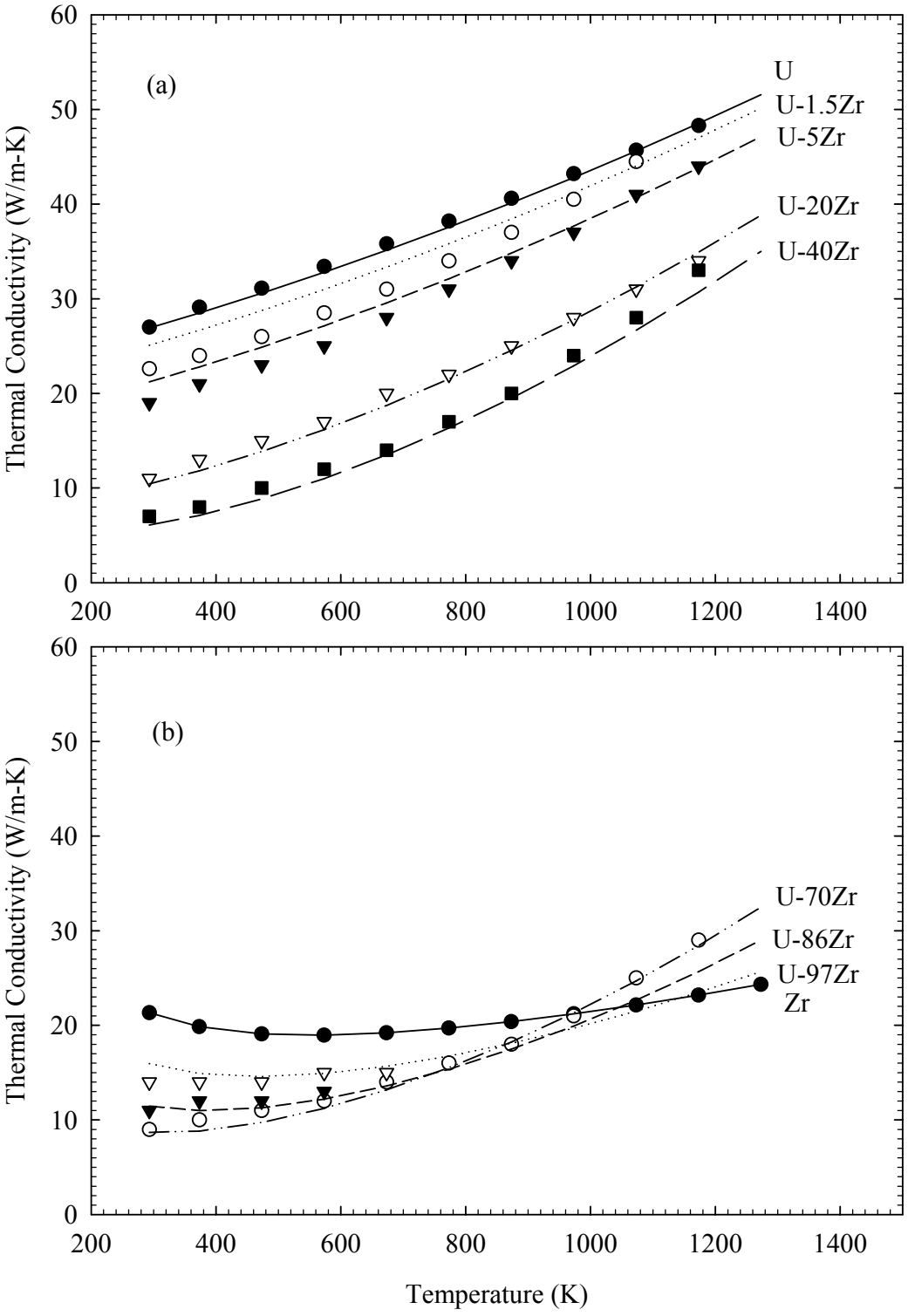

Fig.6-2 Comparison between correlation predictions (lines) and data (symbols) from Touloukian [1] and from Fink [3]. (a) U-rich Zr-U alloys, (b) Zr-rich Zr-U alloys.The coefficient in front of Zr designates the weight percent of Zr in the alloy.

6.4 Zr-Pu Alloy

No measured data for thermal conductivity of Zr-Pu alloy is available in the literature, and estimates have to be made. The thermal conductivity of the alloy is modeled for four separate phase regions, namely, δ-Pu, α-Zr, δ-Pu+α-Zr and (ε-Pu, β-Zr) solid solution phases.

6.4.1 δ-Pu phase

The δ-Pu phase has a high solid solubility for Zr; up to about 40 wt% Zr can make solid solution into the δ-Pu without producing a new phase.

In order to estimate the effect of Zr dissolving into the δ-Pu, an alloy that has the similar alloying behavior must be used. γ-U phase in U-Mo alloy is close to this purpose; it has also a cubic structure and a wide range of Mo solid solubility, up to ~20 wt% Mo.

The thermal conductivity data of U-Mo were available from Refs. 1, 21 – 23. Among these, only data from Refs. 21 and 23 dealt with the γ-U phase. The decrease in the thermal conductivity of the γ-U as a function of Mo content was correlated. Assuming that Zr dissolution in the δ-Pu also has the same effect as Mo does in the γ-U, the decrease correlation was scaled down by the ratio of $k_{\delta\text{-Pu}}/k_{\text{U}}$. As a result, the thermal conductivity correlation for the Zr-dissolved δ-Pu phase was obtained as

$$k_{\delta-Pu(Zr)} = \left(1-\sqrt{1-x_{Pu}}\right)k_{\delta-Pu} + \sqrt{1-x_{Pu}}\;\; k_{c,Zr} \tag{11}$$

where x_{pu} is the Pu weight fraction and $k_{\delta\text{-Pu}}$ is given by Eq.(2). $k_{\text{c,Zr}}$ was obtained as

$$k_{c,Zr} = 29.469 - 118.811\, x_{Pu} + 88.893\, x_{Pu}{}^{2} + 0.0117\, T + 1.922\times10^{-5}\, T^{2} - 0.00716\, x_{Pu}\, T$$

The valid temperature range is between 540 and 870 K.

6.4.2 α-Zr phase

Similar to the δ-Pu phase for Zr, the α-Zr phase also has a high solubility for Pu; the α-Zr phase can accommodate up to ~20 wt% Pu. The same argument as for the Pu-rich side is made for this phase too. As a result, the thermal conductivity correlation for this phase takes an identical form as

$$k_{\alpha-Zr(Pu)} = \left(1-\sqrt{1-x_{Zr}}\right)k_{Zr} + \sqrt{1-x_{Zr}}\,k_{c,Pu} \tag{12}$$

where $k_{c,Pu}$ is given by

$$k_{c,Pu} = 30.57 - 82.301\,x_{Zr} + 71.456\,x_{Zr}^{\ 2} + 0.01895\,T + 8.111\times10^{-6}\,T^2 - 0.02453\,x_{Zr}\,T$$

6.4.3 δ-Pu + α-Zr

In this phase, the alloy is a mixture of two separate phases: δ-Pu and α-Zr. Then, the alloy thermal conductivity can be modeled by the Bruggeman equation, Eq.(8). The weight fractions of each phase, δ-Pu or α-Zr, were calculated by the lever rule. And then, they are converted to the volume fractions by the following formula

$$v_{\delta-Pu} = \frac{\rho_{\alpha-Zr}\,x_{\delta-Pu}}{\rho_{\delta-Pu} - \left(\rho_{\delta-Pu} - \rho_{\alpha-Zr}\right)x_{\delta-Pu}}, \tag{13a}$$

$$v_{\alpha-Zr} = 1 - v_{\delta-Pu} \tag{13b}$$

where x is the weight fraction and ρ is the density of each phase. The temperature-dependent densities of δ-Pu and α-Zr were used.

Fig.6-3 shows the thermal conductivity of the Zr-Pu alloy as a function of the Zr concentration for the δ-Pu, α-Zr and δ-Pu + α-Zr phases. The temperature range of above 540 K

was used. Each isothermal line is generated by three composite equations given by Eqs. (8), (11) and (12).

6.4.4 (ε-Pu,β-Zr) solid solution

For this higher temperature phase, the thermal conductivity correlation of Zr-U, Eq.(10), is considered to be applicable. Prediction results by Eq.(10) for only high temperatures above 873 K were scaled down to fit the correlation. The correlation is analogous to Eq.(10), namely,

$$k_{\varepsilon-Pu,\beta-Zr} = \left(1-\sqrt{1-x_{Zr}}\right)k_{Zr} + \sqrt{1-x_{Zr}}\ \left\{x_{Zr}\ k_{c,Pu,Zr} + \left(1-x_{Zr}\right)k_{\varepsilon-Pu}\right\} \tag{14}$$

where k_{zr} is given by Eq.(2), $k_{\varepsilon\text{-Pu}}$ by Eq.(3b), and

$$k_{c,Pu,Zr} = -98.806 + 147.895\ x_{Zr} - 26.883\,x_{Zr}^{\ 2} + 0.0512\ T + 8.699\times10^{-6}\ T^2 - 0.0601\ x_{Zr}\ T$$

In Fig.6-4, the thermal conductivity of Pu-Zr at temperatures above 873 K is shown. The alloying effect is salient at low temperatures, but diminishing at high temperatures.

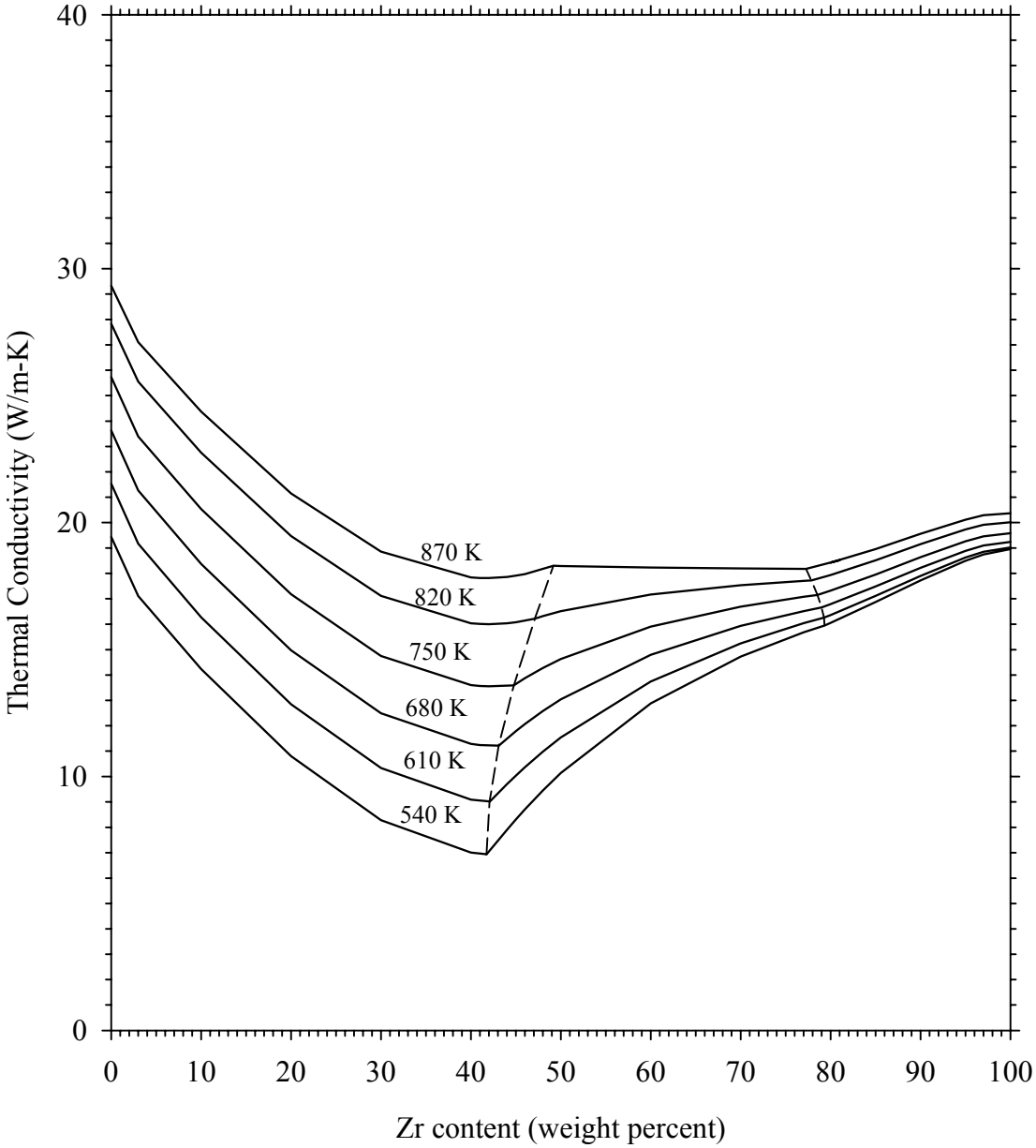

Fig.6-3 Thermal conductivity of Zr-Pu alloys versus Zr content at the temperature range of 540 – 870 K.
The dashed lines indicate the phase transitions.

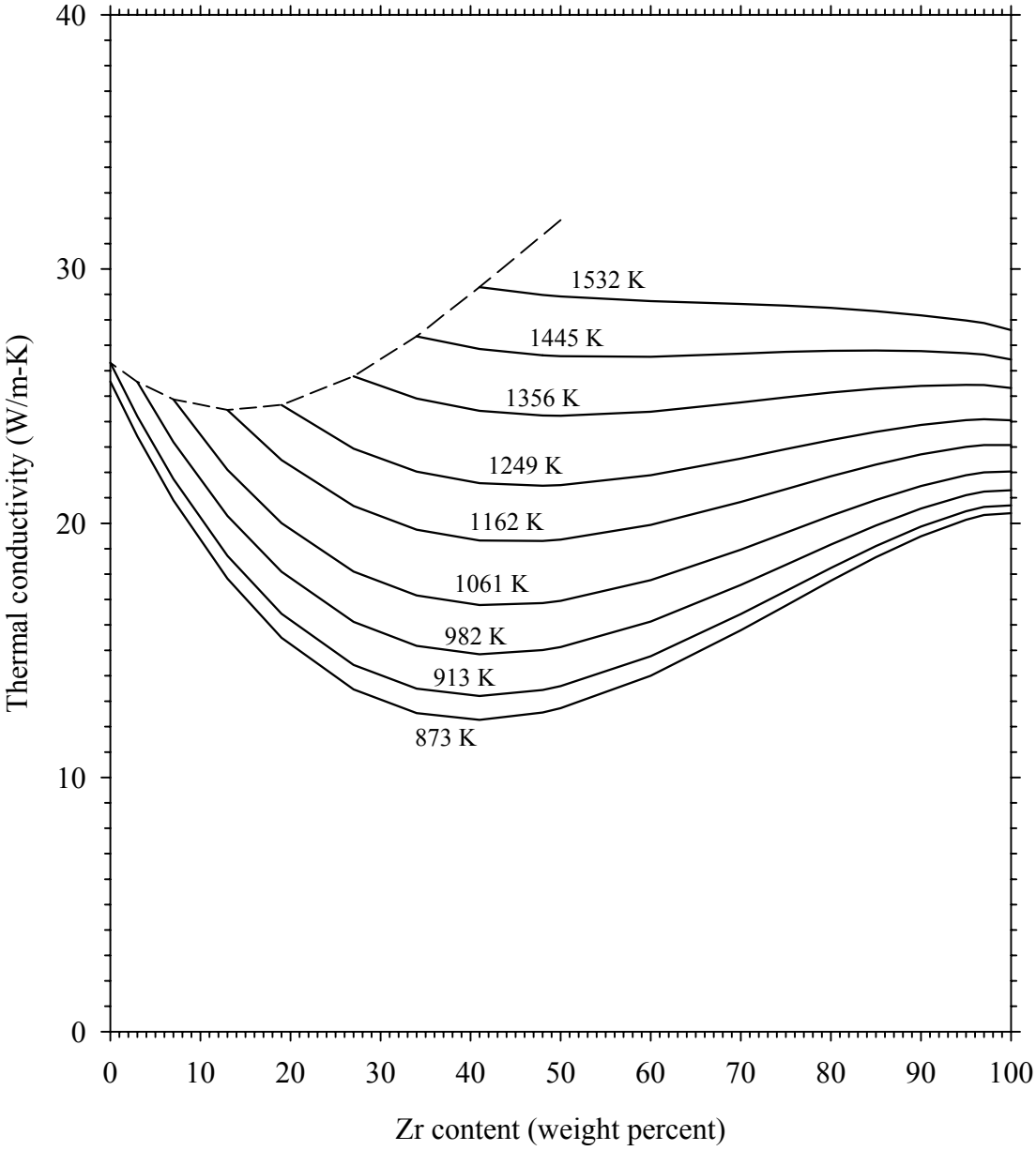

Fig.6-4 Thermal conductivity of Zr-Pu alloy versus Zr content
at the temperature range of 873 – 1532 K.
The dashed line shows the phase transition (solidus line).

6.5 Zr-Pu-Am and TRU-Zr Alloys

As discussed in subsect.6.2, the thermal conductivity of Zr-Pu-Am alloy is provided by Eq.(9) as

$$k_{Zr-Pu-Am} = k_{Zr-Pu}\, v_{Zr-Pu}{}^{2} + k_{Zr-Am}\, v_{Zr-Am}{}^{2} + 4 v_{Zr-Pu} v_{Zr-Am} \frac{k_{Zr-Pu} k_{Zr-Am}}{k_{Zr-Pu} + k_{Zr-Am}} \qquad (9)$$

The thermal conductivity of the Zr-Pu binary alloy has been established in subsect.6.4. Only information for Zr-Am must be known. The thermal conductivity of this alloy, however, has never been measured. This restricts the use of Eq.(9). Therefore, the thermal conductivity of the Zr-Pu alloys is recommended for the Zr-Pu-Am alloy at the present time. In practice, Pu content should be increased according to the amount of Am.

The TRU fuel composition is approximately 63 w%(Zr)+31 w% (Pu) + 4 w% (Am) + 2 w% (Np) + other actinides.

Addition of up to 8 w% Np in Pu had almost negligible effect on the thermal conductivity of Pu even at room temperature [24]. This suggests that the impurity effect by the existence of the small amount (~2 w%) Np and other actinides typical in TRU-Zr fuel can be negligible at the fuel operating temperatures. As a result, the Zr-Pu-Am alloy correlations given in Eq.(9) or Zr-Pu correlations given in Eqs.(11)-(14) are also recommended at the present time.

6.6 References for Section 6

1. Y. S. Touloukian, et al., Thermophysical Properties of Matter, vol. 1, IFI/Plenum, New York (1970).
2. Y. Takahashi, M. Yamawaki and K. Yamamoto, J. Nucl. Mater., 154, 141 (1988).
3. J. K. Fink and L. Leibowitz, J. Nucl. Mater. 226, 44 (1995).
4. T. A. Sandenaw, in The metal Plutonium, ed., A. S. Coffinberry and W. N. Miner, Univ of Chicago Press, pp.152 – 156 (1961).
5. R. Schenkel, Solid State Communications, 23, 389 (1977).
6. W. Muller, R.Schenkel, H.E.Schmidt, et al., J. Low Temp. Phys., 30, 561 (1978).
7. J.A. Lee, in Progress in Nucl. Energy, Series v: Metallurgy and Fuels, III, pp.453-467 (1961).
8. S. Tamura, J. Mater. Sci. Lett., 15, 1752 (1996).
9. A. Matthiessen and C. Vogt, Annal, Physik. (Leipzig), 122, 19 (1864).
10. K. Schroder, CRC Handbook of Electrical Resistivities of Binary Metallic Alloys, CRC, Boca Raton, FL (1983).
11. D. A. G. Bruggeman, Annal. Physik., 24, 636 (1935).
12. R. Landauer, J. Appl. Phys., 23, 779 (1952).
13. Z. Hashin and S. Shtrikman, J. Appl. Phys., 33, 3125 (1962).
14. J.P. Stora, Nucl. Technol., 17, 225 (1973).
15. T.J. Shankland and A.G. Duba, Geophys. J. Int., 103, 25 (1990).
16. F.D. Stacey and O.L. Anderson, Phys. Earth and Planetary Interiors, 124, 153 (2001).
17. G.N. Dul'nev and Yu.P. Zarichnyak, Thermal conductivity of mixtures and composition materials [in Russian; Teploprovodnost' Smesei I Kompozitsionnykh materialov], Energiya, Leningrad (1974).
18. Yu.P. Zarichnyak and T.A. Lisnenko, Izv. Vyssh. Uchebn. Zaved., Priboroster., 19, No.5 (1976).
19. Yu.P. Zarichnyak and T.A. Lisnenko, Inzhenerno-Fizicheskii Zhurnal (Byelorussian SSR), 33, 642 (1977); Journal title of translation: Journal of Engineering Physics (USA) (1978).
20. G.L. Hofman, unpublished information, Argonne National Laboratory (1985).
21. T. Matsui, T. Natsume and K. Naito, J. Nucl. Mater., 167, 152 (1989).

22. H.A. Saller, R.F. Dickerson, A.A. Bauer and N.E. Daniel, Battelle Memorial Institute, Report BMI-1123 (1956).
23. E.L. Francis, UKAEA Report IGR-R/R-287 (1958).
24. K.A. Long, Plutonium and other actinides, Eds. H. Blank and R. Lindner, North-Holland Pub. Co., Amsterdam, pp.449–457 (1976).

Section 7 Diffusion Coefficient

7.1 Elemental Self Diffusion

7.1.1 Plutonium

The diffusion coefficient is expressed as follows:

$$D = D_o \exp\left(-\frac{Q}{RT}\right) \tag{1}$$

where D_o is the pre-exponential factor in cm^2/s, Q the activation energy in J/mole, and R the gas constant, equal to 8.314 J/mole-K.

The self-diffusion coefficient of plutonium has been determined in the ε-phase by Dupuy [1,2] and in the δ-and γ-phases by Tate [3,4]. The data obtained are tabulated in Table 7-1. The self-diffusion coefficient of the δ-phase is approximately two orders of magnitude lower than that of the ε-phase. This is attributed to the fact that this phase has the closest packing structure of all the plutonium phases.

Table 7-1 Plutonium Self-diffusion Coefficient

Ref.	Phase	D_o cm^2/s	Q J/mole
1	ε	2×10^{-2}	7.74×10^{4}
2	δ	4.5×10^{-3}	9.96×10^{4}
3	γ	2.1×10^{-5}	6.99×10^{4}

7.1.2 Zirconium

The self-diffusion data for the polycrystalline α-Zr are available by several authors [5-7]. The three data sets are consistent among themselves. The empirical formula given by Marzocca and Povolo [5] is recommended here.

$$D = \frac{D_1 D_2}{D_1 + D_2} \tag{2}$$

where D_1 is for high temperature, given by $D_1 = 1.59 \times 10^{-9} \exp\left(-111.87 \times 10^3 / RT\right)$ cm^2/sec and for low temperature $D_2 = 1.08 \times 10^5 \exp\left(-351.04 \times 10^3 / RT\right)$ cm^2/sec.

Willaime and Massobrio [8] obtained the self-diffusion coefficient in the β-Zr by fitting the measured data in the literature as $D_0 = 1.598 \times 10^{-11}$ cm^2/sec and $Q = 1.746 \times 10^5$ J/mole.

7.1.3 Other Minor Actinide Elements

No data on the self-diffusion of other minor actinides has been found in the literature. Schmitz [9] measured the diffusion coefficients of actinides in UO_2 at the temperature range of 1523 – 1873 K. The Schmitz data are tabulated in Table 7-2 for comparison.

Table 7-2 Diffusion of Actinides in Uranium Dioxide

Diffusing element	D_o cm^2/s	Q J/mole
U	0.9	4.35×10^5
Pu	0.2	4.10×10^5
Am	0.03	3.85×10^5

Although the Schmitz data are inapplicable directly to the metallic alloy fuels, the diffusion parameters of all actinides in UO_2 are close to each other.

7.2 Pu-Ga and Pu-Al Alloy Interdiffusion

Interdiffusion in the alloys of plutonium with gallium and aluminum, which are used for stabilizing the δ or ε phase, has been investigated [10-13]. Table 7-3 shows a comparison between the data from the literature. As seen in the pure plutonium self-diffusion, the interdiffusion coefficient in the δ-phase of Pu alloys is lower than that of the ε-phase alloy.

Table 7-3 Interdiffusion Coefficient of Pu Alloys

Additives and content (at%)	Phase	D_o cm^2/s	Q J/mole	Ref.
1 Ga	δ	0.1	1.39×10^5	9
3 and 7.9Ga	δ	1.3	1.56×10^5	10
3 and 9.1 Al	δ	2.25×10^{-4}	1.07×10^5	11
0.48 to 2.6 Ga	ε	5.1×10^{-4}	5.52×10^4	12

7.3 Pu-Zr Alloy Interdiffusion

Zanghi and Calais [14] measured the self-diffusion coefficient of Pu in the Pu-40at%Zr alloy for the temperature range of 953 – 1113 K. They found that D_0=0.04 cm^2/sec and Q=1.241×10^5 J/mole.

The interdiffusion in the (ε-Pu,β-Zr) solid solution has been studied by Remy et al. [15]. The interdiffusion coefficient, $\widetilde{D} = \widetilde{D}_o \exp(-Q/RT)$, was measured as a function of temperature and composition as shown in Table 7-4.

The intrinsic diffusion coefficients D_{pu} and D_{Zr} were determined by solving the following set of equations with the measured data

$$\widetilde{D} = N_{Pu} D_{Zr} + N_{Zr} D_{Pu} \tag{3a}$$

and

$$D_{Pu} / D_{Zr} = J'_{Pu} / J'_{Zr} \tag{3b}$$

where J'_{Pu} and J'_{Zr} are the integrated fluxes during the diffusion anneal across the marked plane, N_{Pu} and N_{Zr} the atomic fractions of the components, and D_{Pu} and D_{Zr} the diffusion coefficients of the components in the alloy. As a result, it was possible to obtain D_{pu} and D_{Zr}. As shown in Table 7-5 and Fig.7-1, Pu has a larger diffusivity than Zr.

Table 7-4 Interdiffusion Coefficient in (ε-Pu,β-Zr)

Pu content (at%)	Temperature (K)	$\widetilde{D}$ (cm^2/sec)	Q (J/mole)	$\widetilde{D}_0$ (cm^2/sec)
20	1173	4×10^{-9}		
20	1123	2×10^{-9}		
20	1073	8.4×10^{-9}		
20	1023	2.7×10^{-9}	1.84×10^{5}	7×10^{-1}
30	1123	2.8×10^{-9}		
30	1073	1.5×10^{-9}		
30	1023	6.2×10^{-9}		
30	973	2.7×10^{-9}	1.44×10^{5}	1×10^{-2}
40	1173	5×10^{-9}		
40	1083	2.9×10^{-9}		
40	1073	2.5×10^{-9}		
40	1023	1.4×10^{-9}		
40	973	6.8×10^{-10}	1.19×10^{5}	1.5×10^{-3}
50	1083	5.2×10^{-9}		
50	1073	4.9×10^{-9}		
50	1023	2.9×10^{-9}		
50	973	1.5×10^{-9}	9.83×10^{4}	2.5×10^{-4}
60	1083	8.2×10^{-9}		
60	1023	5.2×10^{-9}		
60	973	3×10^{-9}	7.74×10^{4}	9×10^{-5}

Table 7-5 Intrinsic Diffusion Coefficients of Pu and Zr in Pu-Zr Alloys

for the Pu Concentration Range of 20 – 50 at%

	Pu Concentration (at% Pu)	Q (J/mole)	D_0 (cm^2/sec)
D_{Zr}	20	1.88×10^5	8×10^{-1}
	30	2.05×10^5	7.5×10^{-1}
	40	1.67×10^5	2×10^{-1}
	50	1.21×10^5	1.5×10^{-4}
D_{Pu}	20	1.84×10^5	6×10^{-1}
	30	1.76×10^5	4×10^{-1}
	40	1.13×10^5	1×10^{-3}
	50	1.17×10^5	3×10^{-2}

For the α-phase Zr-Pu alloys with Pu content up to 3at%, the interdiffusion coefficient was reported at the temperature range of 973 – 1073 K [16]. The data are tabulated in Table 7-6.

Table 7-6 Interdiffusion Coefficients of Pu-Zr Alloys

Pu Content (at% Pu)	Q (J/mole)	$\widetilde{D}_0$ (cm^2/sec)
0.15–0.3	2.26×10^5	0.1
1.5–3.0	2.72×10^5	11.1

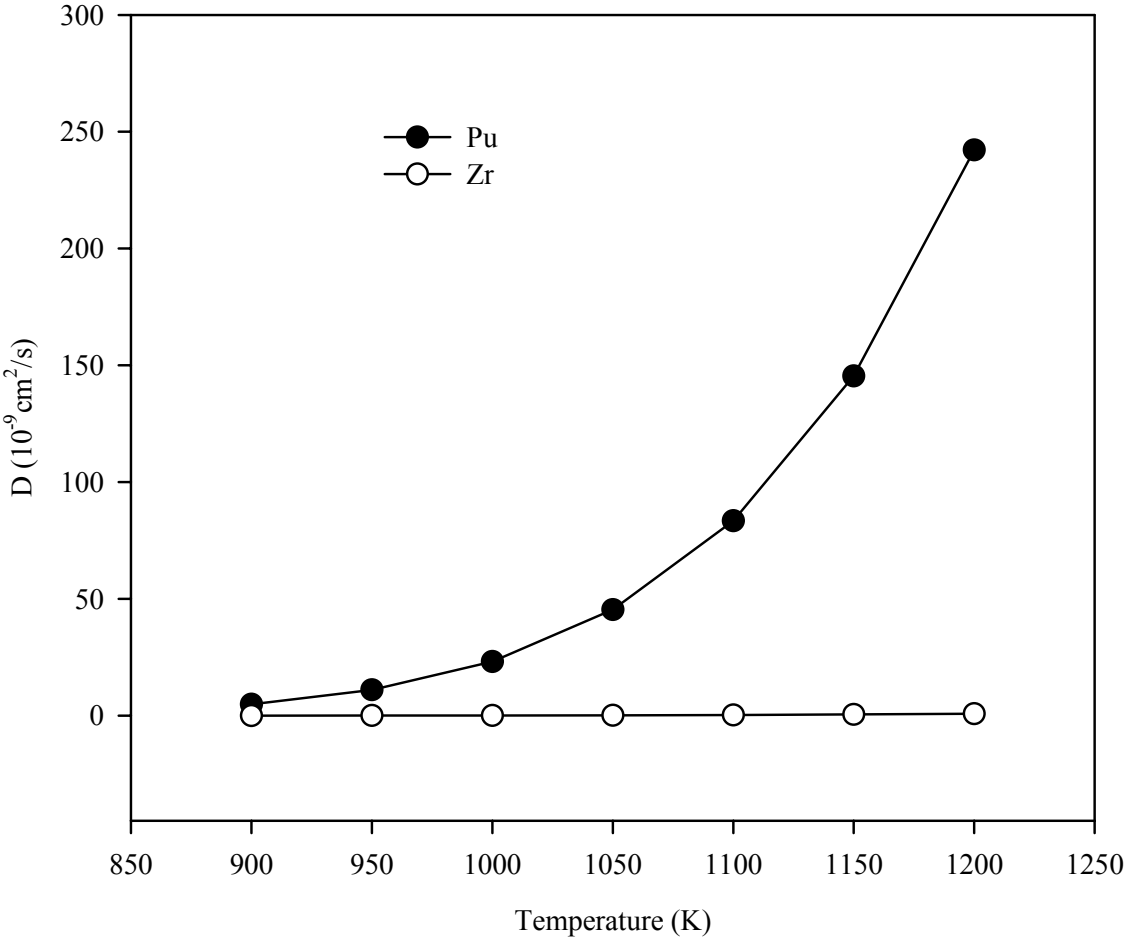

Fig.7-1 Intrinsic diffusion coefficients of Pu and Zr in (ε-Pu,β-Zr) solid solution at 1000 K for 50 at% (Pu) + 50 at% (Zr).

7.4 Constituent Redistribution

7.4.1 U-Pu-Zr Alloy

Constituent redistribution in metallic fuel occurs due to solid-state diffusion under thermal and thermodynamic driving forces, and it is enhanced by irradiation. As a result, originally homogeneous fuel turns into an inhomogeneous alloy. The inhomogeneity in a metallic nuclear fuel causes phase transformation, reduction in solidus temperature, and local enrichment in fissile atoms, all of which lead to variations in fuel physical and mechanical properties and, consequently, in fuel performance such as abnormal swelling and gas release.

For metallic nuclear fuels, this phenomenon was observed as early as 1960s. Murphy and co-workers [17] reported that their irradiated U-Pu-Zr fuel rods showed three concentric microstructural zones containing different Zr and U concentrations in each zone. They suggested that the change in composition might be due to only Zr migration. Later Harbur et al. [18] found that out-of file tests could also cause constituent redistribution, which means that only thermal gradient could generate a driving force large enough for measurable amount of constituent redistribution. During the course of the IFR (Integral Fast Reactor) fuel development, more irradiation tests were conducted for U-base alloy fuels to reveal this phenomenon more in detail [19-22]. The observations from these tests confirmed some features known before and revealed new facts. The following is a brief summary of the observations from the IFR fuel tests.

- The postirradiation test fuels commonly showed three distinctive concentric zones: Zr enriched center zone, Zr depleted intermediate zone and slightly Zr enriched outer cooler zone. U migrated in the direction opposite to Zr. Pu showed a negligible change. The annular zone structure was due not only to the difference in porosity but also to the local composition changes. Microprobe scan signals of typical constituent redistribution profiles are plotted in Fig.7.2 by taking data from Ref.20.

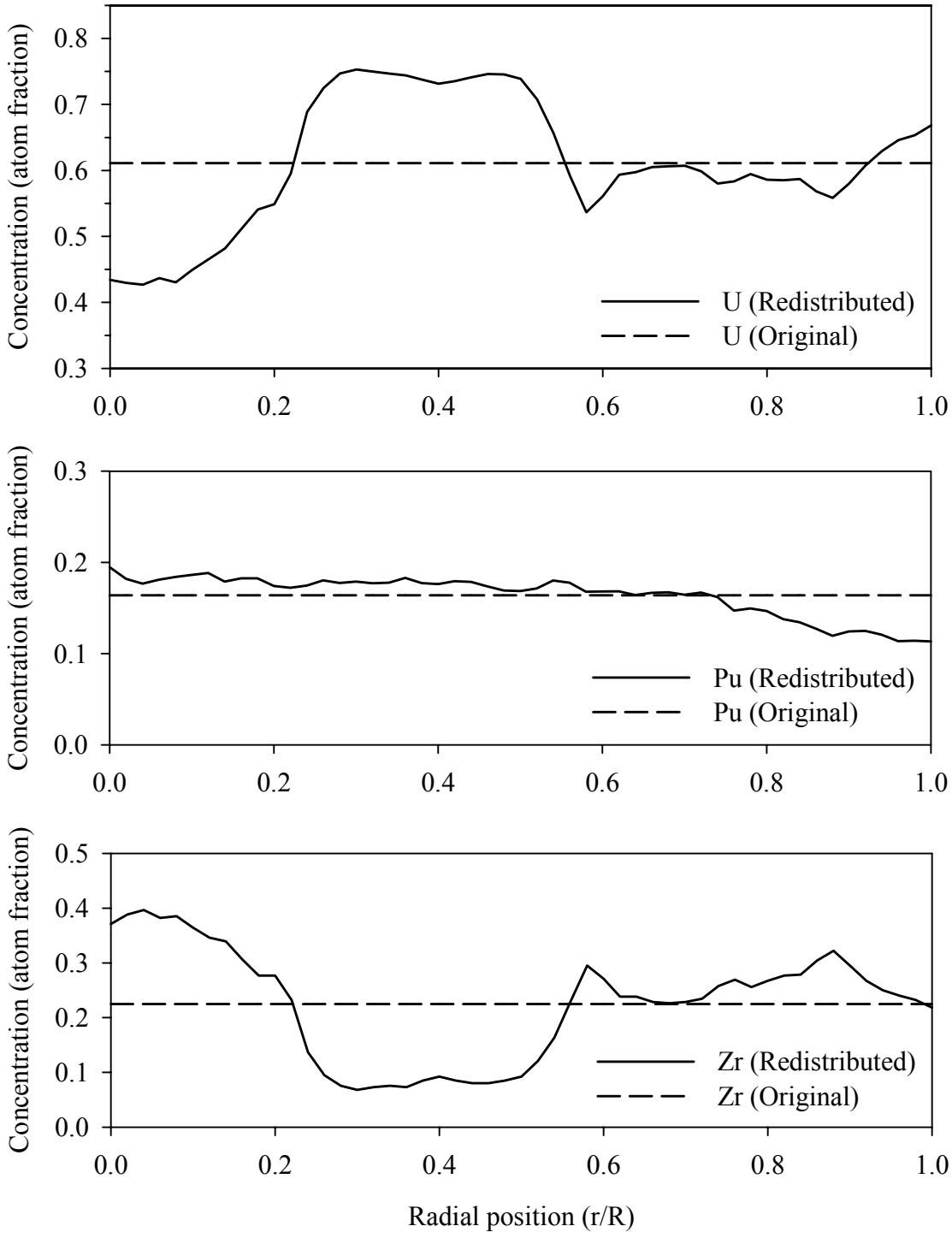

Fig.7-2 Contituent redistribution profiles of U-Pu-Zr fuel at 1.9 at% burnup [20]

- Although Pu showed negligible migration in U-Pu-Zr fuel, it enhanced Zr and U migration when its concentration was greater than 8wt%. As noticed by Porter et al. [19], this may be related to the high gaseous swelling rate in the high-Pu content fuels. The high bubble growth was commonly observed in the high-Pu fuels. The high temperature in the high porosity region is considered to provide the favorable condition for constituent migration. This hypothesis is supported by the observation that constituent redistribution tends to saturate at burnup of ~6 at%, where gas swelling is restricted by external stress. The Pu contribution can be estimated by comparing the migration data for U-Pu-Zr fuel with those for U-Zr fuel. The migration in U-Pu-Zr fuel was faster than U-Zr fuel. The level of migration achieved at 5 at% burnup for the U-Zr fuel could be achieved at 1.9 at% burnup in the U-Pu-Zr fuel (see figures 1 and 2 in Ref.20).

- The major driving force for constituent migration is the occurrence of a multi-phase regime across the fuel. During fuel irradiation, the fuel center region (the hottest region) is occupied by the γ phase, the intermediate region by the $\gamma + \zeta$, and the outer region by the $\delta + \zeta$. The solubility of Zr in these phases varies distinctively. Therefore, the chemical activities of fuel constituents change radially and create the driving force for diffusion. Irradiation of fuel is known to enhance migration by increasing diffusivity of the migrating species where more point defects become available for diffusion.

7.4.2 Zr-TRU Alloy

An analysis of the interdifusion processes of the TRU-Zr multicomponent system is not available in the literature mainly because of its complexity. Even in the simplest case of one-dimensional diffusion in a three-component system, the system of equations could not be rigorously solved although the diffusion coefficients were independent of composition and the Kirkendall effect was neglected [23]. There has been no constituent redistribution study for Zr-TRU alloys either.

There are some studies on the redistribution behavior of U-base metallic alloys including some minor actinides [24]. From ex-reactor thermal tests, Kurata and co-workers found that Np migrated from the hot and cold regions to the intermediate region in the U-19Pu-10Zr-2Am-3Np-3.6Nd-1.2Ce-0.2Y system. Here the coefficient in front of the element designates the concentration of the element in weight percent. The inclusion of MA (minor actinide) and RE (rare earth) in the U-Pu-Zr alloy tended to drive U and Zr out of the intermediate temperature region and enriched Pu, Np, Am and RE. The expelled U and Zr from the region migrated to the hotter region. This finding was contradictory because U was known to move the opposite direction of Zr. In general, Am did not show a remarkable migration at temperatures below 1020 K.

The postirradiation data of the minor actinide (MA) burning experiments in the EBR-II were available where U-Pu-Zr-MA fuels were irradiated [25]. Fig.7-3 shows a postirradiation optical image and constituent redistribution profiles. As shown in the figure, these tests revealed that U, Pu, and Zr behaved the same way as IFR U-Pu-Zr fuel, regardless of the MA inclusion. The Am signal slightly increased at the fuel center and fuel outer region. This suggests that Am migrated from the fuel intermediate region to the fuel center accompanying Zr movement, and followed U from the intermediate region to the outer region. It is also remarkable that Am precipitated in the high porosity regions, showing large peaking signals exactly where U, Pu, and Zr signals drop. There is no Am peak in the intermediate region where no large pore is observed. Np, however, showed a virtually uniform and flat signal, indicating negligible migration and no precipitation behavior like Am.

Theses alloy systems, U-Pu-Zr including several percent of MA, however, are different from the current AAA fuel design options, where Zr is the major constituent. Therefore, the simple extrapolation from the knowledge of U-base alloys to Zr-base alloys may not be accurately applicable to the AAA fuel. Consequently, future works are recommended to study constituent redistribution of Zr-TRU alloys theoretically as well as experimentally.

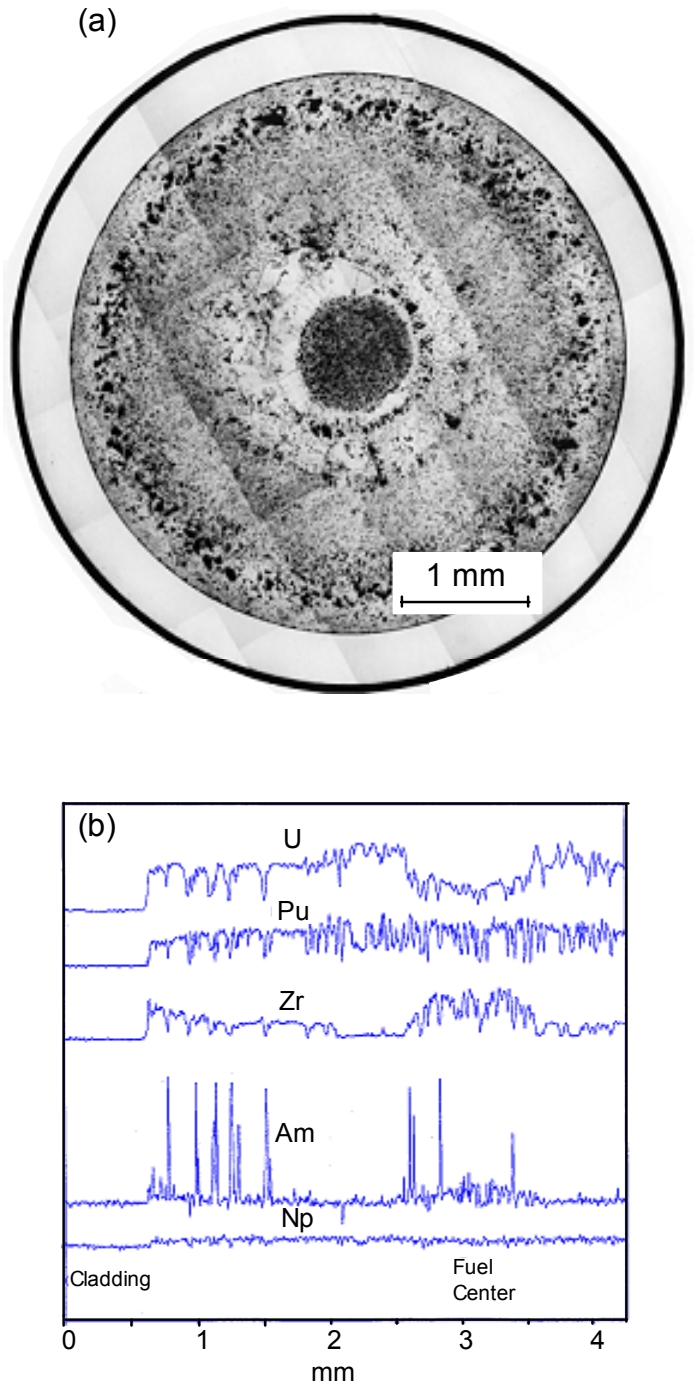

Fig.7-3 Postirradiation results of X501 test: (a) Postirradiation optical image, (b) Wavelength dispersive spectroscopy (WDS) signals. The fuel was composed of U-20.2Pu-9.1Zr-1.2Am-1.3Np (wt%) and irradiated to ~6at% burnup [25].

7.5 References for Section 7

1. M. Dupuy and C.R. Head, CEA-CEN/FAR, Fontenay-aux-Roses, France, Compt. Rend., Ser. C, 236, 35 (1964).
2. D. Calais and J.A. Cornet, Memoires Scientifiques Rev. Metallurg, 69, 493 (1972).
3. R.E. Tate and E.M. Cramer, Trans. Am. Inst. Met. Engr., 230, 639 (1964).
4. R.E. Tate and G.R. Edwards, Proc. Symposium on Thermodynamics with Emphasis on Nuclear Materials and Atomic Transport in Solids, IAEA, Vienna (1966).
5. A.J. Marzocca and F. Povolo, J. Mater. Sci. Letters, 6, 431 (1987).
6. W. Frank, Defect and Diffusion Forum, 66-69, 387 (1989).
7. J. Hotvath, F. Dyment and H. Mehrer, J. Nucl. Mater., 126, 206 (1984).
8. F. Willaime and C. Massobrio, Mat. Res. Soc. Symp. Proc., 209, 293 (1991).
9. F. Schmitz and R. Lindner, J. Nucl. Mater., 17(2), 259 (1965).
10. A.L. Rafalski, M.R. Harvey and D.N. Rietenberg, Trans. Am. Soc. Metals, 60, 721 (1967).
11. G.R. Edwards, R.E. Tate and E.A. Hakkila, J. Nucl. Mater., 25(3), 304 (1968).
12. R.E. Tate, G.R. Edwards and E.A. Hakkila, J. Nucl. Mater., 29(2), 154 (1969).
13. M.R. Harvey, J.H. Doyle, A.L. Rafalski and D.H. Riefenbere, J. Less-common Metals, 23(4), 446 (1971).
14. J. Zanghi and D. Calais, Plutonium and Other Actinides, Eds. H. Blank and R. Lindner, p.525 (1976).
15. C. Remy, M. Dupuy and D. Calais, J. Nucl. Mater., 34, 46 (1970).
16. J.C.Lauthier, A. Van Cracynest and D. Calais, J. Nucl. Mater., 23(1), 111 (1967).
17. W.F. Murphy, W.N. Beck, F.L. Brown. B. Koprowski and L.A. Neimark, Argonne National Laboratory, Report ANL-7602 (1969).
18. D.R. Harbur, J.W. Anderson and W.J. Maraman, Los Alamos Scientific Laboratory, Report LA-4512 (1970).
19. D.L. Porter, C.E. Lahm and R.G. Pahl, Metallurg. Trans. A, 21A, 1871 (1990).
20. G.L. Hofman, S.L. Hayes and M.C. Petri, J. Nucl. Mater., 227, 277 (1996).
21. R.G. Pahl, C.E. Lahm, R. Villareal, W.N. Beck and G.L. Hofman, Proc. Int'l Conf. on Reliable Fuels for Liquid Metal Reactors, Tucson, AZ, USA, Sept. 7-11, p.3-36 (1986).

22. R.G. Pahl, D.L. Porter, C.E. Lahm and G.L. Hofman, Metallurg. Trans. A, 21A, 1863 (1990).
23. G.B. Fedorov and E.A. Smirnov, Diffusion in Reactor Materials, Atomizdat Publishers, Moscow, 1978; Translated from Russian, U.S Dept. of Commerce, NTIS (1984).
24. M. Kurata, T. Inoue and C. Sari, J. Nucl. Mater., 208, 144 (1994).
25. M.K. Meyer, S.L. Hayes, D.C. Crawford, R.G. Pahl, and H. Tsai, Proc. ANS Conf. on Accelerator Applications in the New Millennium, Reno, NV, Nov.11-15 (2001).

Section 8 Elastic Constants

8.1 Modulus of Elasticity

8.1.1 Pu-Zr alloy

The dynamic modulus of elasticity of Pu-Zr alloys is not available in the literature. The data for element Pu and Zr can be found. The measured properties depend significantly on the fabrication history. For instance, carbon contamination during melting affects the measured data much.

Young's modulus for annealed Zr is tabulated in Ref.1 at the temperature range of 66 – 1233 K. Data for Zr were also taken from Ref.2. Two sets of data for crystal bar and sponge Zr were also available from Ref.3. These are compared in Fig.8-1. The data for the crystal bar Zr show the higher extreme whereas the data from Ref.1 show the lower extreme. The data from Ref.2 fall in the middle of the two extremes. The fabrication process of the specimen of Ref.1, however, is not known. Therefore, data from Ref.2 is selected in this report.

The data for Pu are available only from Ref.1. The available data are only up to the γ-to-δ phase transition temperature. Therefore, the values at higher temperatures are approximated by assuming that the value at the phase transition is continuous to the melting point. The data obtained are shown in Fig.8-2. As seen in the figure, the Young's modulus of Pu decreases abruptly as temperature increases. This behavior is entirely different from that of uranium.

There is no measurement available for Pu-Zr alloy in the literature. Nevertheless, the correlation fitting such as the one given in Ref.4 cannot be applicable either, because of the changes related to the allotropic phase transitions. Based on the data assessed above, the classical law of mixtures is recommended to obtain the elastic constant for the Pu-Zr alloys as a function of temperature and composition, i.e.,

$$E_{Pu-Zr} = \mathrm{v}_{Zr} E_{Zr} + (1 - \mathrm{v}_{Zr}) E_{Pu} \qquad (1)$$

where v is the volume fraction. The volume fraction can be derived from the weight fraction by the formula,

$$v_{Zr} = \frac{\rho_{Pu}\, x_{Zr}}{\rho_{Zr} - (\rho_{Zr} - \rho_{Pu}) x_{Zr}} \qquad (2)$$

where ρ is the density and x the weight fraction.

The values yielded by Eq.(1) are for 100 %TD alloys. Therefore, for alloys with porosity, another correction is needed. This is discussed below.

8.1.2 Porosity Correction

The elastic constant of a metal generally decreases as porosity increases. Hofman, et al. [4] developed a method to correct Young's modulus due to porosity introduction. They reduced the Young's modulus of the U-Zr alloys that contained porosity by multiplying the value of a 100 % dense metal with a correction factor. The same method is assumed applicable for the Pu-Zr alloys. Therefore, the modulus of elastic constant for the Pu-Zr alloys is given by

$$E = (1 - 1.2\, P)\, E_{100} \qquad (3)$$

where P is the porosity and E_{100} is the Young's modulus of the 100 % TD Pu-Zr alloys.

8.1.3 TRU-Zr Alloy

No measurement of the elastic constant for the TRU-Zr alloys is found at the present time. Therefore, the information for Pu-Zr alloy can be approximately used instead.

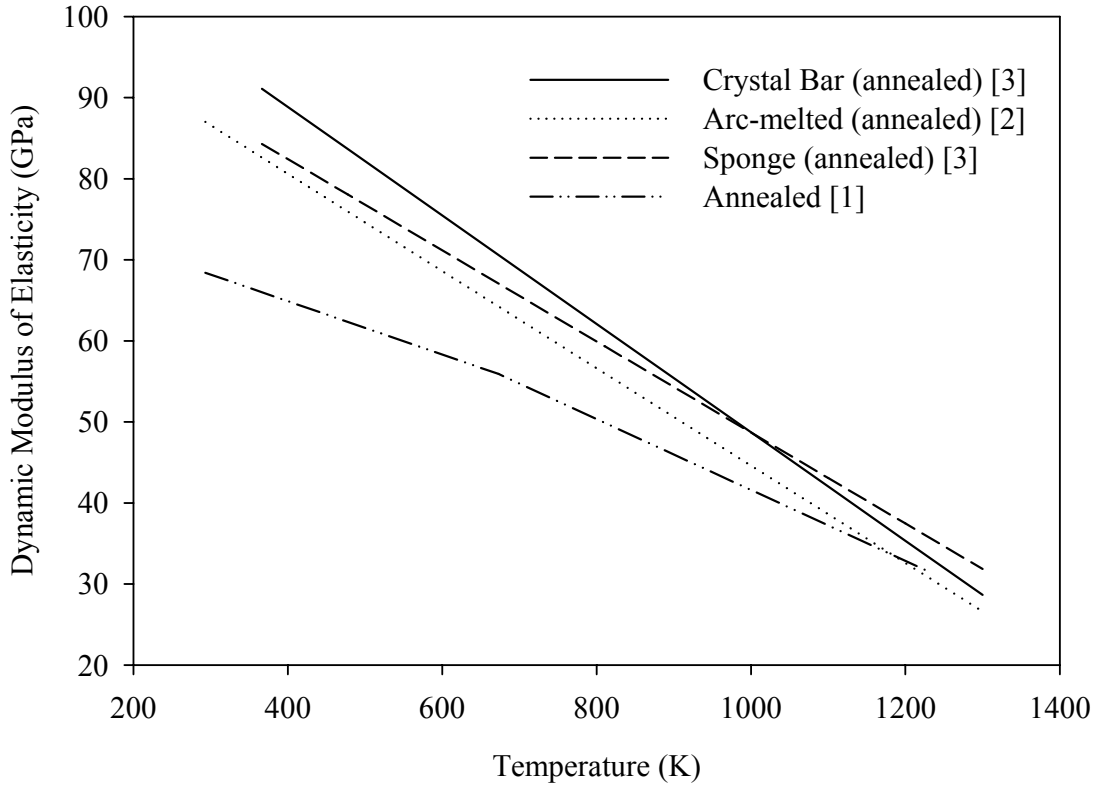

Fig.8-1 Dynamic modulus of elasticity of pure Zr

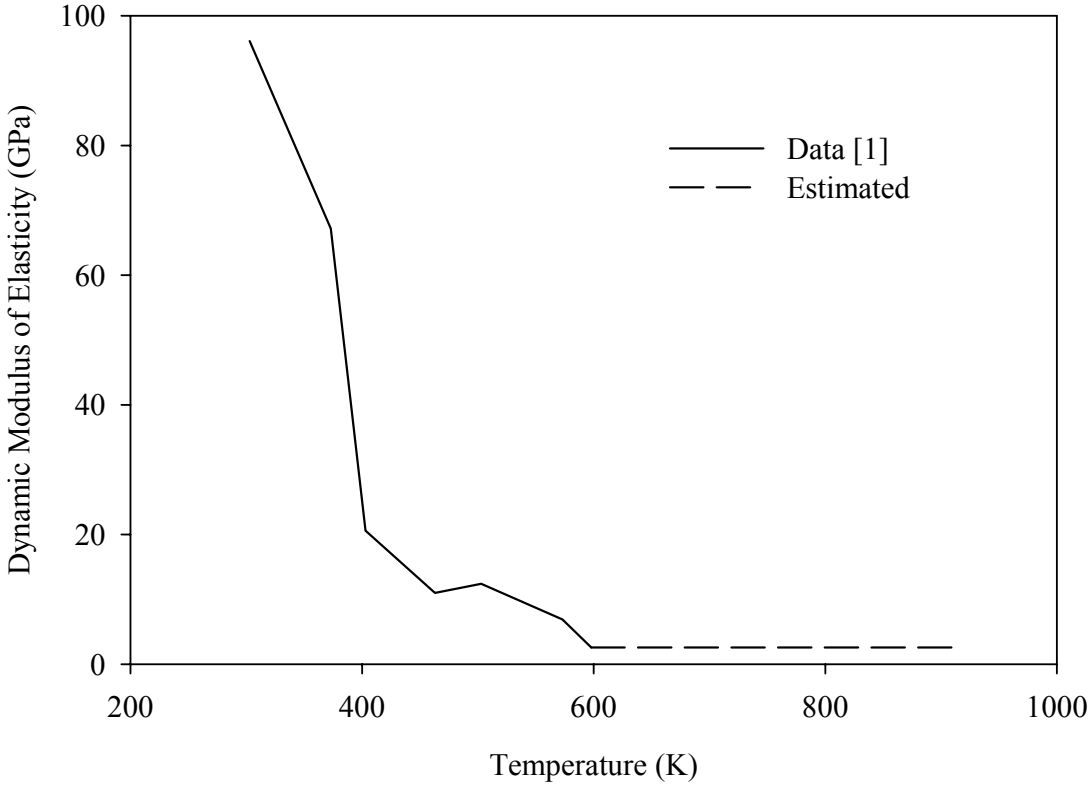

Fig.8-2 Dynamic modulus of elasticity of pure Pu

8.2 Poisson's Ratio

8.2.1 Pu-Zr alloy

In the literature, room temperature data for pure elements are available. At room temperature, the Poisson's ratio for crystal bar Zr is 0.33 and that for sponge Zr is 0.35 [5]. α-Pu has Poisson's ratio of 0.21, and U has 0.23 [1].

The Poisson's ratio of Pu-Zr is not reported at the present time. Hofman [4] provided a correlation for Poisson's ratio of U-Zr alloys. Based on his correlation, the correlation of Poisson's ratio for Pu-Zr alloys is fitted using the Zr-rich data and allowing the disadvantage of adding Pu instead of U to Zr as follows:

$$\upsilon_{Pu-Zr} = 0.368 \frac{1 - 0.599\, x_{Pu}}{1 - 0.384\, x_{Pu}} \left(1 + 1.796 \frac{T - 600}{2125} \right) \tag{4}$$

where x_{Pu} is the Pu weight fraction and T is the temperature in K. The temperature term is normalized with the Zr melting temperature 2125 K. Fig.8-3 shows the predictions made by using Eq.(4).

8.2.2 Porosity Correction

It has been known that Poisson's ratio decreases as porosity increases [4]. In order to implement the effect of porosity in the alloy fuel, the same method as for Young's modulus is used; Poisson's ratio of Pu-Zr alloys that have density less than 100 %TD is obtained by multiplying a correction factor, i.e.,

$$\nu = (1 - 0.8\ P)\ \nu_{100} \tag{5}$$

where P is the porosity and ν_{100} the Poisson's ratio of 100 %TD alloys.

8.2.3 TRU-Zr Alloy

No measurement on Poisson's ratio for TRU-Zr alloys is found at the present time. Therefore, the information for Pu-Zr alloy can be approximately used instead.

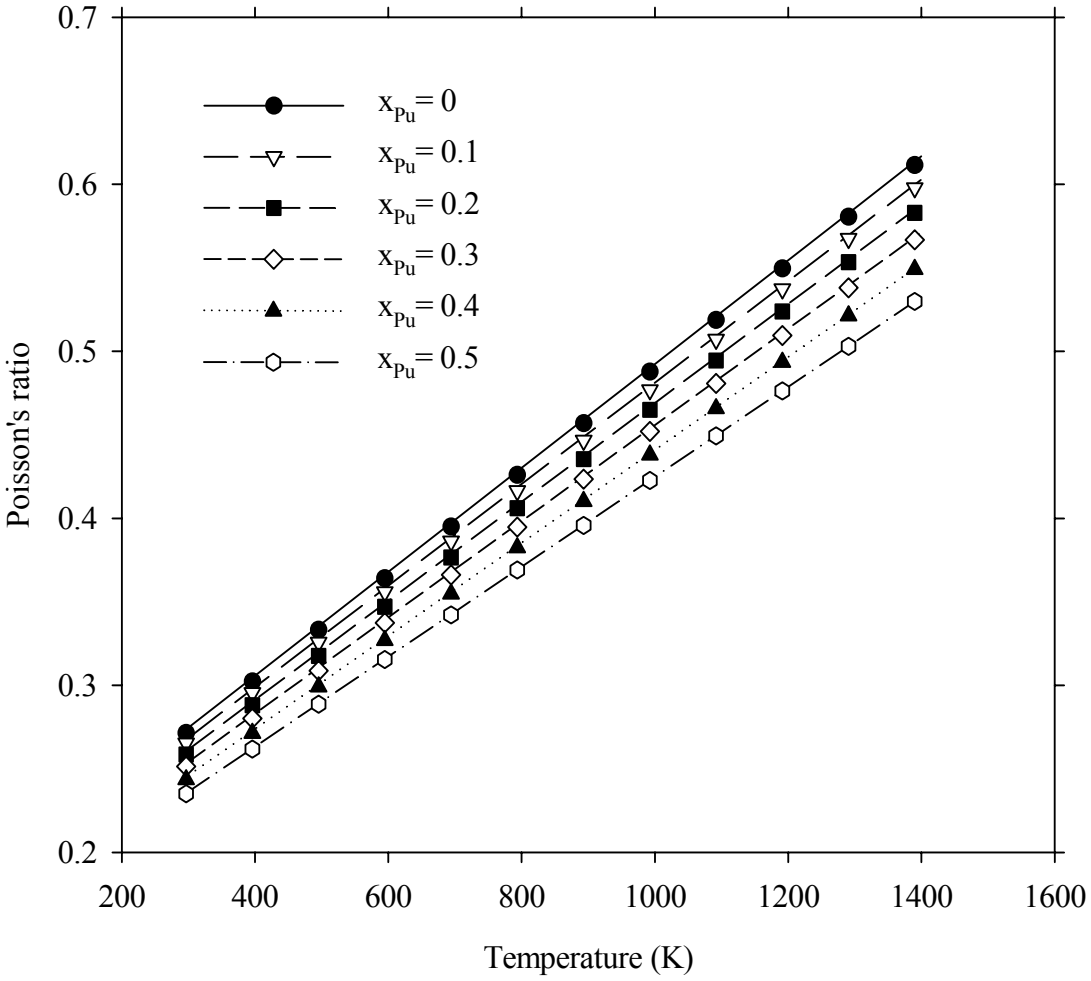

Fig.8-3 Poisson's ratio of Pu-Zr alloys for Pu concentrations up to 0.5 in weight fraction

8.3 References for Section 8

1. G.V. Samsonov, Handbook of the Physicochemical Properties of the Elements, Translated from Russian, IFI/Plenum (1968).
2. F.A. Rough, An Evaluation of Data on Zirconium-uranium Alloys, Battelle Memorial Institute, Report BMI-1030 (1955).
3. H.A. Schwope and G.T. Muehlenkamp, The variation with temperature of the Dynamic Modulus of Elasticity and the Internal Friction of Zirconium, USAEC Report BMI-T-23, Battelle Memorial Institute (1950).
4. G.L. Hofman, unpublished information, Argonne National Laboratory (1985).
5. C.R. Tipton, Jr., Materials, in Reactor handbook, Vol.1, p.711, Interscience Publisher, Inc., New York (1960).

Section 9 Creep

9.1 U-Zr Alloy

The creep of the Zr –rich Zr-U alloys is predominantly determined by the Zr matrix. The minimum secondary creep rate of arc-melted iodide Zr is available as follows [1]:

$$\dot{\varepsilon}_{Zr} = \frac{1\times10^{-23}}{t}\exp\left(\frac{-1.12\times10^{-4}}{T}\right)\sigma^{6.12} + \exp\left(44.84 - \frac{38{,}700}{T}\right)\sinh\left(\frac{5.52\times10^{-5}\,\bar{\sigma}^{2}}{T}\right) \quad (1)$$

where T is in K, t in hour and σ is tress in lb/in^2, and $\bar{\sigma}$ is true stress in lb/in^2.

Douglass [2] used the following relation for the secondary creep rate for zirconium and zirconium alloys:

$$\dot{\varepsilon}_{Zr} = A\exp\left(\frac{-Q_1}{RT}\right)\sigma^{n} + \frac{B}{d^3}\frac{\Omega}{kt}wD_{gb}\,\sigma\exp\left(-\frac{Q_2}{RT}\right) \quad (2)$$

where A, B are constants, Q_1 is the activation energy for slip deformation at high stresses, Q_2 the activation energy for grain boundary diffusion, R the gas constant, d the grain diameter, Ω the atomic volume of the unit cell, D_{gb} the grain boundary diffusion coefficient, w the effective width of the grain boundary, and n the stress exponent.

Hofman developed the creep rate correlation based on theoretical models and data fitting, applicable commonly to metallic U-Zr and U-Pu-Zr fuel [3]:

$$\dot{\varepsilon} = 5.0\times10^{3}\,\sigma\exp\left(\frac{-2.17\times10^{5}}{RT}\right) + 6.0\,\sigma^{\mathrm{n}}\exp\left(\frac{-2.17\times10^{5}}{RT}\right) \quad (3)$$

where $\dot{\varepsilon}$ is in s^{-1}, σ the equivalent stress in MPa, T in K, and R the gas constant, equal to 8.314 J/mole.

Comparison of Eq.(2) and Eq.(3) revealed an important fact that the correlations take basically the same form. This implies that the creep rate for U-rich U-Zr alloys and Zr metal behaves analogously. In this context, we assume that the creep correlation for the Zr-rich Zr-U alloys can also be obtained using Eq.(3).

The U concentration effect is considered. A polynomial for the U concentration effect is augmented to Eq.(3). The final form for minimum creep rate for Zr-rich Zr-U alloys takes the form:

$$\dot{\varepsilon} = \left[A\sigma \exp\left(\frac{-Q_1}{RT}\right) + B\sigma^{n} \exp\left(\frac{-Q_2}{RT}\right)\right]\left(C + D\,x_U + E\,x_U{}^2\right) \qquad (4)$$

where x_U is the U concentration in wt%, and the other parameters hold identical meanings from Eq.(3).

Assuming Q_1 and Q_2 the same, the activation energy of the Zr-rich Zr-U alloys is set equal to the activation energy of the α-Zr self diffusion, which is 2.17×10^5 J/mole [5]. This value happens to be identical to the activation energy of the U-rich U-Zr alloys.

The zirconium creep data showed that n varied from 7.5 at low stresses to about 4.7 at high stresses [2]. Hofman claimed that, for the U-rich U-Zr alloys, n ranged from 1 at low stresses to 4.5 [3]. This suggests that Zr creep has an abnormal dependence on stresses. As a recommendation, the average value of the two sources is taken for the Zr-U alloys, i.e., n= 6.

The creep data for Zr-rich Zr-U alloys were found in the literature [4] and tabulated in Table 9-1. Eq.(4) is used to fit the measured data, and the constants in the equation are determined. As a result, the constants in Eq.(4) were fixed as follows:

$$\dot{\varepsilon} = \left[1.16\times10^{8}\,\sigma \exp\left(\frac{-2.17\times10^{5}}{RT}\right) + 7.26\,\sigma^{6} \exp\left(\frac{-2.17\times10^{5}}{RT}\right)\right] \times\left(2.14\times10^{5} - 1.14\times10^{4}\, x_U + 193.2\, x_U{}^{2}\right) \quad (5)$$

where $\dot{\varepsilon}$ is in 10^{-6}/hr, σ is the equivalent stress in MPa, R is the gas constant equal to 8.314 J/mole, T in K, and x_U the uranium concentration in wt%.

The correlation fits the data very well with the correlation coefficient $R^2 = 0.9982$ and the standard deviation in the creep rate of 1.01×10^{-3} hr^{-1}.

9.2 Zr-Pu Alloy

Assuming that Pu behaves similarly as U in the Zr-rich Zr-U alloys, Eq.(5) is recommended for the creep rate correlation for the Zr-rich Zr-Pu alloys with a change of x_U to x_{Pu}.

9.3 TRU-Zr Alloy

As there is no data for this type fuel, the correlation for Pu-Zr alloys is recommended for use at the present time.

Table 9-1 Creep Data for Zr-rich Zr-U Alloys

Fabrication History [a]	U Content (wt%)	Test Temp. (K)	Stress (MPa)	Time for 1% elongation (hr)	Min. creep rate (10^{-6}/hr)	Test duration (hr)	Total Elongation (%)
1	52.9	1253	3.448	0.16	55,000	1.8	37
1	52.9	1088	3.448	56	130	169	15.1
2	41	723	137.9	1,000			
2	41	723	72.4	10,000			
2	41	723	68.95		0.8		
3	36.3	1253	3.448	0.5	20,000	21	65.3
1	27.7	1253	3.448	0.57	17,000	7.5	36.2
1	27.4	1088	3.448	40	216	162.7	12.3
4	22	773	75.85	100			
4	22	773	57.92	1,000			
4	22	773	37.92	10,000			
4	22	773	68.95		100		
4	22	723	131.0	100			
4	22	723	103.4	1,000			
4	22	723	57.9	10,000			
4	22	723	68.9		3		
4	22	673	262.0	100			
4	22	673	206.9	1,000			
4	22	673	124.1	10,000			
4	22	673	68.9		0.8		
5	3.66	533	206.9		Nil	700	5.25
5	3.66	533	186.2		Nil	600	2.60
5	3.66	533	158.6		Nil	600	1.45
5	3.66	533	151.7		10	2,000	0.96
5	3.66	533	137.9		7	2,000	0.39

[a] 1: Double arc melted, forged, and rolled at 1063 K.
2: Arc melted from iodide zirconium and biscuit uranium, rolled at 1173 K, and water quenched; reheated to 848 K, held 24 hr, and furnace cooled.
3: Induction melted, cast in a copper crucible, and rolled at 1088 K.
4: Arc melted from iodide zirconium biscuit uranium with a consumable electrode, rolled at 948 K, annealed at 1073 K, and furnace cooled.
5: Double arc melted, forged, and rolled to sheet at 948 K; anneal straightened at 1033 K, cold rolled to 25% reduction in area, and annealed 1 hr at 863 K.

9.4 References for Section 9

1. B. Lustman and F. Kerze, Jr., The Metallurgy of Zirconium, McGraw-Hill Book Co., Inc., New York (1955).
2. D.L. Douglass, The Metallurgy of Zirconium, International Atomic Energy Agency (1971).
3. G.L. Hofman, unpublished information, Argonne National Laboratory (1985).
4. F.A. Rough, Battelle Memorial Institute, Report BMI-1030 (1955).
5. V.S. Lyashenko, V.N. Bykov and L.V. Pavlinov, Fiz. Metall. Metalloved. 8(3), 362 (1959); Physics Metals Metallography, 8(3), 40 (1960).

Section 10 Swelling

10.1 Basic Swelling Correlation

In this subsection, a swelling rate is developed for 100% TD fuel under the conditions of no external pressure and no fission gas release.

The volume change during irradiation (i.e., swelling) of a metallic fuel has been reviewed in several places [1-3]. Most of the studies, however, were focused on the U-rich U-Zr and U-Pu-Zr alloys. The swelling data for the Zr-rich U-Zr alloys, under the condition where all fission gas generated is retained in the fuel, could be found from KAPL reports [4-6]. There is no swelling data available for the Pu-Zr alloy.

To establish a swelling correlation for the Pu-Zr alloys, the swelling behavior of the Zr-rich Pu-Zr alloys is assumed similar to that of the Zr-rich U-Zr alloys. The effect of the uranium concentration in the alloys was reported negligible [6]. Lacy and Leary found no difference in the swelling pattern and amount among the Zr-U alloys containing 7 – 22 wt% U [6].

The swelling data of other fuel types such as oxides and carbides revealed that the swelling is a function of temperature and burnup [7,8].

The theoretical swelling rate for Zr-U alloys, which is calculated from the volume change due to fissions without considering the additional volume increase by gas bubble growth and cavitation, is 2.5 %ΔV/V per at% burnup [6]. Since the volume increase due to fission gas atoms is ~0.2% [1], the KAPL value is considered to be too high. Barnes [9], however, supported this value by reporting the solid-fission-product swelling rate of 2.3 %ΔV/V per at% burnup. The swelling rate due to non-soluble nongaseous fission products is more recently calculated as 1.2 % per at% burnup for U-Pu-Zr [1]. This value, however, is based on the assumption that 70% alkali (Cs, Rb) and 20% alkaline earth (Sr, Ba) generated are soluble in Na bond, being excluded for fuel volume increase. The solid fission product swelling depends on various parameters such as neutron energy, fission nucleus, matrix, etc. Therefore, knowing the exact solid swelling rate

is extremely complex. For a more conservative result, if the solubility of the alkali and alkaline earth elements into Na bond is reduced to a minimum, the swelling rate increases to 1.5 %ΔV/V per at% burnup. Since there is no measured data for Zr-Pu alloys, the swelling rate due to the nongaseous fission products for these alloys is recommended as 1.5% per at% burnup.

The KAPL data are well parameterized with respect to burnup and temperature. The correlation is obtained for unrestrained 100 %TD fuel and for no fission gas release, as follows:

$$R = 1.5 + 1.93 \times 10^{8} \left(1 - 3.58B + 3.45B^{2}\right) \exp\left(-\frac{1.59 \times 10^{4}}{T}\right) \quad (1)$$

where R is the swelling rate in (%ΔV/V)/(at% burnup), B is burnup in at% and T temperature in K.

The volume increase as a function of burnup is plotted in Fig.10-1. The figure shows that the amount of fuel swelling is extremely large because no fission gas was allowed to release.

10.2 Swelling under External Stress

External stress retards swelling. The swelling appears to saturate when there is enough free volume available in the fuel to accommodate the volume increase by swelling [1,10,11]. The free volume can be provided by as-fabricated porosity and cavities generated by irradiation. As-fabricated porosity of alloy fuels, however, is negligible.

The internal pressure of a gas bubble under a mechanical equilibrium state is given by

$$p_i = p_{ex} + \frac{2\gamma}{r} \quad (2)$$

where p_i is the bubble internal pressure, p_{ex} is the external pressure and $2\gamma/r$ is the surface tension force. When the external pressure is larger than that needed for equilibrium, the bubble will not grow, which terminates further swelling.

The cavities generated by anisotropic growth of grains have lower than equilibrium pressure [1]. These cavities will provide space for swelling of solid fission products as well as fission gas, when external pressure is large enough. It is worth noting that the external pressure only affects fission gas swelling by restricting gas bubble growth. The external pressure enough to stop (apparent) swelling is generated by the fuel-to-cladding contact caused by fuel swelling and fuel thermal expansion of the fuel. When the fuel has a solid bond with cladding, external pressure exerts from the beginning of irradiation.

The swelling under external pressure situation can be modeled by multiplying an empirical exponential term to the gaseous swelling as follows:

$$R = 1.5 + 1.93\times10^{8}\left(1 - 3.58B + 3.45B^{2}\right)\exp\left(-\frac{1.59\times10^{4}}{T}\right)\exp\left(-0.1p_{c}\right) \tag{3}$$

where p_c is the contact pressure in MPa. Notice again that R is the swelling rate; therefore, the total amount of fuel swelling can be obtained by integrating Eq.(3) with respect to burnup.

10.3 Swelling Correlation with Fission Gas Release

As swelling proceeds, the porosity (due to fuel cavitation and bubble growth) increases in fuel, which eventually yields the interconnections of bubbles and pores, and gives free pathways for gas release. Beck [13] showed that most of fission gas was released from the fuel at ~30% swelling. This suggests that, once swelling reaches 30%, the gaseous swelling diminishes sharply. As a result, the swelling rate is primarily due to the nongaseous fission products. This situation leads to a composite swelling rate such as

$$R = 1.5 + 1.93\times10^{8}\left(1 - 3.58B + 3.45B^{2}\right)\exp\left(-\frac{1.59\times10^{4}}{T}\right)\exp\left(-0.1p_{c}\right), \text{ for S<30\%,}$$

$$R = 1.5\text{, for } 30\% < \text{S} \tag{4}$$

For example, the swelling of Zr-Pu alloys irradiated at 20 MPa external pressure with fission gas release is plotted in Fig.10-2. The amount of fuel swelling should be overpredicted because no gas release was assumed until swelling reaches ~30%.

In order to reduce cladding strain at high temperatures, a free volume must be provided to cope with the swelling of fuel. From EBR-II experiments, this was accomplished by allowing 75% smeared density in the fuel [1]. Since typical fuel alloys do not include as-fabricated porosity, a gap between fuel and cladding is designed. At high temperatures, since it is ductile, an alloy fuel is easily deformed without a severe cladding deformation if appropriate amount of free volume is allows. Another way of providing a free volume is to include a central void.

10.4 Other Consideration: Effect of He Generation from Americium

Helium gas is generated from Am transmutation with a rate 6.8 times higher than that of fission gas (Xe and Kr combined) during thermal neutron irradiation [14] and 4.7 times higher for fast neutron irradiation [15]. This suggests that TRU containing Am will swell additionally due to He generation. Although He is easier to release than Xe and Kr, the swelling rate due to He is assumed approximately the same as that of fission gas, for gas release from the metallic fuel is mainly due to the interconnection of bubbles. Therefore, the swelling rate due to He gas is 0.2% per percent fuel burnup, considering only that He atoms remains as atoms. This yields the additional swelling rate, which is additive to the swelling rate obtained in Eq.(4),

$$R_{He} = (0.2)(4.7)\, x_{Am} \tag{5}$$

where R_{He} is in (%ΔV/V)/(%burnup), x_{Am} the americium atomic fraction in TRU. Notice that x_{Am} is in TRU not TRU-Zr alloy. As a result of the preliminary ATW design, x_{Am} is ~10% of TRU. For this americium concentration, the fuel swells 0.094% per percent burnup, which is almost negligible compared to other uncertainties.

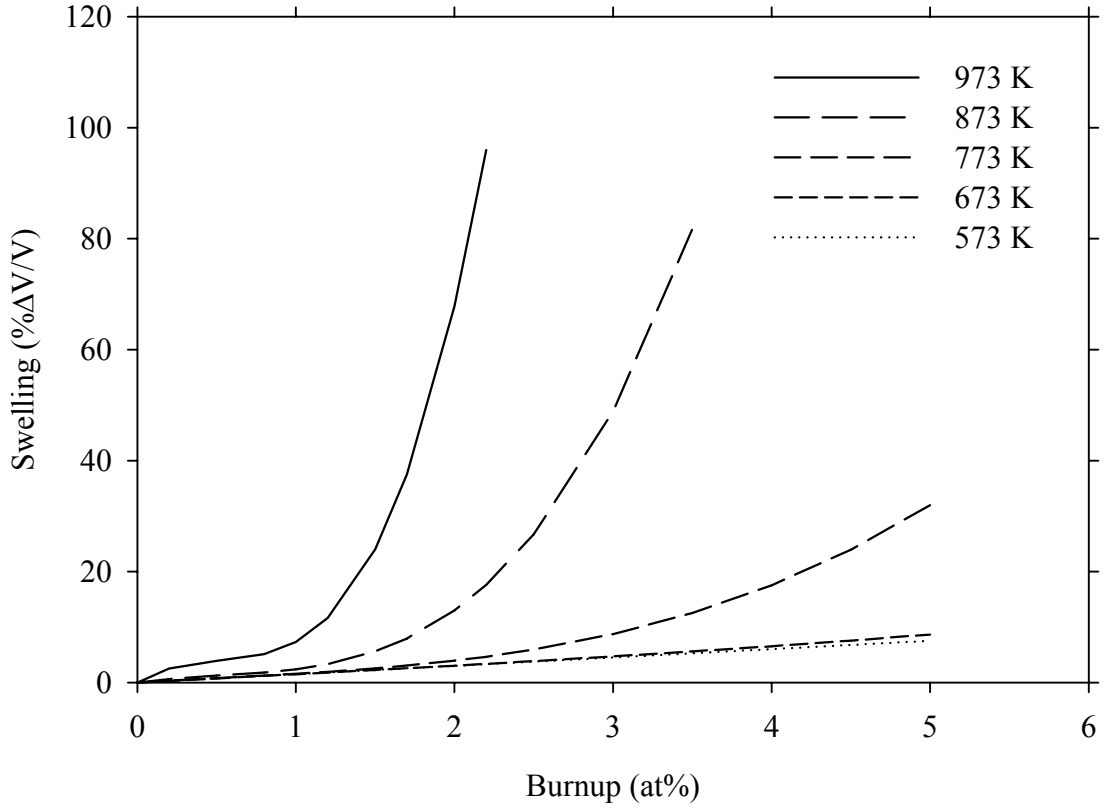

Fig.10-1 Swelling of fuel versus burnup for irradiated Zr-U alloys

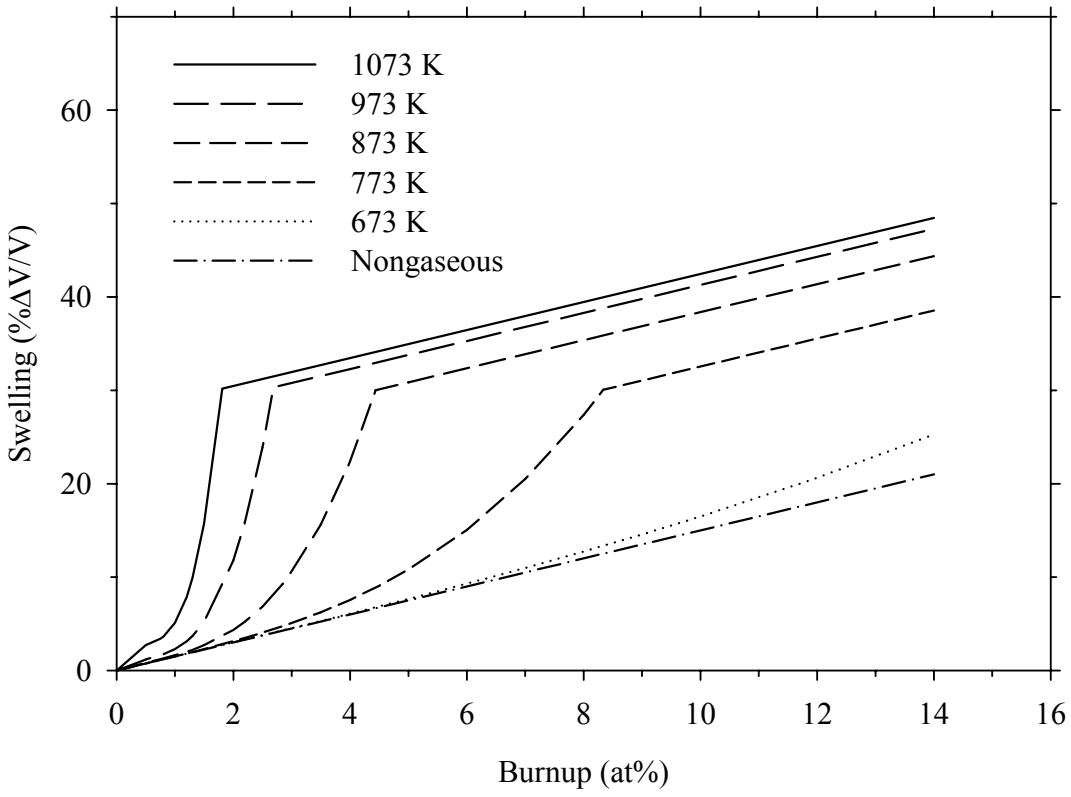

Fig.10-2 Zr-Pu fuel swelling versus burnup under 20 MPa external pressure with fission gas release

10.5 References for Section 10

1. G.L. Hofman and L.C. Walters, Metallic Fast Reactor Fuels, in Materials Science and Technology, A comprehensive Treatment, R.W. Cahn et al., editor, V.10A, 1994.
2. A Boltax, in Nuclear Reactor Fuel Elements, Metallurgy and Fabrication, Chap.9, A.R. Kaufmann, editor (1962).
3. H. Blank, J. Less-common Metals, 121, 583 (1986).
4. W.V. Johnston, The Effect of Postirradiation Annealing of Uranium-zirconium Alloys, Knolls Atomic Power Laboratory, Report KAPL-1562 (1956).
5. W.V. Johnston, The Effect of Transients and Longer-time Anneals on Irradiated Uranium-zirconium Alloys, Knolls Atomic Power Laboratory, Report KAPL-1965 (1958).
6. C.E. Lacy and E.A. Leary, Irradiation Performance of Highly Enriched Fuel, Knolls Atomic Power Laboratory, Report KAPL-1552 (1958).
7. H. Zimmermann, J. Nucl. Mater., 105, 56 (1982).
8. SCDAP/RELAP5/MOD 3.2 Code manual, MATPRO-A Library of Materials Properties for Light Water Reactor Accident Analysis, NUREG/CR-6150, Vol.4, Rev.1, INEL-96/0422 (1998).
9. R.S. Barnes, et al., Proc. Second International Conf. on the Peaceful Uses of Atomic Energy, Geneva (1958).
10. C.R. Tipton, Jr., Materials, in Reactor handbook, Vol.1, p.711, Interscience Publisher, Inc., New York (1960).
11. Y. Koo, B. Lee and D. Sohn, J. Nucl. Mater., 280, 86 (2000).
12. H. Zimmermann, J. Nucl. Mater., 75, 154 (1978).
13. W.N. Beck, Argonne National Laboratory, Report ANL-7388 (1968).
14. R.J.M. Konnings, et al., J. Nucl. Mater., 282, 159 (2000).
15. M.K. Meyer and S.L. Hayes, Argonne National Laboratory, Nuclear Technology Division Memorandum 8 (2001).

Section 11 Gas Release

11.1 Fission Gas Release

The fission gas release data for metallic fuels are available in the literature [1-3]. The review of these data can be summarized as follows:

- Fission gas release is largely dependent on fuel swelling.
- Fission gas release is not directly determined by burnup and temperature; it is determined rather by development of porosity interconnection than gas atom diffusion in the matrix.
- Gas release is independent of alloying elements.
- The difference between Pu and U for fission gas release is negligible.
- Fission gas release is negligible until fuel swells ~20%.

Based on the data by Beck [3], the correlation for fission gas release is obtained.

$$F = 0, \text{ for } S < 19.5\% \tag{1a}$$

$$F = -258 + 333\left[1 - \exp\left(0.077\,S\right)\right], \text{ for } 19.5\% < S \tag{1b}$$

where F is the fission gas release in percent and S is fuel swelling in %. The fuel swelling is obtained from the correlation provided in Sect.1.9. Fig.11-1 compares the data obtained from Beck [2] and predictions by Eq.(1).

11.2 He Gas Release

Because gas release in TRU-Zr alloys is chiefly determined by the connections of bubbles, not by individual gas diffusion, He gas release can be represented by the same correlations for fission gas given in Eq.(1).

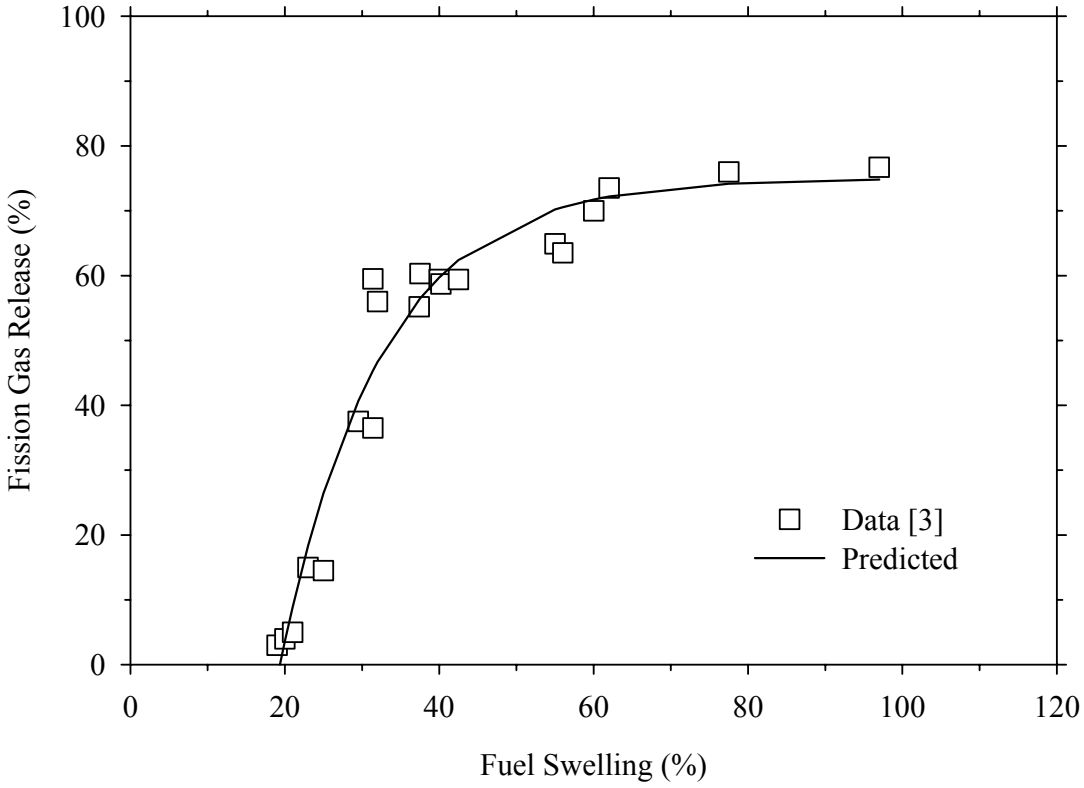

Fig.11-1 Comparison of fission gas release data and predictions by Eq.(1)

11.3 References for Section 11

1. G.L. Hofman and L.C. Walters, Metallic Fast Reactor Fuels, in Materials Science and Technology, A comprehensive Treatment, R.W. Cahn et al., editor, V.10A (1994).
2. R.S. Barnes, J. Nucl. Mater., 11(2), 135 (1964).
3. W.N. Beck, Argonne National Laboratory, Report ANL-7388 (1968).

PART B

Nitride Fuels

PART B

Nitride Fuels

Preface

The purpose of PART B is to provide the best available fuel materials properties and performance models of the (Pu,Zr)N and (TRU,Zr)N solid-solution fuels for fuel design and safety calculation of the Advanced Accelerator Assisted (AAA) system. PART B parallels PART A, Metal Alloy Fuels, in form and topics.

The solid solution of the mononitrides of transuranic elements (i.e., Pu, Np, Am, Cm, etc) with zirconium mononitride, designated as (TRU,Zr)N, is one of the primary candidate fuel types for the AAA system, together with metallic TRU-Zr alloy fuels studied in Argonne National Laboratory.

The data found in the literature were critically reviewed and assessed to provide the recommended ones. For the convenience of the user, most of the materials properties are given in model correlations; performance models are also provided in mathematical formulas. Tabulations were made in some cases where these were regarded to allow more flexibility for the user.

The information for the materials properties of (Pu,Zr)N and (TRU,Zr)N, however, is in many cases nonexistent in general. Therefore, where no data exists, the values and models based on theoretical estimations are made. Extrapolations from the similar ceramic materials such as (U,Pu)C and (U,Pu)N, which have relatively more data, are inevitably relied upon. The justifications for this will be possible only when sufficient measured data become available in the future.

Section 1 General

1.2 Unit Conversion

Throughout this report the units in the SI (i.e., metric) system are preferentially used. Where more convenient, cgs units are also adopted. The following unit conversions are used. Any data given in English units are converted to the corresponding SI units.

1.1.1 Mass

1 lb = 0.45359 kg

1.1.3 Length

1 cm = 0.01 m
1 in. = 0.0254 m
1 ft = 0.3048 m

1.1.3 Temperature

The basic unit for temperature is the absolute temperature in Kelvin (K), which is related to the Celsius scale by

T (K) = T (^{o}C) +273.15

When a temperature is given in the other frequently appearing temperature scale, Fahrenheit (^{o}F), it is converted in Kelvin as follows:

$$T(K) = \frac{5}{9}\left[T(^{o}F) - 32\right] + 273.15$$

In the case where ^{o}F is involved in a unit conversion, however, it is transformed to K as follows:

$$K = \frac{5}{9}(^{o}F)$$

1.1.4 Pressure

Pascal is adopted as the basic unit for pressure. Pressure given in atm, bar, torr (mmHg) and psi (lb/in^2) is converted to Pa (i.e., N/m^2) as follows:

1 atm = 101325 Pa
1 atm = 760 torr
1 bar = 100,000 Pa
1 torr (mmHg) = 133.322 Pa
1 psi = 6895 Pa

1.1.5 Energy, Heat

Joule is the basic unit for energy and heat. Energy given in calorie is converted to joule by using the following unit conversion.

1 cal = 4.184 J
1 Btu = 1055 J
1 MeV = 1.602×10^{-13} J

1.1.7 Thermal Conductivity

1 Btu/hr-ft-^{o}F = 1.731 W/m-K
1 Cal/sec-cm-^{o}C = 418.7 W/m-K

1.2 Fundamental Constants

Table 1-1 Fundamental Constants

Symbol	Quantity	Value
R	Gas constant	8.314 J/mole-K
N_A	Avogadro's Number	6.02217×10^{23} mole^{-1}

1.3 Metal Element and Nitride Data

Table 1-2 Metal Element Data [1–3]

Element	Atomic Number	Atomic mass [a]	Nominal density [b] (g/cm^3)
Zr	40	91.224	6.506
Pu	94	(242) [c]	19.840
Am	95	243.0614	13.670
Np	93	237.0482	20.250

a : based on ^{12}C=12.0000

b: at 293 K

c: mass number of the longest-lived isotope, Pu-242 [3]

Table 1-3 Nitride Data [4]

Nitride	Molecular weight	Nitrogen content (wt%)	Crystal structure		Lattice constant *a* (Å)	Melting Point (K)
			Unit cell	Structure type		
ZrN	105.22	13.31	Cubic	NaCl	4.537	3253
PuN	256.00	5.47	Cubic	NaCl	4.906	3023
NpN	251.00	5.58	Cubic	NaCl	4.8979	3103
UN	252.07	5.55	Cubic	NaCl	4.89	3123
AmN	- [a]	-	-	-	-	-
CmN	-	-	-	-	-	-

a: No data available

1.5 References for Section 1

1. J.R. Lamarsh, Introduction to Nuclear Engineering, Addison-Wesley Pub. Co., Menlo Park, California (1983).
2. J. Emsley, The Elements, Clarendon Press, Oxford (1998).
3. N.N. Greenwood and A. Earnshaw , Chemistry of the Elements, 2nd edition, Butterworth, UK (1997).
4. G.V. Samsonov and I.M. Vinitskii, Handbook of Refractory Compounds, IFI/PLENUM, NewYork-Washigton-London (1980).

Section 2 Heat Capacity

2.1 ZrN

The heat capacity correlation of ZrN exists in Kubaschewski book [1].

$$C_p = 46.44 + 7.03 \times 10^{-3} T - \frac{7.20 \times 10^5}{T^2} \quad (1)$$

where C_p is the heat capacity in J/K-mole and T in K. This correlation was adopted by Spear [2]. Kogel et al. [3] developed a model to better calculate the heat capacity of ZrN. Their correlation can be represented by the following equation and is compared in Fig.2-1 with the Kubaschewski correlation.

$$C_p = 45.86 + 6.82 \times 10^{-3} T - \frac{5.54 \times 10^5}{T^2} \quad (2)$$

Eq.(2) predicts lower values than the Kubaschewski correlation at temperatures above 500K, but both generally predict fairly consistently with each other. Because the Kogel correlation is more updated, Eq.(2) is recommended here.

2.2 PuN

The heat capacity of PuN presented in Kubaschewski [1] is

$$C_p = 44.89 + 1.548 \times 10^{-2} T \quad (3)$$

Here, Cp is in J/K-mole and T in K. Another heat capacity correlation for PuN was offered by Oetting [4] as

$$C_p = 45.0002 + 1.542 \times 10^{-2} T \quad (4)$$

Matsui [5] critically reviewed the heat capacity data of PuN and argued that the Oetting correlation is most reliable. Fig.2-2 shows a comparison between the correlations found in the literature. The correlations by Oetting and by Kubaschewski are almost identical. The data reported by Alexander [6] are generally lower than both correlations by Oetting and by Kubaschewski. From this observation, it is considered that either Oetting or Kubaschewski can be selected. For this handbook, the correlation given by Kubaschewski, Eq.(3), is recommended, because it is based on a more extensive data base.

2.3 (Pu,Zr)N

The heat capacity data of ZrN and PuN solid solution, (Pu,Zr)N, has never been reported. Therefore, the Neumann-Kopp rule [7] is recommended to obtain the heat capacity of the solid solution. According to this rule, the specific heat of (Pu,Zr)N is estimated as

$$C_p = a_{ZrN}\, C_{p,ZrN} + a_{PuN}\, C_{p,PuN} \tag{5}$$

where C_p is the heat capacity of (Pu,Zr)N and a the molecular fraction of PuN and ZrN in the solid solution. For instance, if $(Pu_{0.2}Zr_{0.8})N$ is given, a_{PuN} is equal to 0.2 and a_{ZrN} 0.8. $C_{p,ZrN}$ and $C_{p,PuN}$ are obtained in the proceeding subsections, namely, Eq.(2) and Eq.(3), repsectively.

As an example, the heat capacity of $(Pu_{0.2}\ Zr_{0.8})N$ is compared in Fig.2-3 with those of ZrN and PuN and is tabulated in Table 2-1.

2.4 (TRU,Zr)N

The heat capacity data of TRU nitrides are scarce. Arai, et al., [8] estimated the heat capacity of NpN based on the method provided in Kubaschewski [7]. The correlation, however, apparently underpredicts. No heat capacity data is found for other TRU nitrides. Therefore, as an approximation, the correlation for (Pu,Zr)N is recommended for (TRU,Zr)N regarding the TRU content as the Pu content.

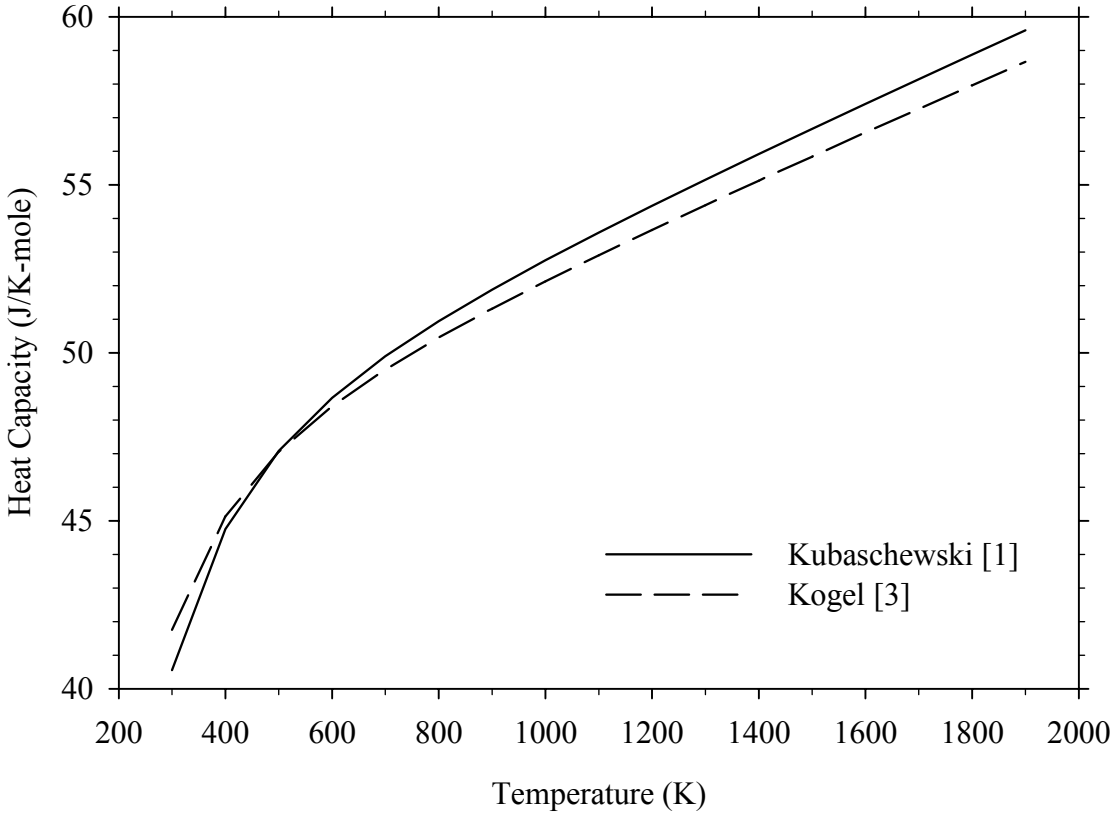

Fig.2-1 Heat capacity of ZrN

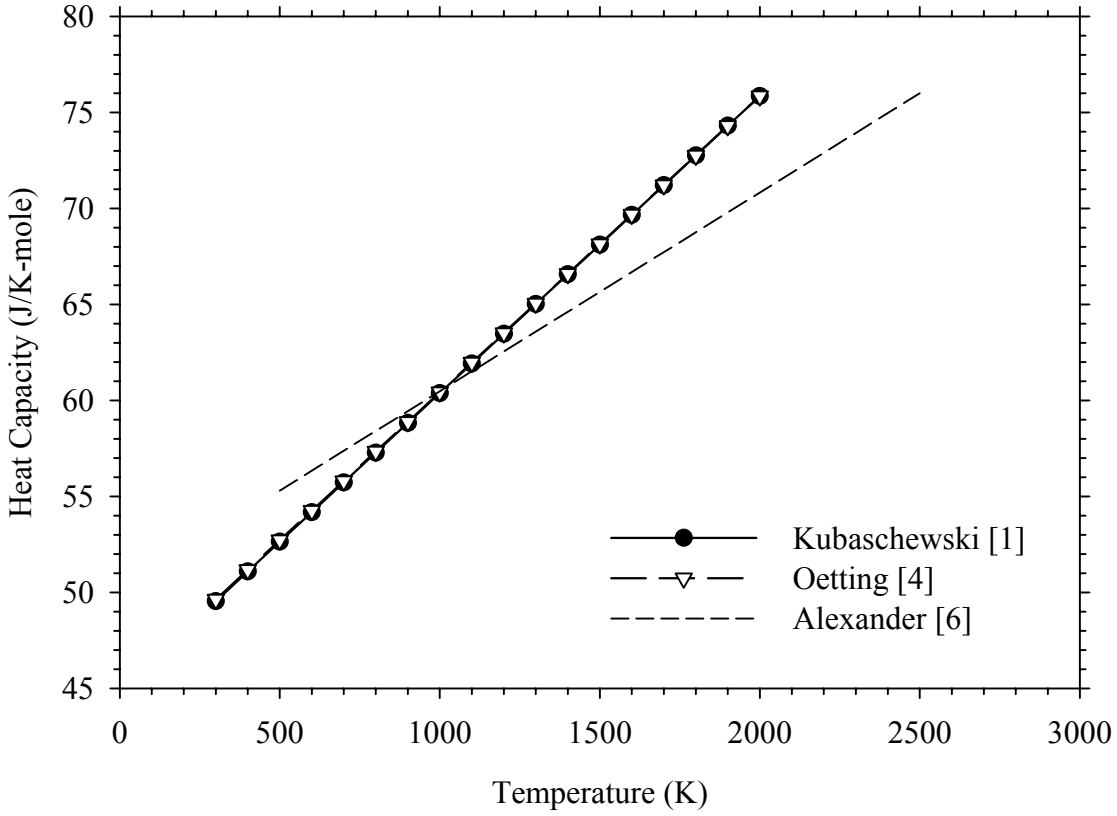

Fig.2-2 Comparison of the heat capacity data of PuN in the literature

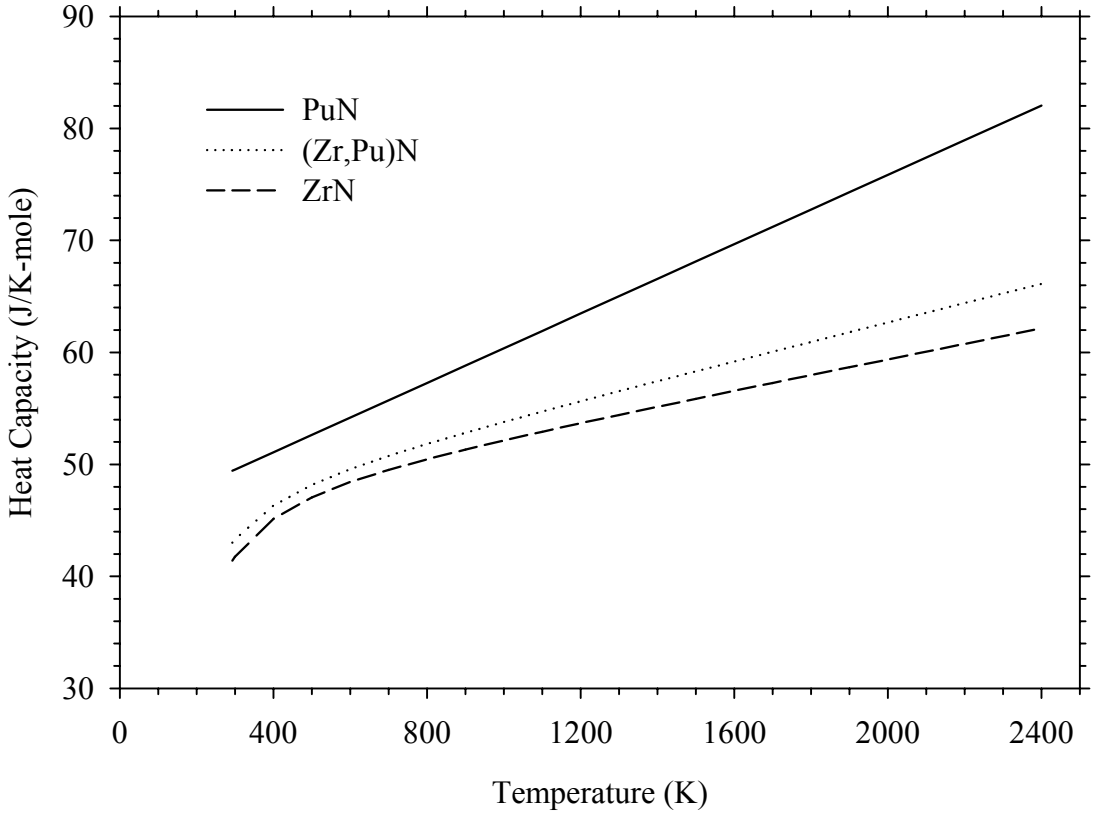

Fig.2-3 Comparison of the heat capacity of PuN, ZrN and (Pu,Zr)N

Table 2-1 Recommended Heat Capacity Values for PuN, ZrN and $(Pu_{0.2}Zr_{0.8})N$

Temperature (K)	PuN (J/K-mole)	ZrN (J/K-mole)	$(Pu_{0.2}Zr_{0.8})N$ (J/K.mole)
293	49.426	41.405	43.009
300	49.534	41.750	43.307
400	51.082	45.126	46.317
500	52.630	47.054	48.169
600	54.178	48.413	49.566
700	55.726	49.503	50.748
800	57.274	50.450	51.815
900	58.822	51.314	52.816
1000	60.370	52.126	53.775
1100	61.918	52.904	54.707
1200	63.466	53.659	55.621
1300	65.014	54.398	56.521
1400	66.562	55.125	57.413
1500	68.110	55.844	58.297
1600	69.658	56.556	59.176
1700	71.206	57.262	60.051
1800	72.754	57.965	60.923
1900	74.302	58.665	61.792
2000	75.850	59.362	62.659
2200	78.946	60.750	64.389
2400	82.042	62.132	66.114

2.5 References for Section 2

1. O. Kubaschewski, C.B. Alcock and P.J. Spencer, Materials Thermochemistry, 6th edition, Pergamon Press, New York (1993).
2. K.E. Spear and J.M. Leitnaker, J. Am. Ceramic Soc., 51 (12), 706 (1968).
3. S.P. Kogel, R.G. Avarbe and T.N. Chizhik, Izvestiya Akademii Nauk SSSR, Neorganicheskie Materialy, 9(10), 1665 (1983).
4. F.L. Oetting, J. Chem. Thermodynamics, 10, 941 (1978).
5. T. Matsui and R.W. Ohse, High Temperature – High Pressure, 19, 1 (1987).
6. C.A. Alexander, J.S. Ogden and M.P. Rausch, Report BMI-659, Battelle Memorial Institute (1975).
7. O. Kubaschewski and C.B. Alcock, Metallurgical Thermochemistry, Fifth Ed., pp183-184, Pergamon Press, New York (1979).
8. Y. Arai, Y. Okamoto and Y. Suzuki, J. Nucl. Mater., 211, 248 (1994).

Section 3 Vapor Pressure

Data for vapor pressures over (TRU,Zr)N are not found in the literature. Therefore, vapor pressures over individual nitrides composing (TRU,Zr)N are collected and reviewed in the following subsections.

3.1 Vapor Pressures over PuN

The major vapor species over PuN are N_2 and Pu(g). There are several places that have information for these [1–7]. Table 3-1 summarizes the information and Fig.3-1 compares the consistency between the data. The consistency among the data from the literature is excellent. Matsui and Ohse [7] obtained the vapor pressure correlations by assessing the existing data in the literature. As shown in Fig.3-1, the N_2 and Pu vapor pressures by Matsui and Ohse are very close to the most recent data by Ogawa [6]. The results by Matsui and Ohse are considered the most reliable, and, therefore, recommended for this handbook. As a result, the recommended vapor pressures for gas species over PuN are summarized as follows:

$$\log(p_{N_2}) = 4.564 - \frac{2.175\times10^4}{T} \tag{1}$$

where p is in MPa and T in K for T < 2993 K.

$$\log(p_{Pu}) = 5.445 - \frac{2.196\times10^4}{T} \tag{2}$$

$$\log(p_{PuN}) = 7.934 - \frac{3.189\times10^4}{T} \tag{3}$$

$$\log(p_{Pu_2}) = 7.187 - \frac{3.210\times10^4}{T} \tag{4}$$

$$\log(p_{Total\ gas}) = 5.021 - \frac{2.071 \times 10^4}{T} \quad (5)$$

3.2 Vapor Pressures over (Pu,Am)N

The vapor pressures of Pu and Am over PuN containing 0.0027 mol.% AmN are reported [8] as:

$$\log(p_{Pu}) = 4.224 - \frac{2.018 \times 10^4}{T} \quad (6)$$

$$\log(p_{Am}) = 1.033 - \frac{1.613 \times 10^4}{T} \quad (7)$$

where p is in MPa. The corresponding N_2 decomposition pressure is expressed as

$$\log(p_{N_2}) = 4.967 - \frac{2.250 \times 10^4}{T} \quad (8)$$

The N_2 pressure in Eq.(8) is very close to that of pure PuN given in Eq.(1). The vapor pressures are compared in Fig.3-2.

Table 3-1 Vapor Pressure over PuN(s,l) Given in $\log(p/MPa) = A - \frac{B \times 10^4}{T(K)}$

N_2(g)	Pu(g)	PuN(g)	Pu_2(g)	Total gas	T (K)	Ref.
A=4.564 B=2.175	A=5.445 B=2.196				1658 – 1976	1
	A=3.44 B=1.68				1923 – 2240	2
A=4.2125 B=2.0967	A=4.9863 B=2.1056				1400 – 2400	3
		A=7.30 B=3.06			1400 – 2400	4
			A=6.27 B=3.03	A=1.7541 +0.8915 log T B=2.0329	1400 – 2400	5
A=2.38 B=1.57	A=4.07 B=1.84	A=6.38 B=2.80	A=4.44 B=2.51	A=-10.7188 +3.984 log T B=1.5234	2900 – 8000	5
A=4.452 B=2.163	A=5.676 B=2.249				1600 – 2500	6
A=4.564 B=2.175	A=5.445 B=2.196	A=7.934 B=3.189	A=7.187 B=3.210	A=5.021 B=2.071	T < 2993	7
A=2.73 B=1.63	A=4.53 B=1.92	A=7.02 B=2.91	A=5.35 B=2.66	A=-12.69 +4.64 log T B=1.56	2993 < T	7

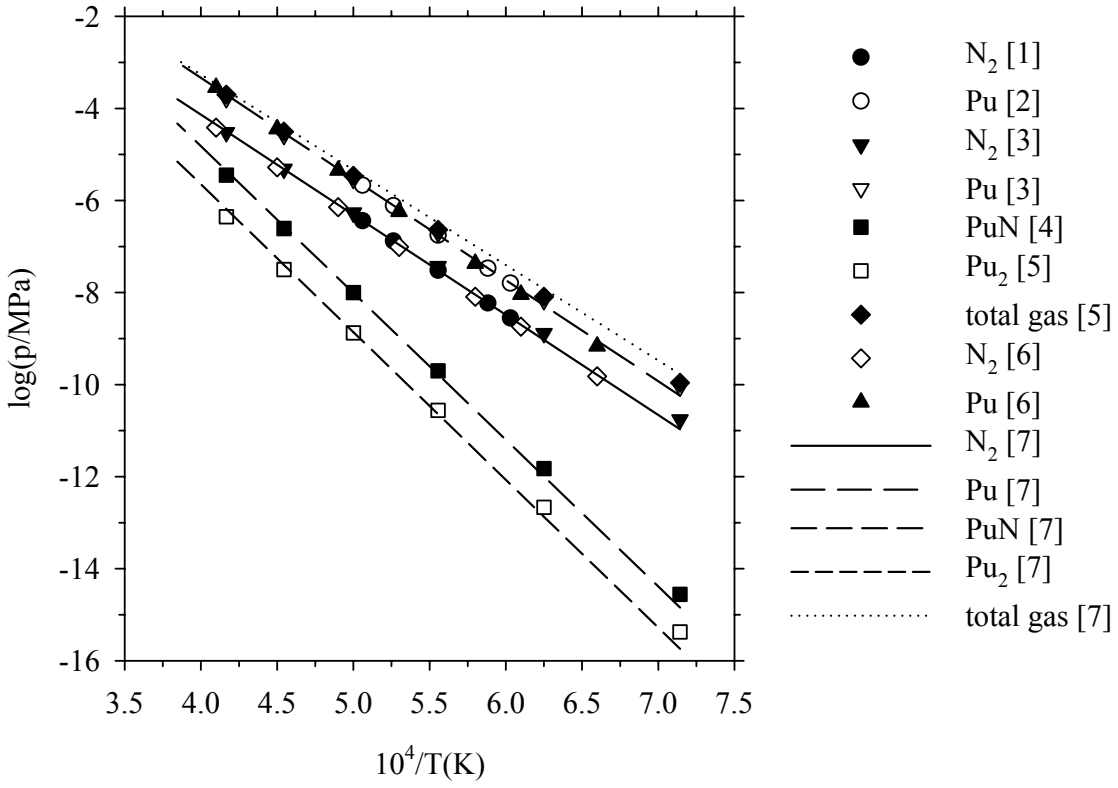

Fig.3-1 Vapor pressures over PuN.
Numbers in brackets are for references.

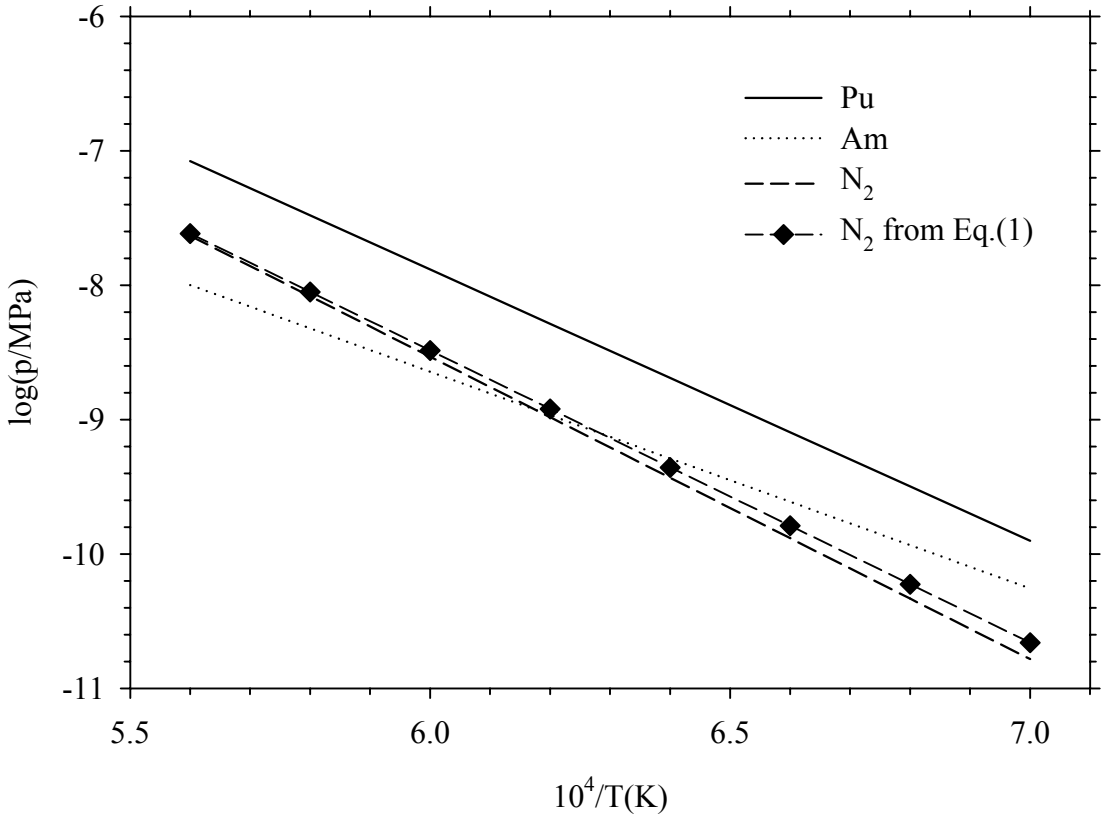

Fig.3-2 Vapor pressures over PuN containing 0.0027 mol.%AmN [8].
N_2 pressure over pure PuN by Eq.(1) is added for comparison.

3.3 Vapor Pressures over NpN

There are a couple of sets of data on the vaporization over NpN [9,10]. The vapor pressure of Np over NpN was obtained by Nakajima [9] as

$$\log(p_{Np}) = 4.26 - \frac{2.22 \times 10^4}{T} \tag{9}$$

where p is in MPa and T in K for $1690 \le T \le 2030\ K$.

For N_2 gas pressure, Nakajima [9] assumed that an extrapolation of Olson and Mulford's equation to the lower temperatures is valid. Therefore, the following equation is recommended for the vapor pressure of N_2 over NpN:

$$\log(p_{N_2}) = 7.193 - \frac{2.954 \times 10^4}{T} + 7.87 \times 10^{-18}\, T^5 \tag{10}$$

3.4 Vapor Pressures over ZrN

The vapor pressures over ZrN are available from Kosolapova [11] and the N_2 pressure over ZrN from Kleykamp [12]. The data are given for the temperature range of 2418 – 2549 K. The following equations are obtained by fitting the data.

$$\log(p_{Zr}) = 2.330 - \frac{2.192 \times 10^4}{T} \tag{11}$$

$$\log(p_{N_2}) = 15.822 - \frac{5.350 \times 10^4}{T} \tag{12}$$

$$\log(p_{ZrN}) = 6.561 - \frac{4.021 \times 10^4}{T} \tag{13}$$

Eqs.(11) – (13) are extrapolated to the lower temperature range, and compared in Fig.3-3 with the data in the literature. The extrapolation for N_2 pressure is consistent with the data estimated by Kleykamp [12].

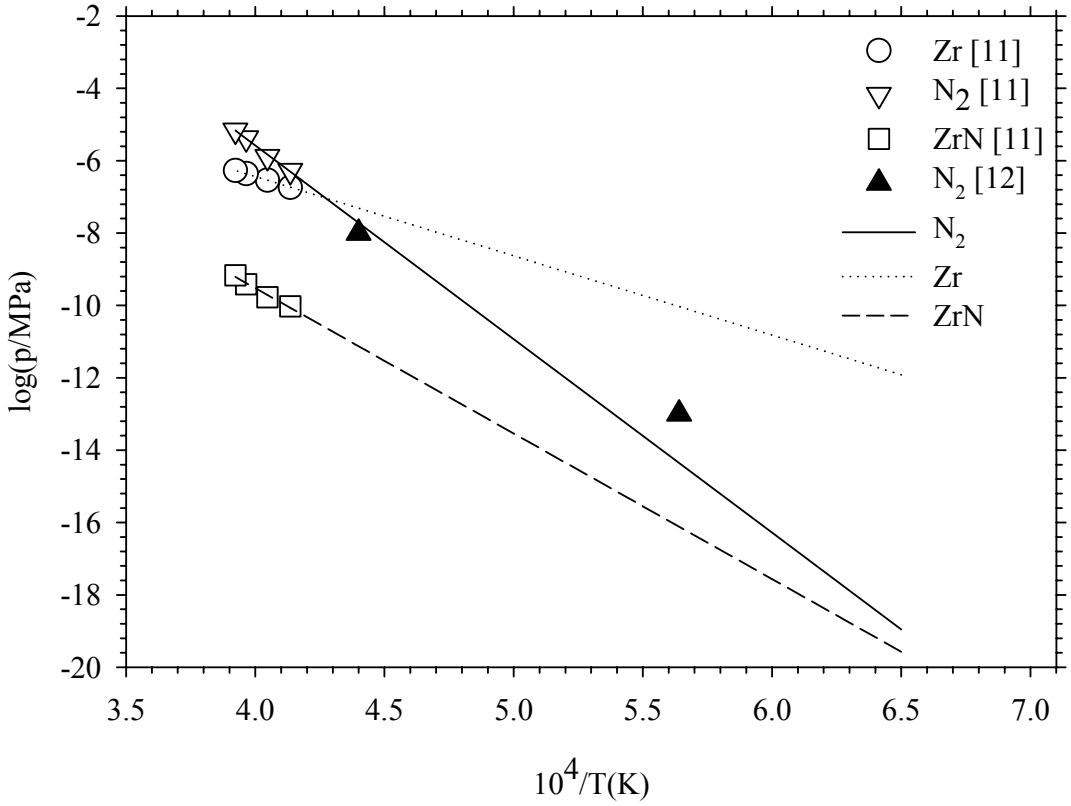

Fig.3-3 Vapor pressures over ZrN. Data (symbols) and extrapolation to lower temperatures (lines).

3.5 References for Section 3

1. R.A. Kent and J.A. Leary, High Temp. Sci., 1, 176 (1969).
2. J.P. Marcon and J. Poitreau, J. Inorg. Nucl. Chem., 32, 463 (1970).
3. A. Sheth and L. Leibowitz, Argonne National Laboratory, Report ANL-AFP-2 (1974).
4. C.A. Alexander, J.S. Ogden and M.P. Rausch, Battelle Memorial Institute, Report BMI-X-659 (1975).
5. A. Sheth and L. Leibowitz, Argonne National Laboratory, Report ANL-AFP-12, 1975.
6. T. Ogawa, J. Nucl. Mater., 201, 284 (1993).
7. T. Matsui and R. Ohse, High Temp. – High Press., 19, 1 (1987).
8. T. Ogawa, T. Ohmichi, A. Maeda, et al., J. Alloys Comp., 224, 55 (1995).
9. K. Nakajima, Y. Arai and Y. Suzuki, J. Nucl. Mater., 247, 33 (1997).
10. W.M. Olson and R.N.R. Mulford, J. Phys. Chem., 70, 2932 (1966).
11. T.Ya. Kosolapova, Handbook of High Temperature Compounds: Properties, production, Applications, p.181, Hemisphere Pub. Co., New York (1990).
12. H. Kleykamp, J. Nucl. Mater., 275, 1 (1999).

Section 4 Thermal Expansion and Density

4.1 Theory

The coefficient of volumetric thermal expansion is a thermodynamic property defined as

$$\alpha = \frac{1}{V}\left(\frac{\partial V}{\partial T}\right)_p \tag{1}$$

where V is the volume and T the temperature. This is called instantaneous coefficient of thermal expansion; it is different from the mean coefficient to be described later. The subscript p implies that Eq.(1) is defined for a constant pressure process. For simplicity, however, the subscript p is dropped in the following equations. For a process where the substance volume changes $V_o \rightarrow V$ according to temperature changes $T_o \rightarrow T$, the mean coefficient is used to describe the process as

$$\overline{\alpha} = \frac{1}{V_o}\frac{V - V_o}{T - T_o} \tag{2}$$

Most measurement values are obtained for length changes and data are given in fractional (or percent) changes of length. The relevant coefficient is the instantaneous coefficient of linear thermal expansion, which is defined as

$$\alpha_l = \frac{1}{L}\left(\frac{\partial L}{\partial T}\right)_p \tag{3}$$

where L is the length of the substance. The corresponding mean coefficient is

$$\overline{\alpha}_l = \frac{1}{L_o}\frac{L - L_o}{T - T_o} \tag{4a}$$

or

$$\overline{\alpha}_l = \frac{1}{\Delta T}\frac{\Delta L}{L_o} \tag{4b}$$

where $\Delta T = T - T_o$ and $\Delta L = L - L_o$. Eq.(4b) is more useful because most data compilations are given in $\Delta L/L_o$.

If the substance is isotropic, the (instantaneous) coefficient of volume expansion is equal to three times the coefficient of linear expansion, i.e.,

$$\alpha = 3\alpha_l \tag{5}$$

The same is not true, however, for the mean coefficients. From Eq.(4) and the fact that $V=L^3$, the following can be shown

$$\frac{V}{V_o} = \left(1 + \Delta T\, \overline{\alpha}_l\right)^3 \tag{6}$$

Applying Eq.(6) into Eq.(2) yields

$$\overline{\alpha} = 3\overline{\alpha}_l + 3\Delta T\, \overline{\alpha}_l^{\,2} + \left(\Delta T\right)^2 \overline{\alpha}_l^{\,3} \tag{7}$$

Comparing between Eq.(5) and Eq.(7), the last two terms in Eq.(7) make the difference. However, the error caused by neglecting those terms in Eq.(7) is generally small.

The corresponding fractional density change can be expressed in terms of linear thermal expansion coefficient by using Eq.(6) as

$$\frac{\Delta\rho}{\rho_o} = \frac{1 - \left(1 + \Delta T\, \overline{\alpha}_l\right)^3}{\left(1 + \Delta T\, \overline{\alpha}_l\right)^3} \tag{8a}$$

where $\Delta\rho = \rho - \rho_o$. Density as a function of temperature can be found by arranging Eq.(8a) as

$$\rho = \left[1 + \frac{1 - \left(1 + \Delta L / L_o\right)^3}{\left(1 + \Delta L / L_o\right)^3} \right] \rho_o \tag{8b}$$

Conversely, the fractional length change ($\Delta V/V_o$) can be determined where the density change is known by

$$\frac{\Delta L}{L_o} = \left(\frac{\rho_o}{\rho} \right)^{\frac{1}{3}} - 1 \tag{8c}$$

4.2 ZrN

4.2.1 Thermal expansion

The thermal expansion coefficient data of ZrN are available from Touloukian [1], and the correlation is

$$\Delta L / L_o = -0.182 + 5.816 \times 10^{-4}\, T + 1.333 \times 10^{-7}\, T^2 - 7.822 \times 10^{-12}\, T^3 \tag{9}$$

where $\Delta L / L_o$ is in % and T in K. The instantaneous linear thermal expansion coefficient is tabulated as a function of temperature [1]. The following correlation was fitted to the data:

$$\alpha_l = 6.572 + 1.825 \times 10^{-3}\, T - 1.203 \times 10^{5}\, / T^2 \tag{10}$$

where α_l is the instantaneous linear thermal expansion coefficient in 10^{-6} K^{-1} and T in K. Eq.(9) and Eq.(10) are recommended for the present handbook and are used to generate values in Table 4-1.

Table 4-1 Thermal Expansion Coefficient and Density of ZrN [1]

T (K)	$\Delta L/L_o$ ($\times 10^2$) [a]	α_l ($\times 10^6$ K^{-1}) [b]	ρ ($g.cm^{-3}$) [c]
293	0.000	5.705 [b]	7.220
300	0.004	5.783	7.219
400	0.071 [a]	6.550	7.205
500	0.141	7.003	7.190
600	0.213	7.333	7.174
700	0.288	7.604	7.158
800	0.365	7.844	7.142
1000	0.525	8.277	7.107
1200	0.694	8.678	7.072
1400	0.872	9.066	7.034
1600	1.058	9.445	6.996
1800	1.251	9.820	6.956
2000	1.452	10.192	6.914
2200	1.659	10.562	6.872
2400	1.874	10.931	6.829

a: For example, this value should read as $\Delta L/L_o = 0.071 \times 10^{-2}$ at T = 400 K.

b: Instantaneous coefficient of linear expansion. This value reads as $\alpha_l = 5.705 \times 10^{-6}$ K^{-1} at 293 K.

c: Calculated based on ρ_o = 7.22 g/cm^3 (at T_o = 293 K) using Eq.(8b).

4.2.2 Density

The density of ZrN at room temperature has been reported several places [2 – 5]. The values, however, are inconsistent among themselves. Samsonov [2,3] indexed two values; one is 7.09 g/cm^3 from the picnometer measurement and the other 7.35 g/cm^3 from the X-ray method. Touloukian [4] recommended 6.84 g/cm^3 for ZrN and 7.30 g/cm^3 for $ZrN_{0.96}$. Recently, Kosukhin et al. [5] reported a picnometric density of $ZrN_{0.93}$ as 7.24 g/cm^3, which is consistent with the Touloukian and the Samsonov's picnometer value, considering the hypostoichiometry. For the present handbook, the average value of Samsonov's two methods, 7.22 g/cm^3, is recommended.

The density change as a function of temperature can be obtained by using Eq.(8b). The thermal expansion and density of ZrN are tabulated in Table 4-1.

4.3 PuN

4.3.1 Thermal expansion

The linear thermal expansion and linear thermal expansion coefficient of PuN are suggested in Touloukian [1]. The thermal linear expansion is

$$\Delta L / L_o = -0.342 + 1.154 \times 10^{-3}\, T + 5.561 \times 10^{-8}\, T^2 - 1.205 \times 10^{-11}\, T^3 \qquad (11)$$

where the thermal linear expansion is in % and T in K. The coefficient of linear thermal expansion is

$$\alpha_l = 11.471 + 1.244 \times 10^{-3}\, T - 4.079 \times 10^{-7}\, T^2 \qquad (12)$$

where the thermal expansion is in 10^{-6} K^{-1} and T in K.

Kurosaki et al. [6] evaluated the thermal expansion of PuN with molecular dynamics method, finding the instantaneous linear thermal expansion coefficient α_l as

$$\alpha_l = 8.861 + 2.324 \times 10^{-3}\, T \qquad (13)$$

Kosolapova suggested $\alpha_l = 7.95 \times 10^{-6}$ K^{-1} for 300 –1300 K [7]. Fig.4-1 compares the data from Touloukian, Kurosaki and Kosolapova. The values by Kurosaki are generally lower than those from Touloukian. Kosolapova data show the lowest extreme. Kurosaki data, Eq.(13), is recommended for the present handbook. The linear thermal expansion, Eq.(11) and the linear thermal expansion coefficient, Eq.(13) are selected and tabulated in Table 4-2.

4.3.2 Density

The room temperature density of PuN can be found in several places [2,3,8]. The values found are 14.23 g/cm^3 by Samsonov and Hausner [2], 14.151 g/cm^3 by Samsonov [3], and 14.24 g/cm^3 by Matzke [8]. The values from Samsonov and Hausner [2] and Matzke [8] are very close, suggesting consistency between the data. Therefore, the average of the values from Ref.2 and Ref.8 is recommended, i.e., the density of PuN is 14.235 g/cm^3. The temperature-dependent density change is given in Table 4-2.

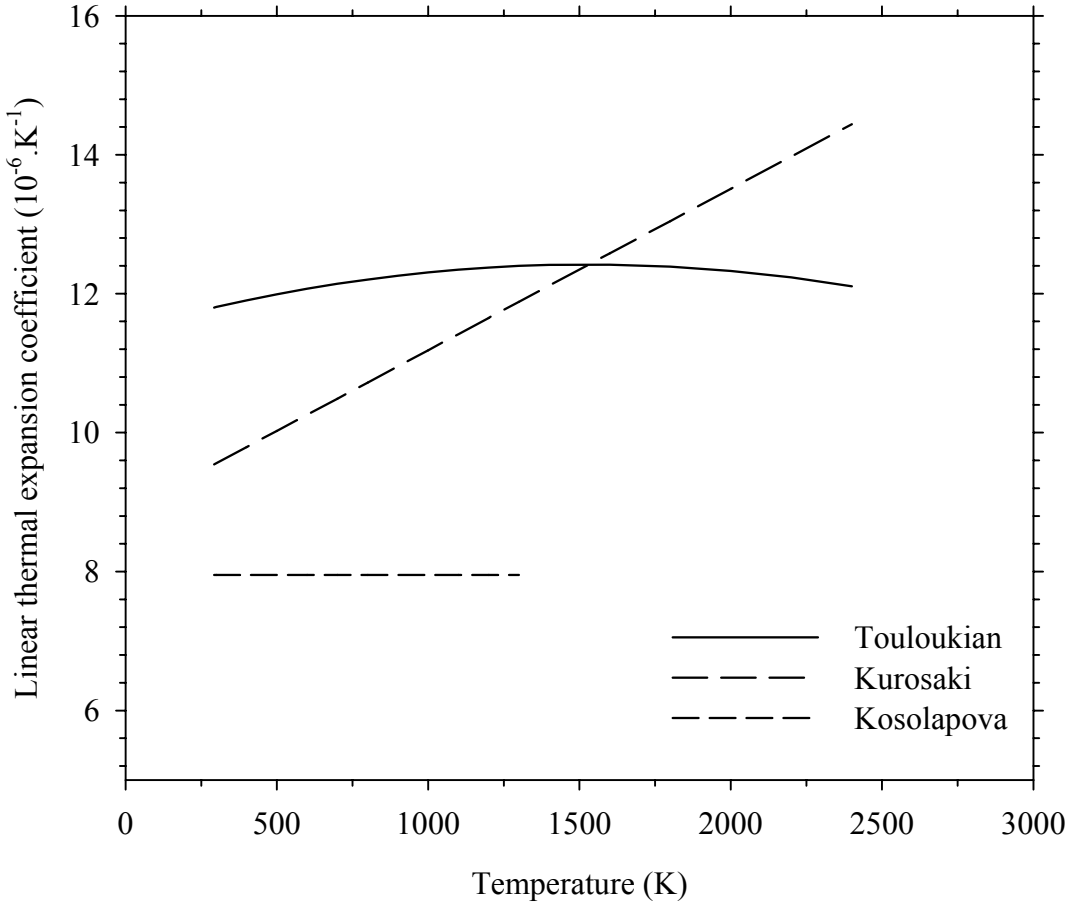

Fig.4-1 Comparison of the linear thermal expansion coefficient of PuN in the literature

Table 4-2 Thermal Expansion Coefficient and Density of PuN

T (K)	$\Delta L/L_o$ ($\times 10^2$) [a]	α_l ($\times 10^6$ K^{-1}) [b]	ρ ($g.cm^{-3}$) [c]
293	0.000	9.542 [b]	14.235
300	0.009	9.558	14.231
400	0.128 [a]	9.791	14.181
500	0.247	10.023	14.130
600	0.368	10.255	14.079
700	0.489	10.488	14.028
800	0.611	10.720	13.977
900	0.733	10.953	13.927
1000	0.856	11.185	13.876
1100	0.979	11.417	13.825
1200	1.102	11.650	13.775
1300	1.226	11.882	13.724
1400	1.350	12.115	13.674
1600	1.597	12.579	13.574
1800	1.845	13.044	13.475
2000	2.092	13.509	13.378
2200	2.338	13.974	13.282
2400	2.581	14.439	13.187

a: For example, this value should read as $\Delta L/L_o = 0.128 \times 10^{-2}$ at T = 400 K.

b: This value reads as $\alpha_l = 9.542 \times 10^{-6}$ K^{-1} at 293 K.

c: Calculated based on ρ_o = 14.235 g/cm^3 (at T_o=293 K) using Eq.(8b).

4.4 (Pu,Zr)N

There are no data for thermal expansion of (Pu,Zr)N in the literature. The simple law of mixtures is recommended. Therefore, the thermal expansion and the coefficient of linear thermal expansion are estimated as

$$(\Delta L / L_0)_{(Pu,Zr)N} = \mathrm{v}_{\mathrm{PuN}} (\Delta L / L_0)_{PuN} + \mathrm{v}_{ZrN} (\Delta L / L_0)_{ZrN} \tag{14}$$

$$\alpha_{(Pu,Zr)N} = \mathrm{v}_{\mathrm{PuN}} \alpha_{PuN} + \mathrm{v}_{ZrN} \alpha_{ZrN} \tag{15}$$

where v is the volume fraction. The composition is typically given by $(Pu_cZr_{1-c})N$. For this case, the molecular fractions of PuN and ZrN in the solid solution need to be converted to the volume fractions by the formula

$$\mathrm{v}_{PuN} = \frac{\rho_{ZrN} M_{PuN} a_{PuN}}{\rho_{PuN} M_{ZrN} - (\rho_{PuN} M_{ZrN} - \rho_{ZrN} M_{PuN}) a_{PuN}} \tag{16}$$

where v is the volume fraction, ρ the density, *M* the molecular weight and *a* the molecular fraction. For the case where $(Pu_cZr_{1-c})N$ is given, the molecular fraction of PuN, c, is equal to a_{PuN} in Eq.(16); $a_{\mathrm{ZrN}} = 1 - c = 1 - a_{\mathrm{PuN}}$. If the composition is given in the weight fractions of each nitride, the volume fractions can be found by using the relationship

$$\mathrm{v}_{PuN} = \frac{\rho_{ZrN} x_{PuN}}{\rho_{PuN} - (\rho_{PuN} - \rho_{ZrN}) x_{PuN}} \tag{17}$$

where *x* is the weight fraction.

The density of (Pu,Zr)N solid solution is also approximated by the law of mixtures.

$$\rho_{(Pu,Zr)N} = \mathrm{v}_{\mathrm{PuN}} \rho_{PuN} + \mathrm{v}_{ZrN} \rho_{ZrN} \tag{18}$$

where ρ is the density of the nitride solid solution.

As an example, the thermal expansion, the coefficient of linear thermal expansion and the density of $(Pu_{0.2}Zr_{0.8})N$ calculated using Eq.(14), Eq.(15) and Eq.(18), respectively, are tabulated in Table 4-3.

Fig.4-2 shows a comparison between the coefficient of the linear thermal expansion of PuN, ZrN and $(Pu_{0.2}Zr_{0.8})N$.

4.5 (TRU,Zr)N

Since there are no data in the literature, the methods used in the previous subsection for (Pu,Zr)N are suggested for (TRU,Zr)N, regarding the TRU content as the Pu content.

Table 4-3 Thermal Expansion, Linear Thermal Expansion Coefficient and Density of $(Pu_{0.2}Zr_{0.8})N$

T (K)	$\Delta L/L_o$ ($\times 10^2$) [a]	α_l ($\times 10^6$ K^{-1}) [b]	ρ ($g.cm^{-3}$)
293	0.000	6.610 [b]	8.874
300	0.005	6.673	8.872
400	0.085 [a]	7.315	8.851
500	0.166	7.717	8.830
600	0.250	8.024	8.808
700	0.335	8.287	8.785
800	0.423	8.526	8.762
900	0.512	8.751	8.739
1000	0.604	8.968	8.715
1100	0.697	9.178	8.691
1200	0.791	9.386	8.667
1400	0.986	9.792	8.617
1600	1.187	10.193	8.566
1800	1.393	10.590	8.513
2000	1.605	10.985	8.460
2200	1.822	11.379	8.406
2400	2.043	11.771	8.352

a: This value should read as $\Delta L/L_o = 0.0856 \times 10^{-2}$ at T = 400 K.

b: This value should read as $\alpha_l = 6.610 \times 10^{-6}$ K^{-1}.

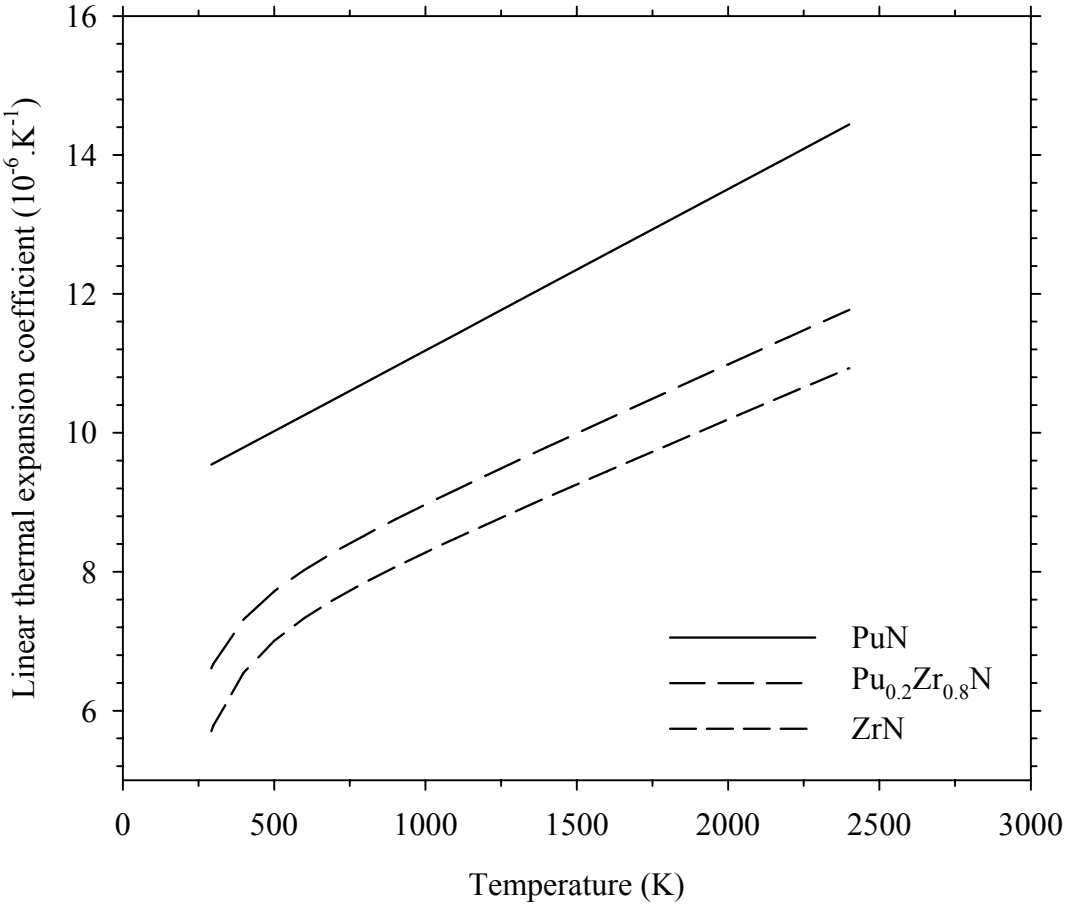

Fig.4-2 Comparison of the linear thermal expansion coefficients of ZrN, PuN and $(Pu_{0.2}Zr_{0.8})N$

4.6 References for Section 4

1. Y.S. Touloukian, R.K. Kirby, R.E. Taylor and P.D. Desai, Thermal Expansion, Thermophysical Properties of Matter, Vol.12, IFI/Plenum, New York-Washington (1975).
2. G.V. Samsonov, Plenum Press Handbook of High-temperature Materials, No.2 Properties Index, Plenum Press, New York (1964).
3. G.V. Samsonov and I.M. Vinitskii, Handbook of Refractory Compounds, IFI/Penum, New York-Washington-London (1980).
4. Y.S. Touloukian, Thermophysical Properties of High Temperature Solid Materials, Vol.5, The Macmillan Co., New York (1967).
5. V.V. Kosukhin, V.F. Funke, I. Minashkin, et al., Izvestiya Akademii Nauk SSSR, Neorganicheskie Materialy, 23(1), 63 (1987).
6. K. Kurosaki, K. Yano, K. Yamada, et al., J. Alloys Compounds, 313, 242 (2000).
7. T. Ya. Kosolapova, Handbook of High Temperature Compounds: Properties, production, Applications, Hemisphere Publishing Co., New York (1990).
8. Hj. Matzke, Science of Advanced LMFBR Fuels, p.62, North-Holland, Amsterdam (1986).

Section 5 Thermal Conductivity

5.1 ZrN

Hedge et al. [1] reported measured data for the thermal conductivity of ZrN at the temperature range of 408 – 2307 K. Touloukian's comparison [2] with other references showed that the Hedge data appeared to be the most reliable. Recently, Kleykamp [3] recommended the Hedge data for the ZrN thermal conductivity, but his data are systematically higher than the Hedge data for all temperature regimes although the difference is small. A parabolic correlation was used to fit the data to yield

$$k_{ZrN} = 1.423 + 2.402 \times 10^{-2}\, T - 6.404 \times 10^{-6}\, T^2 \qquad (1)$$

where k is the thermal conductivity in W/m-K and T in K. Fig.5-1 compares the correlation and the data.

5.2 PuN

The thermal conductivity of PuN can be found in several places [4 – 7]. Among them, the most recent data are by Arai [4]. The temperature dependence of the Arai data is similar to those of Keller [6] at temperatures lower than 1000 K. At temperatures higher than1000 K, however, Keller's data show a decrease as temperature rises while Arai and Alexander data show an increase. Because it reflected the abrupt drop of Keller's data at temperatures beyond 1000 K, the Matzke correlation decreases significantly at temperatures larger than 1600 K. For this handbook, the Arai data are preferred. The parabolic correlation fitted to the Arai data are expressed as follows

$$k_{PuN} = 6.906 + 7.653 \times 10^{-3}\, T - 2.011 \times 10^{-6}\, T^2 \qquad (2)$$

where k is in W/m-K and T in K.

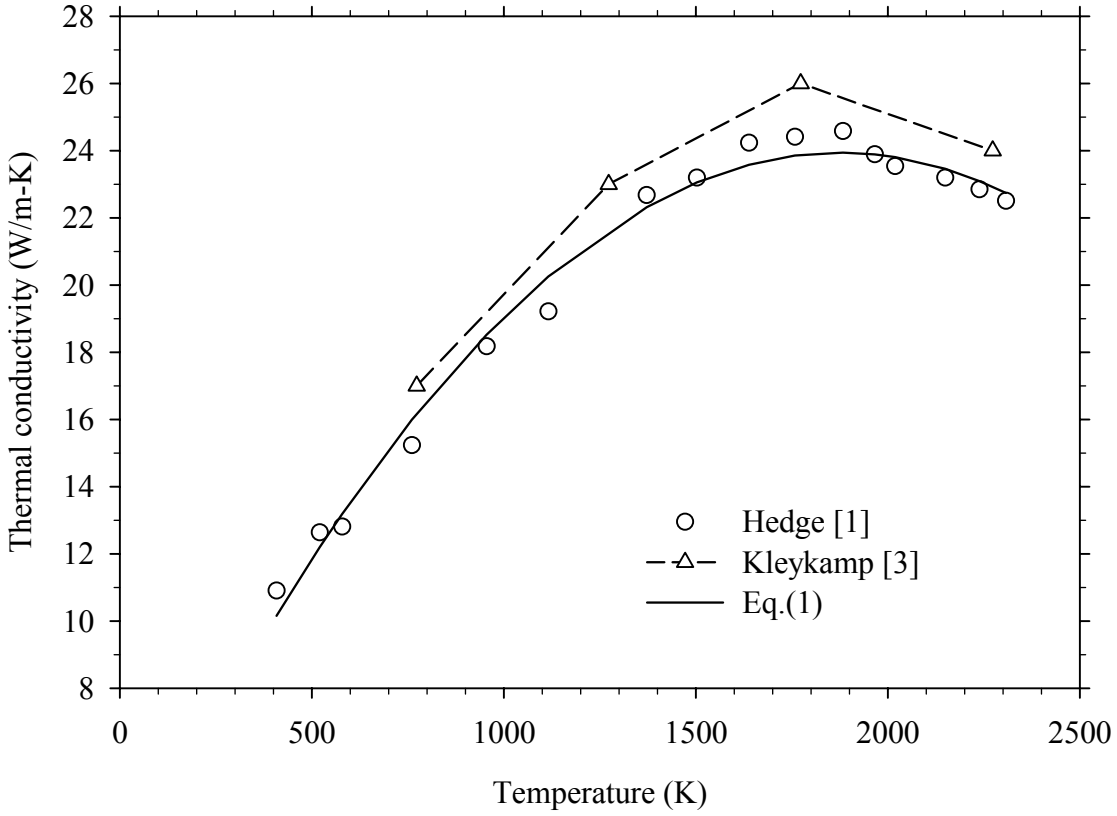

Fig.5-1 Thermal conductivity correlation of ZrN
fitted to the data in the literature

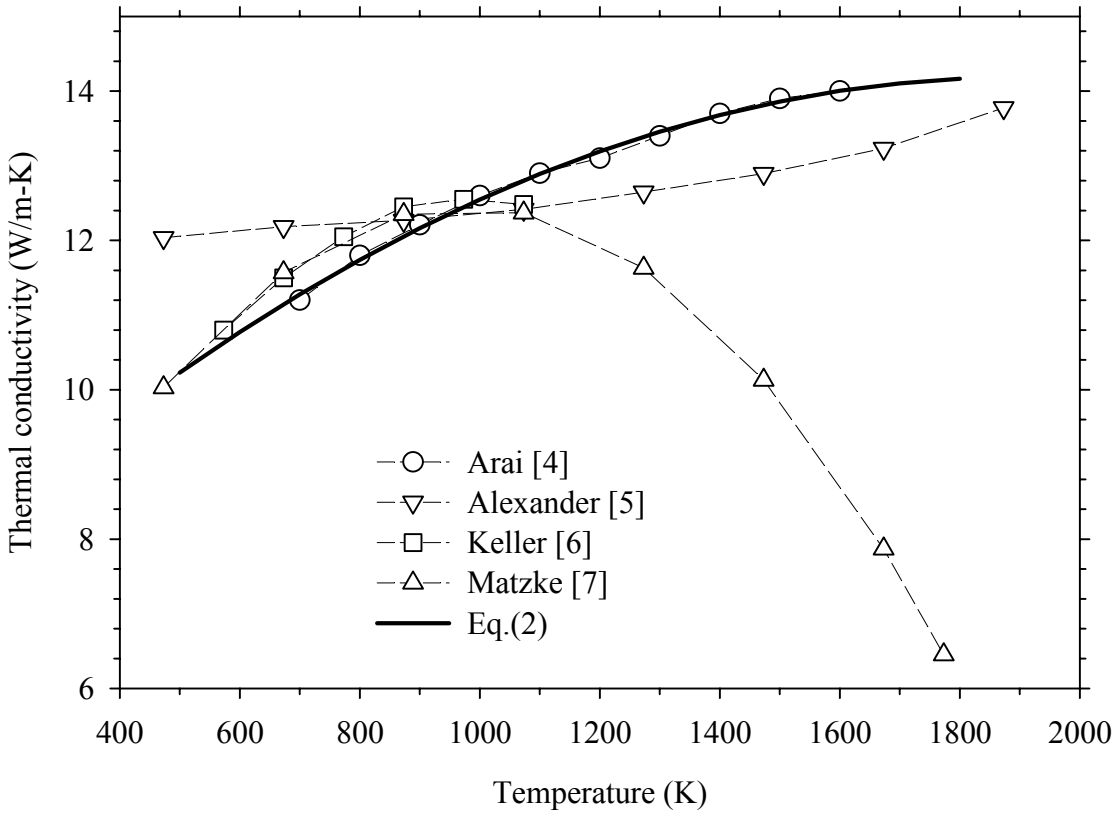

Fig.5-2 Thermal conductivity correlation of PuN fitted to the data in the literature

5.3 NpN

The thermal conductivity of NpN was measured by Arai [8]. The thermal conductivity correlation is

$$k_{NpN} = 7.89 + 1.27 \times 10^{-2}\, T - 4.32 \times 10^{-6}\, T^2 \qquad (3)$$

where k is in W/m-K and T in K.

5.4 (Pu,Zr)N

The thermal conductivity of (Pu,Zr)N is not available in the literature. A method to estimate is needed.

The measured thermal conductivities of (U,Pu)N solid solutions [4] were lower than the values calculated by the averaging method such as Bruggeman formula (see PART A, subsection 6.2). This is attributed to the impurity effect. The discrepancy becomes more noticeable at lower temperatures; at high temperatures above 1100 K, the difference is negligible. Since the current design for AAA nitride fuels adopts a temperature regime lower than 1100 K, the solid solution effect must be considered. More detailed explanation regarding the impurity effect is given in PART A, subsection 6.2.

The thermal conductivity of ZrN (Eq.(1)) is similar to that of UN (from Arai [4]) in temperature dependence, as shown in Fig.5-3. Arai [4] measured the effect of PuN content on the thermal conductivity of (U,Pu)N solid solutions. Considering also the similarities in crystal structure (both cubic NaCl type) and lattice parameter between UN and ZrN, we consider that the solid solution effect of (Pu,Zr)N is also similar to that of (U,Pu)N. The thermal conductivity of (Pu,Zr)N as a function of ZrN content and temperature is obtained using the same scheme in PART A, subsection 6.2.

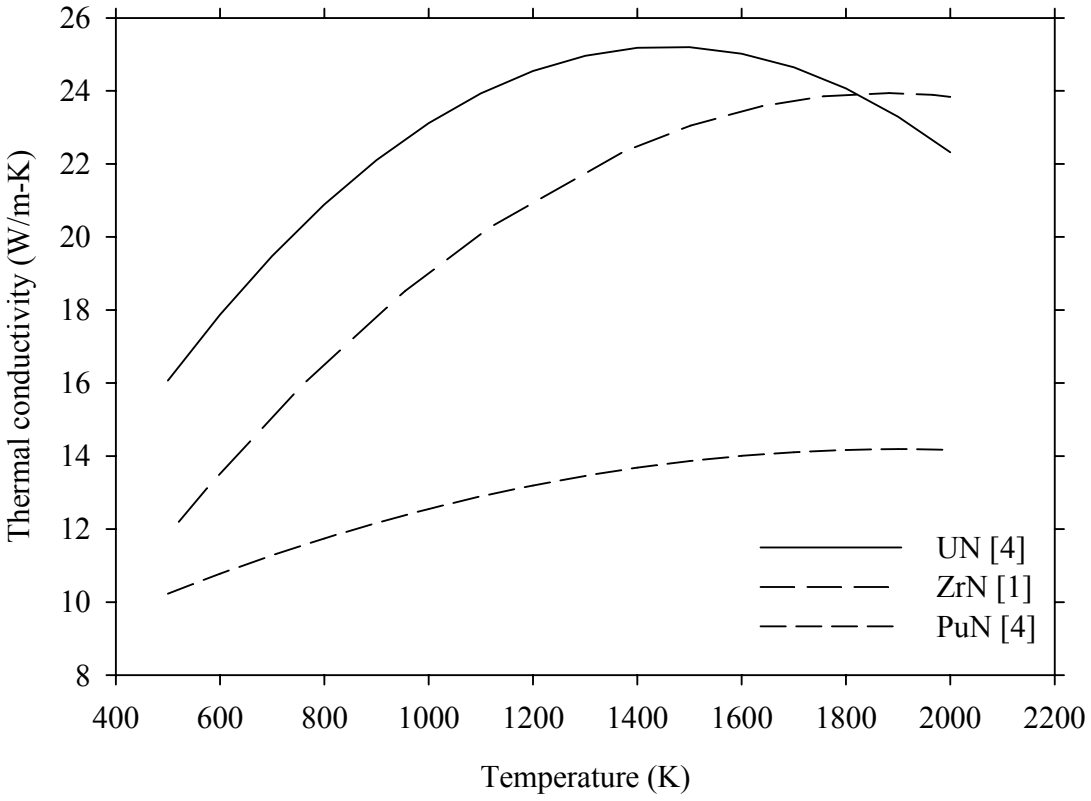

Fig.5-3 Comparison of thermal conductivities of UN, ZrN and PuN

$$k_{(Pu,Zr)N} = \left(1-\sqrt{1-x_{ZrN}}\right)k_{ZrN} + \sqrt{1-x_{ZrN}}\ \left\{x_{ZrN}\ k_m + \left(1-x_{ZrN}\right)k_{PuN}\right\} \tag{4}$$

where k_{ZrN} is given by Eq.(1), k_{PuN} by Eq.(2), and

$$k_m = -8.432 + 14.438\ x_{ZrN} + 0.014\ T - 1.957\times10^{-6}\ T^2 - 1.549\times10^{-3}\ x_{ZrN}\ T \tag{5}$$

Here x_{ZrN} is the molecular fraction of ZrN in (Pu,Zr)N solid solution; frequently, x is also given such as $(Pu_{1-x}Zr_x)N$.

The prediction result by Eq.(4) is compared with ZrN and PuN data from the literature and plotted in Fig.5-4. At lower temperatures, the solid solution thermal conductivity is lower than that of PuN due to the increased impurity effect at low temperatures.

5.5 (TRU,Zr)N

Because there are no data available for the thermal conductivity of (TRU,Zr)N, Eq.(4) is recommended for use as an estimation, regarding the TRU content as the Pu content.

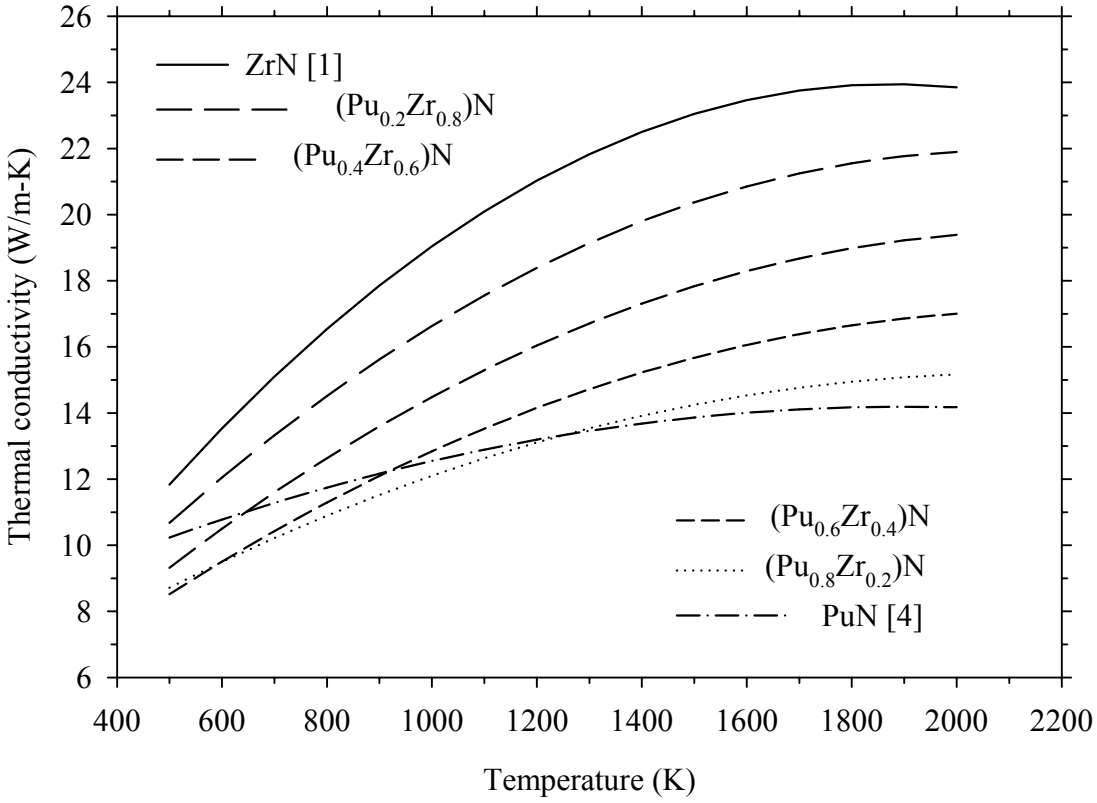

Fig.5-4 Thermal conductivity of ZrN, PuN and (Pu,Zr)N solid solutions

5.6 Porosity Effect

The nitride option for AAA fuel includes approximately 15% as-fabricated porosity. Regardless of the amount, once introduced, porosity reduces the thermal conductivity. There have been many quantitative methods to deal with the effect of porosity on the bulk thermal conductivity. For the present handbook, the Maxwell-Eucken equation is suggested:

$$k_P = \frac{1-P}{1+\beta P} k_{TD} \tag{6}$$

where k_P is the thermal conductivity of a matrix including porosity P, k_{TD} the thermal conductivity of the matrix with 100% theoretical density, and P porosity in fraction. Here β is used to correct the characteristics of pores; the more closed pores, the higher the value. For a high closed pore case, β can be 2 or even 3.

The porosity effect on the thermal conductivity of (Pu,Zr)N fuel containing 15% porosity is calculated as $k_{15} = 0.74\ k_{TD}$, if $\beta = 1$; $k_{15} = 0.65\ k_{TD}$, if $\beta = 2$.

For the current application, $\beta = 1$ is recommended.

5.7 References for Section 5

1. J.C. Hedge, J.W Kopec, C. Kostenko and J.I. Lang, Technical Documentary Report ASD-TDR-63-597, IIT Research Institute (1963).
2. Y.S. Touloukian, R.W. Powell, C.Y. Ho and P.G. Klemens, Thermophysical Properties of Matter, vol. 2, Thermal Conductivity, p.675, IFI/Plenum, New York-Washington (1970).
3. H. Kleykamp, J. Nucl. Mater., 275, 1 (1999).
4. Y. Arai, Y. Suzuki, T. Iwai and T Ohmichi, J. Nucl. Mater., 195, 37 (1992).
5. C.A. Alexander, R.B. Clark, O.L. Kruger and J.L. Robbins, in Plutonium and other Actinides, Eds. H. Blank and R. Lindner, p.277, North-Holland Pub. Co., Amsterdam (1976).
6. D.L. Keller, Battelle Memorial Institute, Report BMI-1845 (1968).
7. Hj. Matzke, Science of Advanced LMFBR Fuels, North-Holland, Amsterdam (1986).
8. Y. Arai, Y. Okamoto and Y. Suzuki, J. Nucl. Mater., 211, 248 (1994).

Section 6 Diffusion Coefficient

6.1 Diffusion in ZrN

The diffusion coefficient for Zr in ZrN is not available in the literature. Desmaison and Smelzer [1] argued that Zr diffusion in ZrN is negligible. Nitrogen diffusion in ZrN is measured by several authors [1 – 6]. The data, however, are not consistent among themselves. The recommended values are obtained by the best fit of the data shown in Fig.6-1. The recommended chemical diffusion coefficient of nitrogen in ZrN, $\widetilde{D}$, given as a solid line in the plot, is

$$\widetilde{D} = 1.086 \times 10^{-5} \exp\left(\frac{-12.73 \times 10^{4}}{RT}\right) \tag{1}$$

where $\widetilde{D}$ is in cm^2/s, R the gas constant in J/mole-K and T in K.

6.2 Diffusion in (U,Pu)N

Information of Pu diffusion in (Pu,Zr)N is not available in the literature. Instead, Matzke [7] collected and reviewed Pu diffusion in (U,Pu)N. The Pu diffusion coefficient obtained for $(U_{0.8}Pu_{0.2})N$ is produced by extracting values from one of the plots in Matzke book, i.e.,

$$D_{Pu} = 4.571 \times 10^{-3} \exp\left(\frac{-43.27 \times 10^{4}}{RT}\right) \tag{2}$$

where D is in cm^2/s, R in J/mole-K and T in K.

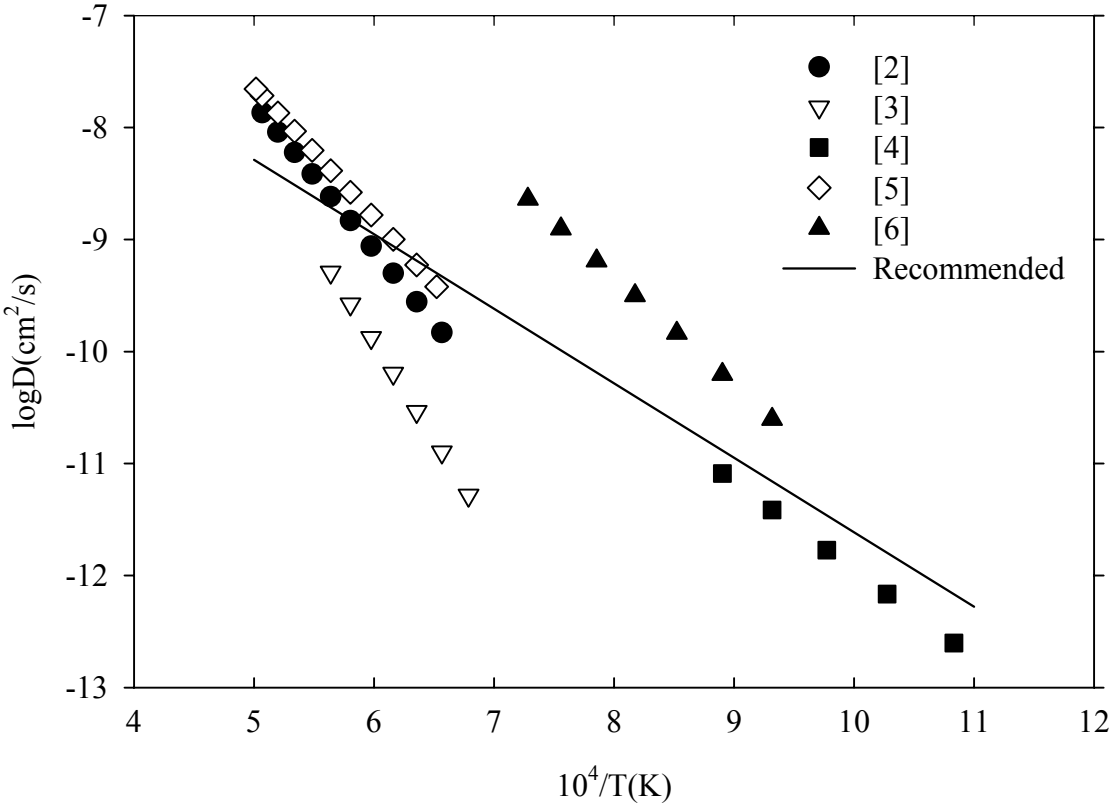

Fig.6-1 Nitrogen diffusion coefficient in ZrN in the literature and recommended fit

D_{Pu} depends on nitrogen pressure, with the relationship $D_{Pu} \propto p_{N_2}^{\frac{1}{n}}$. n increases with temperature, implying D_{Pu} becomes independent on nitrogen pressure at high temperatures. At 1650°C, n=4.8; and at 1810°C n=200 [7].

6.3 Diffusion in (Pu,Zr)N

No information for diffusion of Pu and Zr in (Pu,Zr)N is found in the literature. As a result of the review in subsections 6.1 and 6.2, however, Pu diffusivity is deemed similar to that in (U,Pu)N given by Eq.(2), and Zr diffusivity is negligible. Nitrogen diffusion in (Pu,Zr)N is probably similar to that in ZrN discussed in subsection 6.1.

6.4 Radiation Enhanced Diffusion in (Pu,Zr)N

The irradiation enhanced diffusion of (U,Pu)N is discussed by Matzke [7,8]. The enhancement in diffusion for (U,Pu)N under irradiation is a linear relation of burnup given as follows [7]:

$$D^* = (1.8 \pm 0.5) \times 10^{-30} \dot{F} \tag{3}$$

Here D^* is in cm^2/s and $\dot{F}$ in fissions/cm^3-s. Notice D^* is independent on temperature.

As a result, the total diffusion coefficient of Pu is obtained by adding Eq.(2) and Eq.(3), i.e.,

$$D_t = D_{Pu} + D^* \tag{4}$$

6.5 References for Section 6

1. J.G. Desmaison and W.W. Smelzer, J. Electrochem. Soc., 122 (3), 354 (1975).
2. V.S. Eremeyev, Y.M. Ivanov and A.S. Panov, Izv. Akad. Nauk SSSR, Metal., No.4, 262 (1969).
3. S.K. Iyer, Ph.D. Thesis, University of Pennsylvania, Philadelphia, Pa. (1971).
4. C.J. Rosa and W.C. Hagel, J. Electrochem. Soc., 115, 467 (1968).
5. Y.V. Levinskii, S.S. Kiparisov and Y.D. Strogonov, Izv. Vysshikh Uchebn. Zavedenii, Tsvetn. Met., 13, 91 (1970).
6. J. Paidassi and R. Le Delliou, C.R. Acad. Sci. Paris, Ser. C, 272, 249 (1971).
7. Hj. Matzke, Science of Advanced LMFBR Fuels, North-Holland (1986).
8. Hj. Matzke, J. Less-Common Metals, 121, 537 (1986).

Section 7 Elastic Constants

7.1 Young's Modulus

7.1.1 Fully Dense Nitride

ZrN

Young's modulus or elasticity modulus of ZrN at room temperature is found in several places [1–6]. The values are 328 GPa [1,2], 392 GPa [3], 441 GPa, 500 GPa [4], and 460 GPa [4–6]. Among these values, the most frequent and recent one, 460 GPa, is selected.

The temperature dependence of ZrC, $ZrN_{0.79}$ and $ZrN_{0.89}$ is found in Ref.1. The carbide and nitrides showed the same linear decrease with temperature at the temperature range of 293 – 2000 K. The difference is small. Hence, fitting the data to a linear equation yields

$$E(T) = E_0 \left[1 - 1.33 \times 10^{-4} \left(T - T_0\right)\right] \quad (1)$$

where E_0 is the elasticity modulus at room temperature in GPa and T_0 is room temperature. As a result, recommendation for the elasticity modulus of ZrN is

$$E_{ZrN} = 460 \left[1 - 1.33 \times 10^{-4} \left(T - 293\right)\right] \quad (2)$$

where E is in GPa and T in K.

PuN

The elasticity modulus for PuN has not been measured.

Matzke [7] showed the temperature dependence of the elasticity modulus of (U,Pu)N is a linear relationship between the elasticity modulus and temperature:

$$E(T) = E_0 \left[1 - 0.92 \times 10^{-4} \left(T - T_0\right)\right] \tag{3}$$

where E_0 is the elasticity modulus at room temperature in GPa and T_0 is room temperature.

Matzke argued that the substitution of U by Pu does not change the elasticity modulus of (U,Pu)N, which suggests that PuN behaves similarly as UN, as far as elasticity is concerned [7]. Based on this, the elasticity modulus of PuN is approximated by that of UN. The room temperature elasticity modulus of UN appears in several places [8 – 13]. The values vary in the range 262 – 270 GPa. Among these, 270 GPa from Refs.12 and 13, is recommended, because they are the most recent results.

The temperature dependence is assumed the same as that of (U,Pu)N. Then, the Young's modulus for PuN is given as

$$E_{PuN} = 270 \left[1 - 0.92 \times 10^{-4} \left(T - 293\right)\right] \tag{4}$$

where E is in GPa and T in K.

(Pu,Zr)N

There is no measurement available for the elasticity modulus of (Pu,Zr)N in the literature. The classical law of mixtures is recommended, i.e.,

$$E_{(Pu,Zr)N} = \mathrm{v}_{ZrN} E_{ZrN} + (1 - \mathrm{v}_{ZrN}) E_{PuN} \tag{5}$$

where v is the volume fraction.

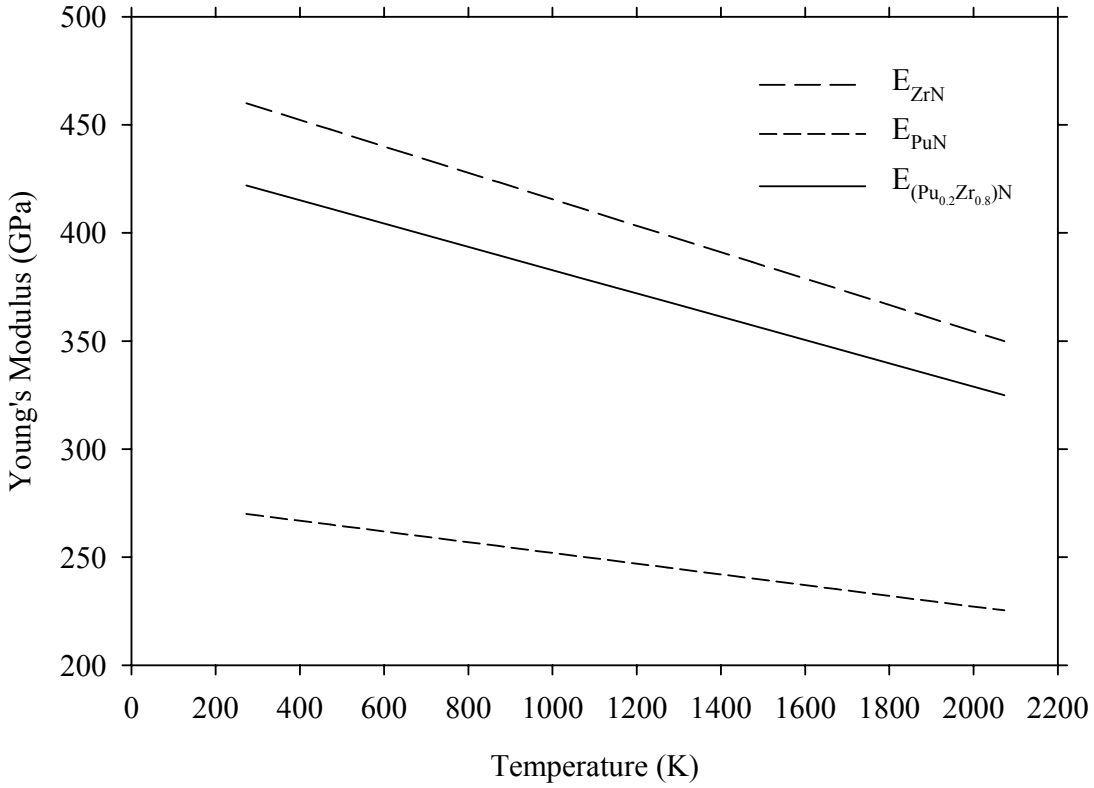

Fig.7-1 Estimated Young's modulus of 100% TD $(Pu_{0.2}Zr_{0.8})N$

The temperature-dependent correlations for E_{ZrN} and E_{PuN} are given in Eq.(3) and Eq.(4), respectively. The volume fraction can be derived from the weight fraction by the formula,

$$v_{ZrN} = \frac{\rho_{PuN}\, x_{ZrN}}{\rho_{ZrN} - (\rho_{ZrN} - \rho_{PuN}) x_{ZrN}} \tag{6}$$

where ρ is the density and x the weight fraction.

If the concentrations of PuN and ZrN are given in atomic fraction of Pu and Zr in (Pu,Zr)N such as $(Pu_{1-a}Zr_a)N$, the volume fraction can be approximated with a good accuracy by the atomic fractions, i.e., $v_{ZrN} \approx a$.

Fig.7-1 shows a prediction result for $(Pu_{0.2}Zr_{0.8})N$ using Eq.(5).

7.1.2 Porosity Correction

The elasticity modulus of UN decreases linearly as porosity increases. There are several methods to implement the porosity effect on the elastic constants. Among them, the linear relation (i.e., Loeb type) is adopted for this handbook; the elasticity modulus due to porosity is reduced by multiplying the value of a 100 % dense UN with a correction factor (1–αP), where α ranges 2.3 – 2.7 [8 – 10] and 2.7 for (U,Pu)N [7]. The same method is assumed applicable for the (Pu,Zr)N with α = 2.7; therefore, the elasticity modulus for the (Pu,Zr)N with porosity is expressed by

$$E^{P}_{(Pu,Zr)N} = (1 - 2.7\ P)\ E^{100}_{(Pu,Zr)N} \tag{7}$$

where $E^{P}_{(Pu,Zr)N}$ is the porosity corrected elasticity modulus of (Pu,Zr)N with porosity P, P is the fractional porosity, and $E^{100}_{(Pu,Zr)N}$ is the elasticity modulus of the 100 % theoretically dense (Pu,Zr)N provided in Eq.(5).

7.2 Poisson's Ratio

7.2.1 Fully Dense Nitrides

ZrN

Poisson's ratio of ZrN was reported as 0.25 [2,3].

The temperature dependence of Poisson's ratio is assumed the same as that of the elasticity modulus given in Eq.(1), i.e.,

$$\nu_{ZrN} = 0.25\left[1 - 1.33\times10^{-4}\left(T - 293\right)\right] \tag{8}$$

where T is in K.

PuN

No measurement for PuN is available; instead, Poisson's ratio of UN is given as 0.28 [13]. The value for UN is assumed applicable for PuN.

Similarly, the temperature dependence of Poisson's ratio of PuN is assumed the same as that of UN given in Eq.(3). As a result, Poisson's ratio for PuN is

$$\nu_{PuN} = 0.28\left[1 - 0.92\times10^{-4}\left(T - 293\right)\right] \tag{9}$$

(Pu,Zr)N

Because there are no data for (Pu,Zr)N solid solution in the literature, the classical law of mixtures, Eq.(5), is also recommended for the Poisson's ratio of (Pu,Zr)N,

$$\nu_{(Pu,Zr)N} = \mathrm{v}_{ZrN}\nu_{ZrN} + (1 - \mathrm{v}_{ZrN})\nu_{PuN} \tag{10}$$

where ν is Poisson's ratio and v the volume fraction. The volume fraction can be derived from the weight fraction by the formula,

$$v_{ZrN} = \frac{\rho_{PuN}\, x_{ZrN}}{\rho_{ZrN} - (\rho_{ZrN} - \rho_{PuN}) x_{ZrN}} \tag{11}$$

where ρ is the density and x the weight fraction.

7.2.2 Porosity Correction

Poisson's ratio of UN decreases almost linearly as porosity increases until the fractional porosity becomes 0.3 [13]. The same effect is assumed for (Pu,Zr)N, Therefore, the Poisson's ratio for (Pu,Zr)N can be recommended as follows:

$$\nu^{\mathrm{P}}_{(Pu,Zr)N} = (1 - 1.13\,\mathrm{P})\, \nu^{100}_{(\mathrm{Pu,Zr})\mathrm{N}} \tag{12}$$

where $\nu^{\mathrm{P}}_{(Pu,Zr)N}$ is the Poisson's ratio of (Pu,Zr)N with porosity P, *P* fractional porosity and $\nu^{100}_{(Pu,Zr)N}$ Poisson's ratio of100% theoretically dense (Pu,Zr)N obtained in Eq.(10).

7.3 References for Section 7

1. T.Ya. Kosolapova, Handbook of High Temperature Compounds, p.502, Hemisphere Publishing Co., New York (1990).
2. S.V. Borisov, B.V. Mitrofanov and G.P. Shveikin, Zvestiya Akad. Nauk SSSR, Neorgan. Mater., 15(12), 2124 (1979).
3. I.N. Frantsevich, E.A. Zhurakovskii and A.B. Lyashchenko, Inorg. Mater., 3, 6 (1967).
4. E. Toeroek, A.J. Perry, L. Chollet and W.D. Sproul, Thin Solid Films, 153, 37 (1987).
5. A.T. Santhanam, in Transition Metal carbides and Nitrides: Application of Transition Metal Carbides and Nitrides in Industrial Tools, Blackie Acad. And Prof., ed., S.T. Oyama, chap.1, p.1, London (1996).
6. A.J. Perry, Thin Solid Films, 193(1,2), 463 (1990).
7. Hj. Matzke, Science of Advanced LMFBR Fuels, North-Holland (1986).
8. H.L. Whaley, W. Fulkerson and R.A. Potter, J. Nucl. Mater., 31, 345 (1969).
9. A. Padel and C.H. de Novion, J. Nucl. Mater., 33, 40 (1969).
10. U. Guinan and C.F. Cline, J. Nucl. Mater., 43, 205 (1972).
11. C. Novion and R. Lallement, Rev. Int. Hautes Temp. Refract., 9(1), 117 (1972).
12. S.A. Balankin, A.S. Bubnov, N.A. Zaitsev et al., Izv. Akad. Nauk SSSR, Ser. Neorgan. Mater., 15(7), 1222 (1979).
13. S.L. Hayes, J.K. Thomas and K.L. Peddicord, J. Nucl. Mater., 171, 271 (1990).

Section 8 Creep

8.1 Fully Dense (Pu,Zr)N

Because of nonexistence of data for ZrN, PuN and (Pu,Zr)N creep, the creep rate for (Pu,Zr)N is assumed that of UN. Two works were found that provided thermal creep data for UN [1,2]. Based on this, two model correlations were generated by independent investigators [3,4]. Among them, the correlation by Hayes et al. [3] follows a simple power law assuming dislocation climb as the dominant creep mechanism, avoiding the complexity of the grain size dependence. On the other hand, Billone's model is represented by the sum of a linear thermal creep and a power-law thermal creep. For the present handbook, the correlation by Hayes et al. is selected, because it is a more recent product. Then, the thermal creep rate can be given by

$$\dot{\varepsilon}_T = 2.054 \times 10^{-3} \sigma^{4.5} \exp\left(-\frac{39369.5}{T}\right) \tag{1}$$

where $\dot{\varepsilon}_T$ is the thermal creep rate in s^{-1}, σ the effective stress in MPa and T temperature in K. Notice that the creep rate is for the steady state regime.

8.2 Porosity Correction

The increase in creep of less than 100%TD nitrides from the fully dense one was modeled using UO_2 data by Hayes et al. [3]. Adopting the Hayes model, the augmentation factor to be multiplied to Eq.(1) for fuels with less than 100% TD is expressed by

$$f(P) = \frac{0.987 \exp(-8.65 P)}{(1-P)^{27.6}} \tag{2}$$

where P is the fractional porosity.

8.3 Irradiation Effect

Nitride fuel is subject to additional creep under neutron irradiation. The additional amount of creep is additive to the thermal creep obtained in Eq.(1), and it is known independent on temperature. Billone et al [4] derived a correlation for creep under irradiation based on the data by Brucklacher and Dienst [5]:

$$\dot{\varepsilon}_I = 1.81\times10^{-32}\left(1+1250\,P^2\right)\sigma\,\dot{F} \tag{3}$$

where $\dot{\varepsilon}_I$ is the additional creep due to irradiation in s^{-1}, P the fractional porosity, σ the effective stress in MPa and $\dot{F}$ the fission rate in fissions/m^3-s.

As a result, the total steady-state creep rate considering all features discussed above is obtained as $\dot{\varepsilon} = \dot{\varepsilon}_T + \dot{\varepsilon}_I$, i.e.,

$$\dot{\varepsilon} = 2.054\times10^{-3}\sigma^{4.5}\exp\left(-\frac{39369.5}{T}\right)\frac{0.987\exp(-8.65\,P)}{(1-P)^{27.6}} + 1.81\times10^{-32}\left(1+1250\,P^2\right)\sigma\,\dot{F} \tag{4}$$

where

$\dot{\varepsilon}$ = the total steady-state creep in s^{-1},

σ = the effective stress in MPa,

T = the temperature in K,

P = the fractional porosity,

$\dot{F}$ = the fission rate in fissions/m^3-s.

8.4 References for Section 8

1. R.R. Vandervoort, W.L. Barmore and C.F. Cline, Trans. Met. Soc., AIME, 242, 1466 (1968).
2. M.H. Fassler, F.J. Huggel and M.A. DeCrescente, Compressive Creep of UC and UN, Pratt and Whitney Aircraft Co., PWAC-482 (1965).
3. S.L. Hayes, J.K. Thomas and K.L. Peddicord, J. Nucl. Mater., 171, 271 (1990).
4. M.C. Billone, V.Z. Jankus, J.M. Kramer and C.I. Yang, Proc. Advanced LMFBR Fuels, Tucson, AZ, eds., J. Leary and H. Kittel, American Nuclear Society, p.516 (1977).
5. D. Brucklasher and W. Dienst, J. Nucl. Mater., 42, 285 (1972).

Section 9 Swelling

9.1 Basic Swelling Correlation

Although extensive swelling data for (U,Pu)C exist, (Pu,Zr)N does not have any measurement data in the literature [1]. Therefore, estimations need to be made. To establish a swelling correlation for (Pu,Zr)N, the swelling behavior of (Pu,Zr)N is assumed similar to that of (U,Pu)C. Swelling of carbides and oxides is known to be determined mainly by temperature and burnup [2,3].

The total swelling is a cumulative result of swelling due to solid fission products and swelling due to fission gas. The solid swelling rate is generally considered independent of temperature and burnup. Matzke [1] recommended swelling rate of 0.6 $\%\Delta V/V$ per at% burnup for (U,Pu)C, excluding the possible contribution from Cs. If Cs is included, the value increases to 1 $\%\Delta V/V$ per at% burnup. Zimmerman [2] used 0.8 $\%\Delta V/V$ in his correlation for (U,Pu)C. Therefore, the Zimmerman value happens to be the average of values with and without consideration of the Cs contribution. Since the behavior of solid fission products in nitrides is probably the same as that of carbides, the solid fission product swelling for (Pu,Zr)N can be deduced from the data for (U,Pu)C. Thus, selecting the Zimmerman data, the swelling rate due to solid fission products for (Pu,Zr)N is given by

$$\dot{S}_s = 0.8 \tag{1}$$

where the swelling rate is in $\%\Delta V/V$ per at% burnup.

There is no data for (Pu,Zr)N gas swelling although some data exist for (U,Pu)C. At the present time, (U,Pu)C swelling data are proposed to be used for obtaining a correlation for (Pu,Zr)N swelling with slight reduction because of less swelling in (Pu,Zr)N than (U,Pu)C.

The correlation by Zimmerman for the fission gas swelling of (U,Pu)C [2] is given below after minor modifications, i.e.,

$$\dot{S}_g^C = C_1\, C_2 \exp\left(-C_2 B\right) \tag{2}$$

where $\dot{S}_g^C$ = unrestrained swelling for (U,Pu)C in $\%\,\Delta V / V$ per at% burnup,

$$C_1 = 10 + \frac{24}{1+\exp\left(\dfrac{1400-T}{74}\right)},$$

$$C_2 = 0.06 + 8.025\times 10^3 \exp\left(-\frac{2.027\times 10^4}{T}\right),$$

B = burnup in at%,

T = fuel average temperature in K during irradiation.

Matzke showed that metal nitrides have distinctively smaller fission gas diffusivity than metal carbides [1]. This results in higher critical temperature for the onset of fission gas swelling, i.e., more fission gas remains in atomic dispersion (or dynamic solution), and resulting in a lower swelling rate. The comparison between the swelling rates of UN and UC is available from Matzke book [1]. In order to include this effect, the temperature-dependent reduction ratio of UN to UC is obtained by fitting the data, and multiplied to (U,Pu)C swelling rate, Eq.(2). Therefore, the swelling rate of (Pu,Zr)N is found as

$$\dot{S}_g^N = (2.732\times 10^{-4}\, T)\, \dot{S}_g^C \tag{3}$$

where $\dot{S}_g^C$ is the gas swelling rates of (U,Pu)C given in Eq.(2).

From Eq.(3), the difference in gas swelling of (U,Pu)C from that of (Pu,Zr)N is noticeable at temperatures only above 1000 K. For gas diffusion is negligible for both fuel types at low temperatures.

The total swelling rate for (Pu,Zr)N is addition of the rates given in Eq.(1) and Eq.(3), i.e.,

$$\dot{S} = 0.8 + 2.732 \times 10^{-4}\, T\, C_1\, C_2\, \exp(-C_2\, B) \tag{4}$$

where $\dot{S}$ is in $\%\,\Delta V / V$ per at% burnup, C_1 and C_2 given in Eq.(2).

9.2 Swelling under External Stress

The total swelling appears to saturate under enough external stress when there is free volume available in the fuel to accommodate the volume increase [4,5]. The free volume can be imparted by as-fabricated porosity and bubbles generated by irradiation. As-fabricated porosity of the current (TRU,Zr)N fuel design for AAA is ~15%.

The internal pressure of a gas bubble under a mechanical equilibrium state is given by

$$p_i = p_{ex} + \frac{2\gamma}{r} \tag{5}$$

where p_i is the bubble internal pressure, p_{ex} is the external pressure and $2\gamma/r$ is the surface tension force. When the external pressure is larger than that needed for equilibrium, the bubble stops to grow, which terminates further swelling.

The external pressure chiefly affects fission gas swelling by restricting gas bubble growth. In addition, as Koo showed [5], more gas can be retained in the grain boundary bubbles under external pressure, which results in less swelling. The external pressure enough to stop apparent swelling may be generated by pressure buildup in the fuel plenum and the fuel-to-cladding contact points. Zimmerman [2] claimed that the noticeable influence of the external stress was found only at temperatures above 1573 K and pressures greater than 30 MPa.

The swelling rate under external pressure situation can be modeled by multiplying an empirical term to the gaseous swelling rate. Using the data by Zimmerman [2], the total swelling rate for this situation is expressed as follows:

$$\dot{S} = 0.8 + 2.732 \times 10^{-4}\, T\, C_1\, C_2\, C_3 \exp(-C_2\, B) \qquad (6)$$

where $C_1 = 10 + \dfrac{24}{1 + \exp\left(\dfrac{1400 - T}{74}\right)}$,

$$C_2 = 0.06 + 8.025 \times 10^3 \exp\left(-\frac{2.027 \times 10^4}{T}\right),$$

$$C_3 = 1 - 0.01\, T \left[1 - \exp\left(-2.396 \times 10^{-4}\, p_c\right)\right],$$

with p_c the external pressure in MPa.

The total swelling is obtainable by integrating Eq.(6) with respect to burnup if needed.

Fig.9-1 shows a comparison between swelling of unrestrained and restrained fuel at the temperature range of 773 – 1773 K.

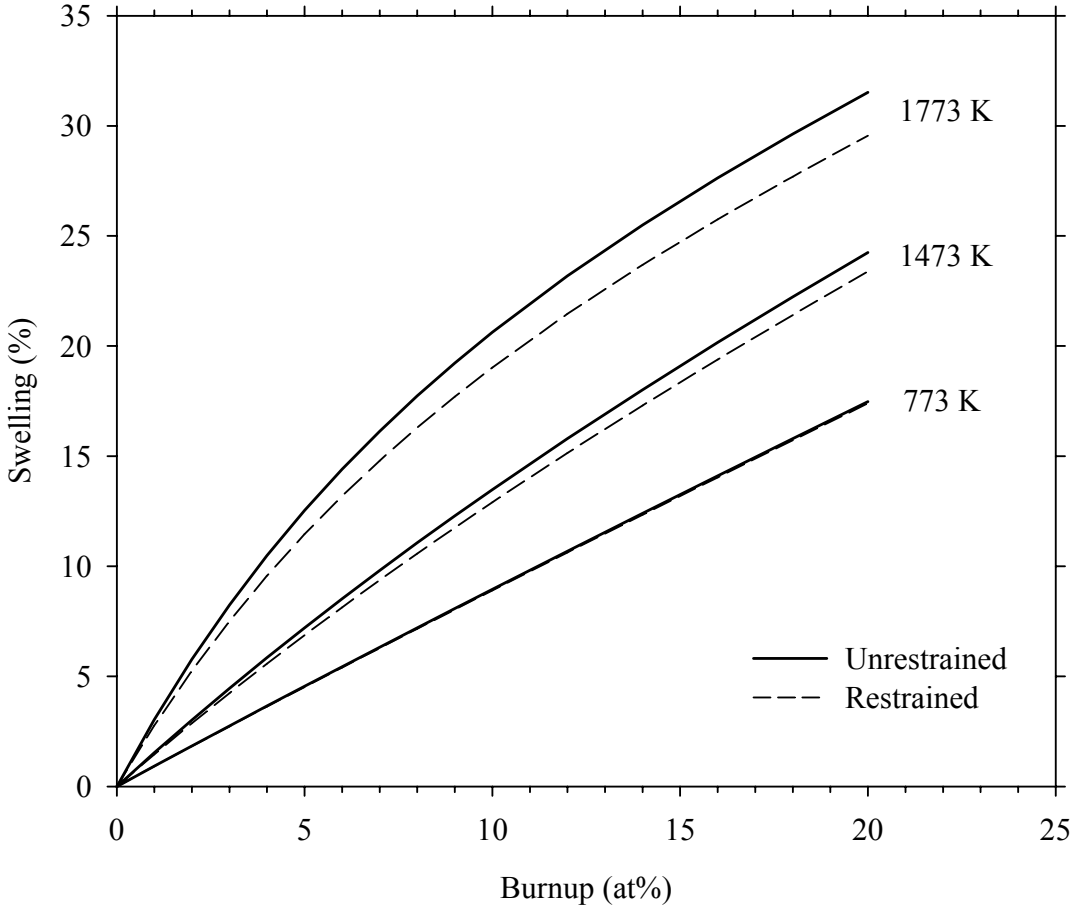

Fig.9-1 Swelling of (Pu,Zr)N with and without external stress of 30 MPa

9.3 References for Section 9

1. Hj. Matzke, Science of Advanced LMFBR Fuels, North-Holland, NewYork, 1986.
2. H. Zimmerman, J. Nucl. Mater., 105, 56 (1982).
3. SCDAP/RELAP5/MOD 3.2 Code manual, MATPRO-A Library of Materials Properties for Light Water Reactor Accident Analysis, NUREG/CR-6150, Vol.4, Rev.1, INEL-96/0422 (1998).
4. C.R. Tipton, Jr., Materials, in Reactor handbook, Vol.1, p.711, Interscience Publisher, Inc., New York (1960).
5. Y. Koo, B. Lee and D. Sohn, J. Nucl. Mater., 280, 86 (2000).

Section 10 Gas Release

10.1 Fission Gas Release Correlation

Currently there are no data for fission gas release from (Pu,Zr)N and (TRU,Zr)N in the literature. However, several data sets and model correlations for fission gas release from UN are available. For a preliminary recommendation, the data and correlations for UN are proposed to be used for (Pu,Zr)N.

Vaidyanathan and Plumlee [1] provided a mechanistic model for 100%TD UN with undetermined coefficients. Storms [2] provided an empirical correlation based on measurement data from UN and (U,Pu)N available in the literature [3 – 5]. The Storms correlation is a function of fuel average temperature, burnup and porosity. The effect of the Pu content in the correlation is considered negligible. For the present handbook, the Storms correlation is recommended, and the correlation is

$$F = 100 \left[1 + \exp\left\{ 7.8 \left(1 - P\right)^{0.77} B^{-0.09} - 0.0025\, T \right\} \right]^{-1} \qquad (1)$$

where F is the percent fission gas release, P the fractional porosity, B at% burnup, and T fuel average temperature in K. Notice that Eq.(1) is not defined at $B = 0$ at%, where obviously $F = 0$.

Fig.10-1 shows a prediction result for (Pu,Zr)N with 15% porosity.

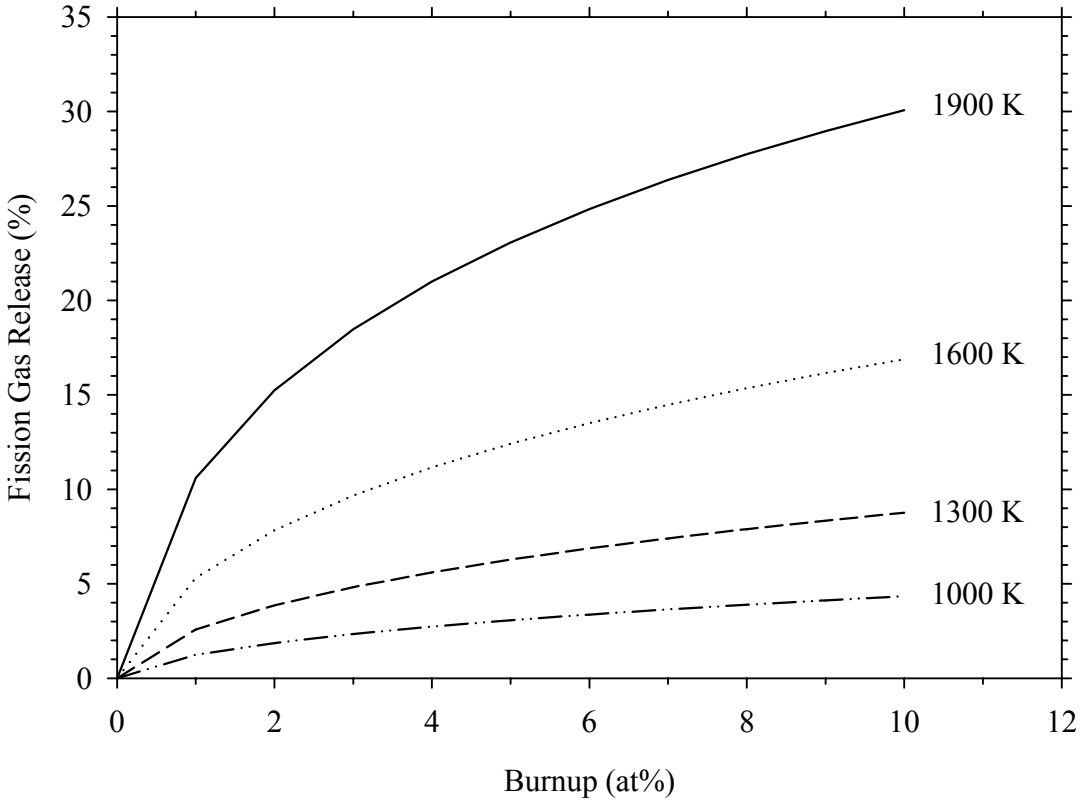

Fig.10-1 Percent fission gas release from (Pu,Zr)N with 15% porosity

10.2 References for Section 10

1. S. S. Vaidyanathan and D.E. Plumlee, AIP Conference Proceedings, 10th Symposium on Space Nuclear Power and Propulsion, M. S. El-Genk and M.D. Hoover, eds., p.251 (1993).
2. E.K. Storms, J. Nucl. Mater., 158, 119 (1988).
3. R. Baars, NITRID: A simple code for analysis of uranium nitride fuel pins, 4th Symposium on Space Nuclear Systems, Albuquerque, NM, Jan. 12-16 (1987).
4. J.K. Thomas, D.E. Brozak and K.L. Peddicord, Material property and irradiation performance correlations for nitride fuels, 5th Symposium on Space Nuclear Power Systems, Albuquerque, NM, Jan. 11-14 (1988); see also Final Project report-5/30/87, Texas A&M University (1987).
5. S.B. Ross, Uranium nitride fuel swelling and thermal conductivity correlations, M.S. Thesis, University of New Mexico, Albuquerque, NM (1987).